CRUSTAL AND LITHOSPHERE DYNAMICS OF THE SOUTHERN PACIFIC AND THE WEST ANTARCTIC MARGIN

FLORIAN WOBBE

A thesis submitted in partial fulfillment of the requirements for the degree of

Doctor of Philosophy in Geosciences

APPROVED DISSERTATION COMMITTEE

Prof. Dr. Vikram Unnithan
Dr. Karsten Gohl
Dr. Klaus Grosfeld
Prof. Dr. Carmen Gaina
Prof. Dr. Rolando di Primio

DATE OF DEFENSE: March 31, 2014

School of Engineering and Science

SUBMITTED:
January 31, 2014

REVISED:
December 10, 2014

SUPERVISORS:
Prof. Dr. Vikram Unnithan (chair of dissertation committee), Jacobs University, Bremen, Germany
Dr. Karsten Gohl, Alfred Wegener Institute, Bremerhaven, Germany

FURTHER MEMBERS OF THE DISSERTATION COMMITTEE:
Dr. Klaus Grosfeld, Alfred Wegener Institute, Bremerhaven, Germany
Prof. Dr. Carmen Gaina, University of Oslo, Oslo, Norway
Prof. Dr. Rolando di Primio, GFZ German Research Centre for Geosciences, Potsdam, Germany

AFFILIATION:
Alfred Wegener Institute, Helmholtz Centre for Polar and Marine Research, Am Alten Hafen 26, 27568 Bremerhaven, Germany

The author conducted the research for this dissertation in the Geophysics working group at the Alfred Wegener Institute for Polar and Marine Research, Bremerhaven. The work was funded by the Earth System Sciences Research School (ESSReS), a graduate school of the Helmholtz Association of German Research Centres at the Alfred Wegener Institute.

SUMMARY

Currently, there is a broad interest in the development of paleotopographic models for the West Antarctic margin, which are essential for robust simulations of paleoclimate scenarios. Recent work has shown that large uncertainties in past topography reconstructions have led to false conclusions about the growth and the extend of Antarctica's ice sheet. The evolution of the polar ice sheets is one of the driving factors of global climate change. Improvements on paleotopographic models are therefore fundamental for a better understanding of the climate in the past.

In this thesis, the author acquired and analyzed a new geomagnetic dataset off the West Antarctic margin, refined the South Pacific plate-tectonic reconstruction, and for the first time estimated the deformation of Antarctica's passive continental margins. The new data constrain the age of the rifted oceanic margin of West Antarctica and indicate that initial seafloor formation propagated westward from the Bellingshausen sector between ~89 and 84 Myr. In the Ross Sea area little continental deformation (<90 km) is observed prior to the breakup of Gondwana. However, further east the independent motion of the Bellingshausen microplate over a period of 22 Myr extended the continental margin by 106–304 km. Subsequent intraplate magmatism further altered the lithosphere. The rifting phase along the Pacific margin of Antarctica was comparatively short. Elsewhere in Antarctica rifting lasted much longer and was slow enough to allow for 300–400 km of margin extension.

The author further determined the total sediment thickness from seismic data, calculated cross-regional total sediment thickness grids of the Southern Pacific, and derived the sediment unloaded basement topography. The data indicate that sediment thickness along the Pacific margin of Antarctica is about 3–4 km larger than previously assumed and that the sediment volume has been underestimated. Hence, the re-evaluation of erosion rates and West Antarctica's topography are eminent to improve our understanding of Antarctica's glaciation history.

Grids of sediment corrected basement depth and residual basement depth of the South Pacific were derived from the sediment thickness and then compared to the present-day state of dynamic topography models. The mean residual basement depth of the Antarctic plate is about 300 m higher than that of the Pacific plate. The observations support the existence of a persistent mantle plume beneath the Ross Sea and the Balleny Islands hotspot area. However, dynamic topography disagrees with the presented residual basement depth of the South Pacific. Consequently, predictions of the South Pacific paleotopography remain speculative until more accurate

dynamic topography models, which explain the anomalous basement depth become available.

ACKNOWLEDGMENTS

Firstly, I want to thank Vikram Unnithan for being my formal PhD advisor and for providing the opportunity to participate various field and short courses as teaching assistant, thus making my PhD time much more enjoyable. My thanks also go to Karsten Gohl for supervising my thesis, for his discussions and suggestions, and for the unforgettable research cruise to West Antarctica yielding more than 6800 helicopter flight bonus miles. Further, I owe Klaus Grosfeld a debt of gratitude. He lent me an ear at a time I had lost the proverbial 'red thread' of my thesis and successfully re-motivated me, which I really appreciate. Also, as Earth System Science Research School coordinator, Klaus did an amazing job of organizing many interesting short courses and activities. For having me at the NGU in Trondheim, Norway, and for teaching me the first steps of plate reconstructions, I want to express my sincere thanks to Carmen Gaina. Likewise, I am grateful to Bryan Davy, Rupert Sutherland, and Dietmar Müller for inviting me to stay at GNS Science, Lower Hutt, New Zealand, and the University of Sydney, Australia, for a fruitful research visit. Special thanks go to Ansa Lindeque for hitting the rough road to the PhD with me, and for being her supportive self throughout the journey, as well as to my officemates Tabea Altenbernd and Stefanie Keßling for their advice and all the scientific and non-scientific discussions. Last but not least, I am deeply grateful to my family, my friends, and colleagues, who were always present when I needed them and who gave me the strength to go ahead.

CONTENTS

LIST OF FIGURES

LIST OF TABLES

1 INTRODUCTION AND MOTIVATION OF THIS STUDY

The geodynamic evolution of the South Pacific is one of the key elements in circum-Antarctic palaeoclimate modeling in terms of boundary conditions. Plate-kinematic rotations of plates and plate segments provide the basis of several fundamental derived datasets, including oceanic paleoage and basement depth. In combination with other data sources, such as sediment thickness and the present-day geometry of continental margins, plate-kinematics help to understand the tectonic processes during continental breakup.

Paleogeography and paleotopography play an important role in global climate change. The global atmospheric and oceanic circulation patterns, for example, are controlled by the location and configuration of landmasses, and the geometry and depth of the seabed. The timing of Gondwana's breakup and the formation of early shallow water passages are crucial for investigating global ocean circulation patterns. Ocean currents contribute only a small amount to the mean poleward heat transport of the earth (e.g., Trenberth and Caron 2001; Czaja and Marshall 2006; Fasullo and Trenberth 2008), yet they are of critical importance in the global heat budget and can trigger global climate transitions from, for example, a greenhouse to an icehouse. The onset of the Antarctic Circumpolar Current (Barker et al. 2007b) after the opening of the Drake Passage (Livermore et al. 2007) and the deepening of the Tasman Gateway in the Eocene–Oligocene transition (Stickley et al. 2004) is considered to be the cause for the glaciation of Antarctica (Barker et al. 2007a). The circulation keeps warm ocean waters away from Antarctica's coast and isolates the continent's climate.

Not only the ocean circulation driven by the geometry of the oceanic basins surrounding Antarctica is responsible for the buildup of the icecaps. The onshore topography of West Antarctica itself is an essential factor for the growth and preservation of ice shields. Existing climate simulations have limitations in accurately depicting the land topography of the past and often rely on the present-day subglacial bedrock topography. In the past, this has led to inaccurate conclusions regarding atmospheric composition and glaciation in the Northern Hemisphere (e.g., DeConto et al. 2008). Recent reconstructions of Eocene–Oligocene topography, however, indicate that much of West Antarctica's topography has eroded since then (Wilson and Luyendyk 2009; Wilson et al. 2012). Consequently, most of West Antarctica lay above sea level in the Early Oligocene and hence was able to support and protect larger ice masses from warm ocean currents (Wilson et al. 2013).

The following section summarizes the main research questions of this thesis and provides the outline for the single publications in Chapters 4 to 7. Each of the topics addressed therein will be concluded in Chapter 8 with an outlook on new research possibilities.

1.1 PLATE-TECTONIC RECONSTRUCTION OF THE SOUTH PACIFIC

The complex plate-tectonic reconstruction of the South Pacific is complicated by a lack of data adjacent to West Antarctica constraining the timing and rate of rifting during continental margin formation. Several models exist that explain the plate-tectonic evolution of the South Pacific (e.g., Molnar et al. 1975; Stock and Cande 2002; Larter et al. 2002; Eagles et al. 2004a). These models are fairly similar for regions with abundant magnetic data. However, the West Antarctic margin geometry is discussed controversial. Especially in the Bellingshausen Sea sector little is known about the type and the thickness of the crust. Hence, it remains speculative whether the southern Bellingshausen Plate margin is of continental or oceanic origin (Eagles et al. 2004b). Newly obtained geophysical data along the continental margin of West Antarctica (Gohl 2007, 2010) provide an opportunity to improve past models of the South Pacific evolution beginning with the breakup of Gondwana. This leads to the first fundamental research questions for this thesis:

Can the plate-tectonic reconstruction of the South Pacific be improved with new geophysical data? What is the initial breakup time? By how much was the West Antarctic continental margin extended prior to the breakup of Gondwana? How long did the deformation last? Which is the exact geometry of the breakup?

1.2 ANTARCTICA'S PRE-RIFT MARGIN GEOMETRY

The implications of extension within the continental crust of rifted continental margins for the global plate circuit are well known since the late 1980s (e.g., Dunbar and Sawyer 1987, 1989). Pre-rift (full-fit) plate-tectonic reconstructions of passive continental margins must consider relative motion by seafloor spreading and by the extension of continental crust during continental breakup. Otherwise, overlaps in the global plate circuit may occur (cf. Figure 2.6).

Although extension during the pre-breakup Australian–Antarctic continental rifting has been considered by Powell et al. (1988) and Royer and Sandwell (1989), recent plate-tectonic models of the South Pacific only account for seafloor spreading (since c. magnetic chron c34y, 84 Myr) and

do not attempt full-fit reconstructions (e.g., Royer and Rollet 1997; Tikku and Cande 1999; Whittaker et al. 2007).

The conjugated continental margins of Australia and Wilkes Land (cf. Figure 2.6) are well investigated in comparison to other regions. But elsewhere, there is very limited data available to better constrain the margin restoration. The extent of Antarctica's continent–ocean transition zones (COTZ), for example, remained largely unknown in the past. Reliable estimates of crustal thickness within the COTZ are scarce and hence it is difficult to reconstruct pre-rift margin geometry. Due to these problems, current plate-tectonic reconstructions of the Gondwana breakup are restricted to two (e.g., Antarctica–India, Gaina et al. 2007; Jokat et al. 2010) or three (e.g., Antarctica–Africa–South America, Jokat et al. 2003; König and Jokat 2006; Eagles and König 2008) plates only and continental extension during the rifting phase cannot be quantified precisely.

New geophysical data along the continental margin of Antarctica permitted a more precise differentiation of oceanic and continental crust, not only indicating that Antarctica's COTZs are much broader than previously thought (Gohl 2008), but also providing an opportunity to study the evolution of the margin geometry of Antarctica:

How much continental deformation took place along the circum-Antarctic passive margins during the breakup of Gondwana? How long did the deformation last? Which is the restored geometry of Antarctica's pre-rift suture?

1.3 SOUTH PACIFIC LITHOSPHERE DYNAMICS

Currently, there is a broad interest in the development of paleotopographic models for the West Antarctic margin, which are essential for robust simulations of paleoclimate scenarios. The ANTscape research initiative, for example, expedites research on the paleogeography and paleoelevation of Antarctica. Reconstructions of the Antarctic topography at the Eocene–Oligocene (c. 34 Myr) transition indicate that West Antarctica's land area decreased by about 20% since then (Wilson and Luyendyk 2009; Wilson et al. 2012). Both, glacial erosion and thermal subsidence, lowered the West Antarctic bedrock elevations. A climate-ice sheet model based on the new paleotopography predicts an earlier onset of glaciation, and an ice volume which is >1.4 times greater than previously thought (Wilson et al. 2013).

Unfortunately, present paleotopographic models still contain large uncertainties and lack information on sediment thickness and geodynamic conditions. For example, the sediment thickness in the Australian–Antarctic region has been underestimated by more than 2000 m (Whittaker et al. 2013). This has implications not only for onshore paleotopography and paleoclimatology, but also for geodynamic conditions of the Southern

Ocean. Reconstructions of basement topography and paleobathymetry all depend on precise sediment thickness estimates.

In the last years the amount of available seismic reflection data along the West Antarctic margin (e.g., Scheuer et al. 2006a, b; Gohl 2007, 2010; Lindeque and Gohl 2010; Uenzelmann-Neben and Gohl 2012; Wobbe et al. 2012; Gohl et al. 2013b; Kalberg and Gohl 2014) increased constantly, allowing the amendment of existing sediment thickness models of the Pacific margin of West Antarctica (e.g., Divins 2003; Scheuer et al. 2006a):

Can the South Pacific sediment thickness grids be improved using new geophysical data? What are the differences to previous sediment thickness and sediment volume estimates? Do the new data change our geodynamic and tectonic understanding of West Antarctica and the South Pacific? What are the implications for sediment thickness-derived datasets such as sediment unloaded basement depth?

2 DATASETS AND METHODS

This chapter gives a brief overview of the data and methods applied. It focusses on details that were not considered in the publications (Chapters 4 to 7). This thesis is essentially based on newly obtained ship- and airborne magnetic data, shipborne gravity data, and marine seismic data. The data were acquired along the continental margin of West Antarctica during two R/V Polarstern cruises in 2006 (ANT-23/4, Gohl 2007) and 2010 (ANT-26/3 Gohl 2010). The first publication includes a comprehensive summary of the data and methods required to obtain full-fit reconstructions of passive continental margins (Section 4.2). The following section provides more detailed information on the non-standard procedures for analyzing ship-magnetic data from Polarstern.

2.1 MAGNETIC DATA PROCESSING

Airborne magnetic data was acquired from specially equipped offshore-configured MBB Bo 105 helicopters operating from R/V Polarstern (Figure 2.1). The helicopters towed a cesium-vapor magnetometer 30 m below the airframe to avoid magnetic disturbances. This reduced the amount of post-processing necessary to obtain optimal results when interpolating the magnetic field over a surface (cf. Section 6.3).

The data from the two three-component fluxgate vector magnetometers mounted on R/V Polarstern's crow's nest (Figure 2.2), however, had to be pre-processed. The ship's ferrous hull caused spurious shifts in the

Figure 2.1. Helicopter towed optically pumped cesium-vapor magnetometer operated from R/V Polarstern.

Figure 2.2. Fluxgate magnetometers installed in R/V Polarstern's crow's nest.

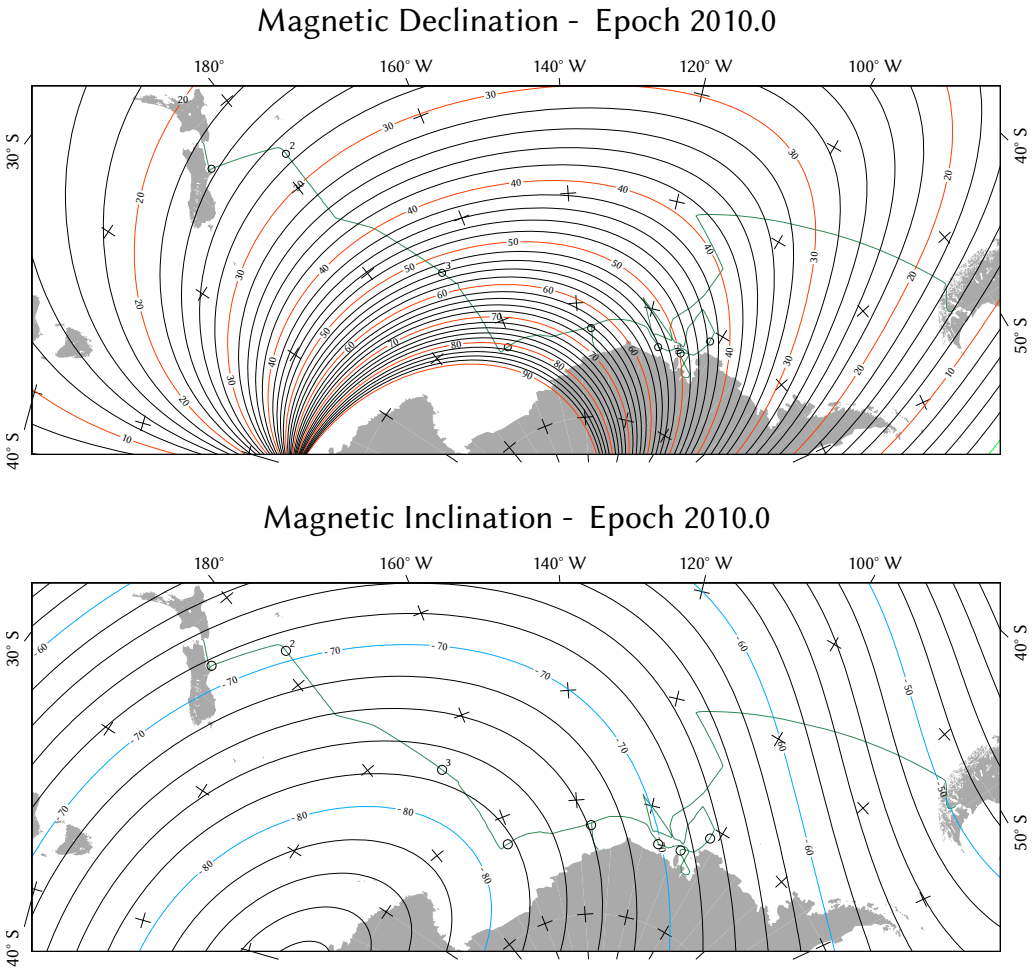

Figure 2.3. Isogonic lines (magnetic declination) and isoclinic lines (magnetic inclination) of the South Pacific (International Geomagnetic Reference Field, IGRF-11, Finlay et al. 2010). Magnetic compensation loops (circles) during R/V Polarstern cruise ANT-26/3 (green line). Lambert conformal conic projection with central meridian 135°W and standard parallels 70°S and 50°S referenced to WGS84.

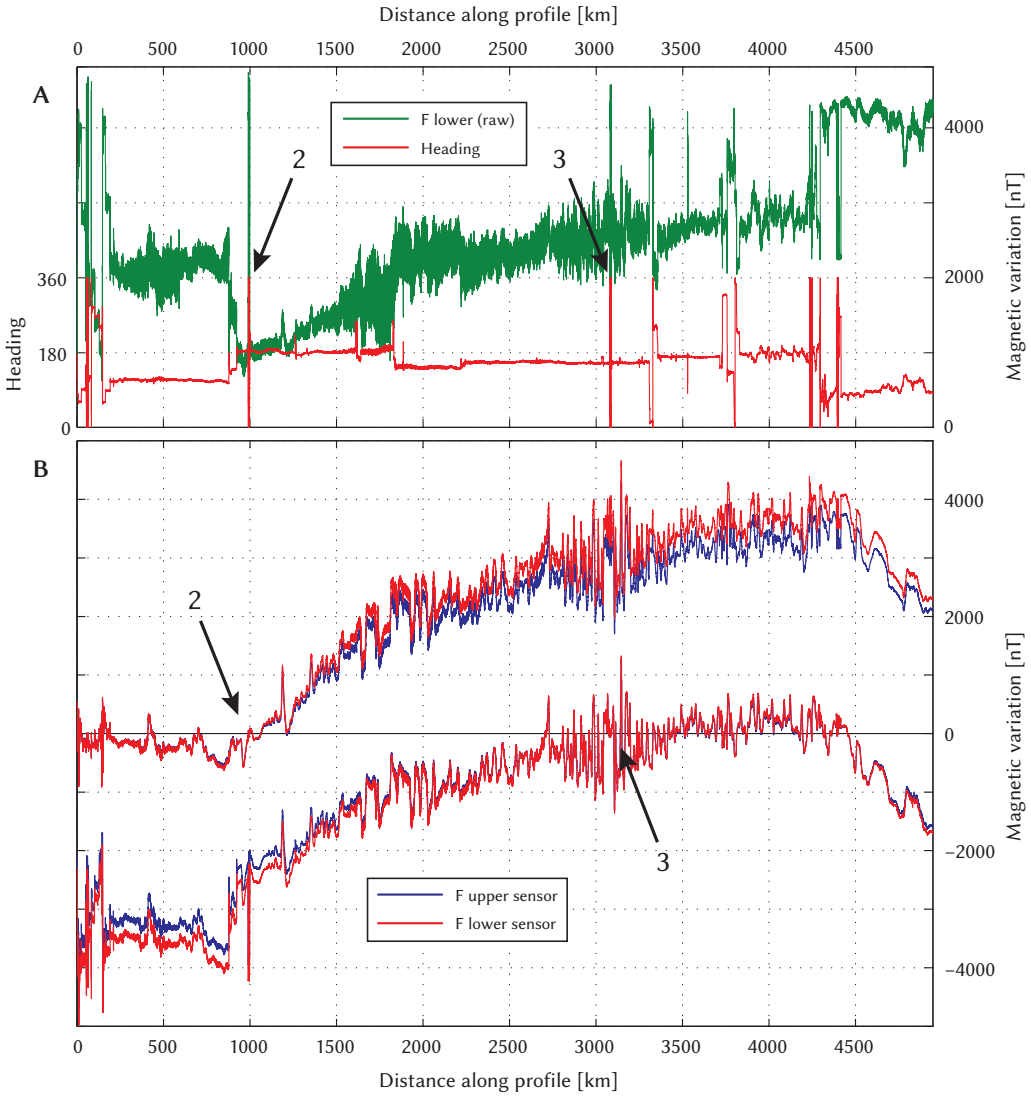

Figure 2.4. Raw and processed data from R/V Polarstern's fluxgate magnetometers during transect from New Zealand to the Ross Sea from 2010-01-31 to 2010-02-15 (Figure 2.2). A – Ship's compass heading and uncompensated total field (F) of lower sensor. B – Compensated ship-magnetic data (cf. König 2006; Gohl 2010; Wobbe et al. 2012) using calibration coefficients from second and third calibration loop (arrows, cf. Figure 2.3).

measured magnetic data which had to be compensated. The largest error stems from the ship's heading with respect to the magnetic north (e.g., Nogi and Kaminuma 1999; König 2006). The same holds true for changes in magnetic declination and inclination (Figure 2.3), which vary considerably even within short range, due to the proximity of the research area to the South Magnetic Pole. A one degree change of the ship's heading or the magnetic declination causes about 300 nT of variation in the horizontal components (cf. Figure 2.4a). The procedure for compensating the perturbations has been established by König (2006) and is described in detail in Section 4.2.2.

It should be noted that the quality of the retrieved ship-magnetic data has to be monitored constantly because the radius of optimal magnetic

data acquisition around a compensation loop cannot be predicted. For operations in the polar regions the radius usually lies between <500 and 1500 km. The point, at which the calibration coefficients of the nearest compensation loop are insufficient to compensate the magnetic readings, can be determined with the following scheme. A first indicator is the steady deviation of the compensated data (total field) from the International Geomagnetic Reference Field (IGRF, Finlay et al. 2010). Values that differ by more than 1000 nT should be considered off-scale (Figure 2.4b). A very good indicator for leaving the radius of optimal data acquisition is the difference of the compensated data from the two separate magnetometer sensors. If the difference is nearly zero, the set of calibration coefficients is sufficient. If the difference increases steadily, the magnetic readings cannot be compensated properly for perturbations and a new compensation loop is required (Figure 2.4b).

2.2 PLATE-TECTONIC RECONSTRUCTION

Plate-tectonic reconstructions are obtained by fitting isochrons from two adjacent plates, which is described in great detail in the second publication (Section 5.1). In this thesis, the open-source software GPlates (Boyden et al. 2011) for interactive plate-tectonic reconstructions was utilized for visually fitting picks of the magnetic spreading anomalies in the South Pacific (Figure 2.5, Section 4.2).

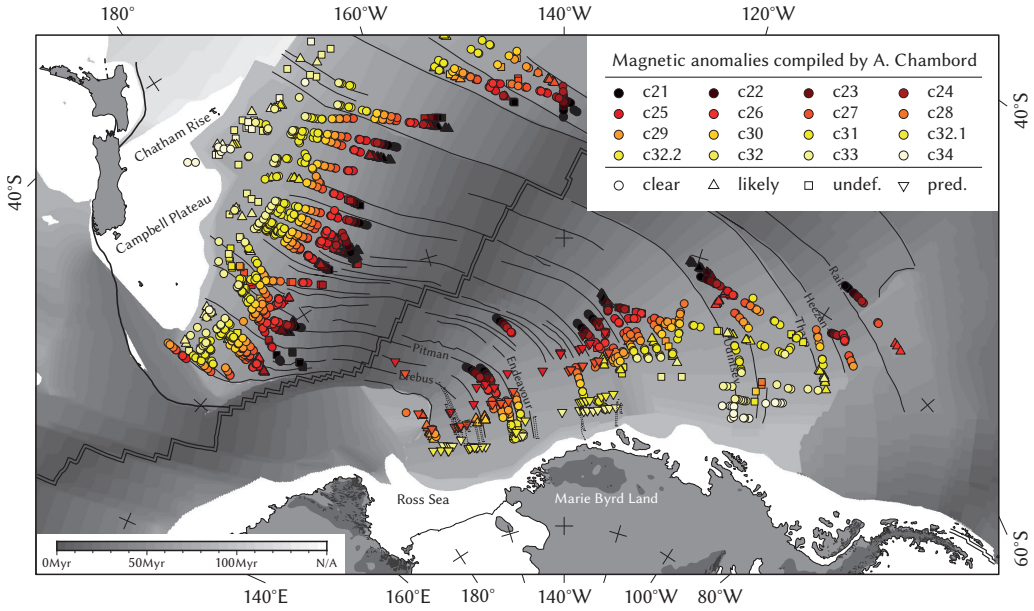

Figure 2.5. Compilation of magnetic anomaly picks on the West Antarctic and the Pacific plate used for plate-tectonic reconstruction in Wobbe et al. (2012). Dotted lines represent helicopter- and ship-magnetic lines (Figure 4.1). Basemap: age of the oceanic crust (Wobbe et al. 2012). Lambert conformal conic projection with central meridian 160°W and standard parallels 75°S and 69°S.

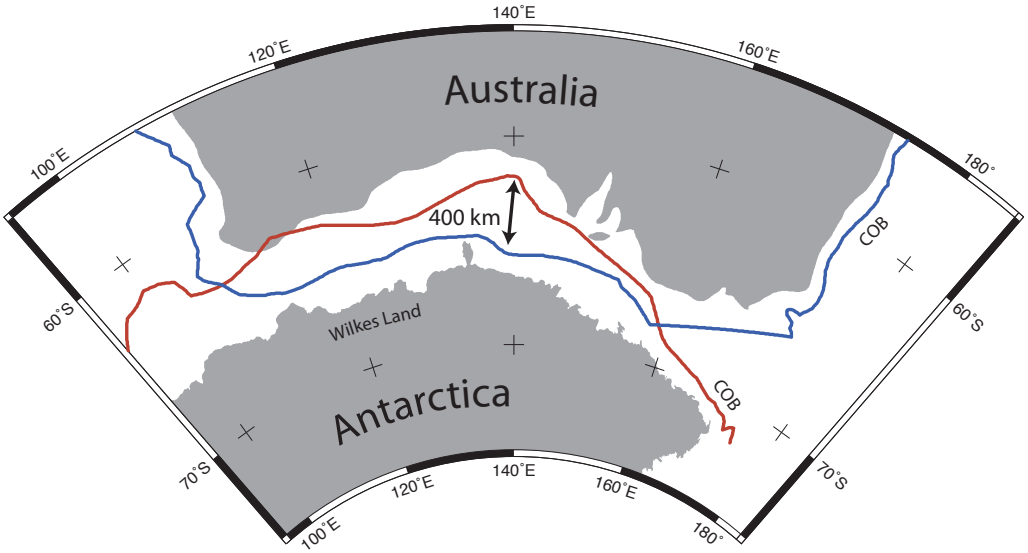

Figure 2.6. Misfit in static plate-tectonic reconstruction (Australia–Antarctica, c. 140 Myr) due to neglected continental deformation. COB – continent–ocean boundary. Polar stereographic projection; Antarctica fixed at its present-day position.

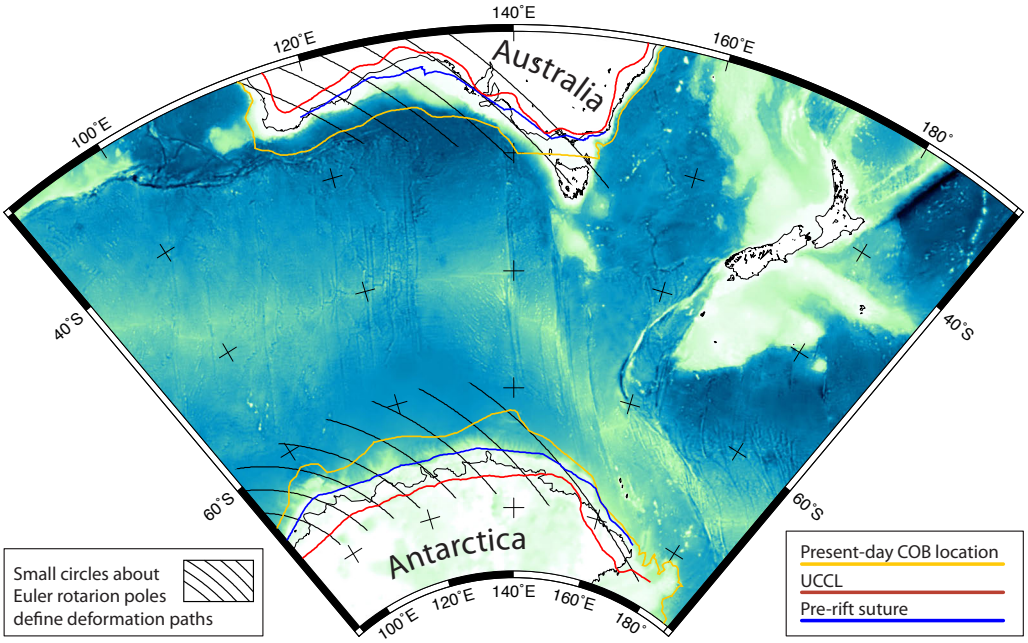

Figure 2.7. Reconstruction of Australian–Antarctic pre-rift suture. COB – continent–ocean boundary, UCCL – Unstretched Continental Crust Limit. Basemap: ETOPO1 bedrock topography (Amante and Eakins 2009). Lambert conformal conic projection with central meridian 140°E and standard parallels 63.75°S and 41.25°S.

In order to obtain full-fit plate-tectonic reconstructions of passive continental margins, intra-plate deformation associated with the breakup process prior to the formation of oceanic crust has to be estimated. Omission of continental extension produces misfits and overlaps in the global plate circuit (Figure 2.6). The procedures of restoring the continent–ocean boundary are illustrated in Section 5.2.

A small C program, betaRotate (c. 1500 lines), written by the author of this thesis in 2009, facilitates the reconstruction of passive continental margins. The command-line utility reads GMT-style line segment files of the landward unstretched continental crust limit (UCCL) and the seaward continent–ocean boundary (COB, Figure 2.7). Given a constant stretching factor, β, and an Euler pole, the program calculates the pre-rift suture by rotating all points along the deformation paths described by the small circles about this rotation pole (Figures 2.7 and 5.2). The rotation angle is determined by the β-factor and the length along each small circle (cf. Section 5.2). Optionally, a second deformation zone may be defined and a different stretching factor can be applied to this zone (cf. Figures 5.2).

The restoration method of betaRotate is essentially the same that was later developed independently by Whittaker et al. (2010) and Williams et al. (2011). The only difference is that Whittaker et al. (2010) and Williams et al. (2011) estimated the stretching along each small circle individually whereas betaRotate integrates the crustal thickness over a larger area and applies an average β-factor for a complete set of COT and UCCL.

2.3 AGE OF THE OCEANIC CRUSTAL AND BASEMENT TOPOGRAPHY

Figures 2.5 and 7.3 show the crustal age of the South Pacific oceanic crust. Using the model ages, the picks of the magnetic spreading anomalies, and the rotation poles from the plate-tectonic reconstruction (Section 4.3.4), a set of isochrons was produced. Prior to gridding, intermediate isochrons were constructed, to get a more densely spaced set of isochrons. This was achieved with the open-source software Intertec, developed by the EarthByte Group. In the last step, the age of the oceanic crust was gridded using a nearest-neighbor interpolation algorithm.

Both, the crustal age grid and the sediment thickness grid (Figure 7.2), provide the basis for derived datasets such as sediment unloaded basement depth (Figure 7.4) and residual basement depth (Figure 7.5) discussed in Section 7.3. Figure 2.8 illustrates how the residual basement depth is calculated by subtracting a model age of the oceanic crust from the sediment unloaded basement depth. Residual basement anomalies can be attributed to asthenospheric flow (Phipps Morgan and Smith 1992), intra-plate volcanism, or deeper mantle flow (Steinberger 2007). Hence,

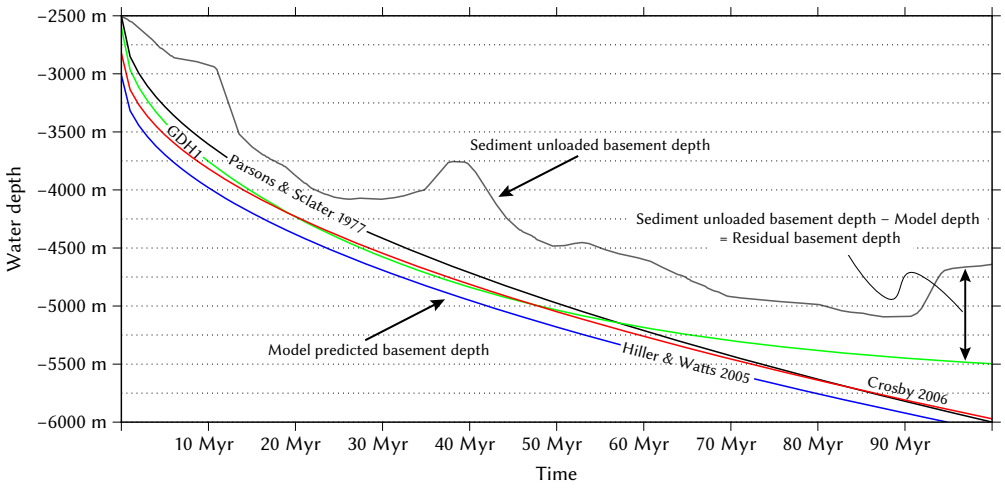

Figure 2.8. Relationship between water depth in the oceans and age of the oceanic crust (Parsons and Sclater 1977; Stein and Stein 1992; Hillier and Watts 2005; Crosby et al. 2006). Illustration of residual basement depth calculation by subtracting the model predicted basement depth from the sediment unloaded basement depth (gray line).

there should be a direct relationship to dynamic topography, which is examined in detail in Section 7.4.

2.4 UTILIZED AND DEVELOPED SOFTWARE

In addition to the software already specified above, several other programs were utilized for data processing, including

- ShipMagComp, a MATLAB routine written by König (2006) for compensating ship-magnetic data from R/V Polarstern,
- MODMAG, a MATLAB program to model marine magnetic anomalies (Mendel et al. 2005),
- zp, an open-source software by Barry Zelt for picking the sea floor and the acoustic basement from seismic data,
- and LCT, a commercial software for forward modeling of the gravity response.

Most figures were created with the Generic Mapping Tools (GMT). Since 2011 the author of this thesis contributed to GMT's code base and improved several features, which are now implemented in the core of the recently released GMT version 5 (Wessel et al. 2013). The new features include increased gridded data hard disc I/O and faster operations on grids in the frequency domain. This is achieved by implementing chunked data I/O via NetCDF-4 and integrating better performing fast Fourier transform algorithms (e.g., FFTW). Especially the data processing, grid

manipulation, and filtering for the fourth publication benefitted from the improved functionality.

3 SCIENTIFIC CONTRIBUTIONS

PUBLICATION I: Wobbe, F., K. Gohl, A. Chambord, and R. Sutherland, 2012. Structure and breakup history of the rifted margin of West Antarctica in relation to Cretaceous separation from Zealandia and Bellingshausen plate motion. *Geochem. Geophys. Geosyst.*, **13**(4), Q04W12. doi:10.1029/2011GC003742.

The authors present a new dataset of air- and shipborne geophysical measurements acquired during R/V Polarstern cruises in the eastern Ross Sea and Bellingshausen Sea in 2006 (ANT-23/4) and 2010 (ANT-26/3). The new data constrain the structure and age of the rifted oceanic margin of West Antarctica. The authors conclude that the Ross Sea area resembles a typical magma-poor margin with little continental deformation (<90 km) prior to the breakup of Gondwana. In the Bellingshausen sector, however, margin extension is estimated to be 106–304 km with abundant evidence for volcanism. The authors develop an improved plate-tectonic reconstruction of the West Antarctic continental margin, which predicts that initial seafloor formation propagated westward from the Bellingshausen sector between ~89 and 84 Myr.

The principal author was in charge of the magnetic data acquisition during the cruise ANT-26/3. Subsequently, he processed and analyzed that data, modeled the continental margin extension, refined the South Pacific plate-tectonic reconstruction, and wrote the manuscript. Karsten Gohl supervised the project and was chief scientist during R/V Polarstern cruises ANT-23/4 and ANT-26/3. Amandine Chambord reinterpreted magnetic anomalies using ship-magnetic data from the GEODAS marine trackline geophysics database (NGDC 2007) and compiled a new set of magnetic anomaly picks on the West Antarctic and the Pacific plate (Figure 2.5). Rupert Sutherland contributed to the data processing and analysis and improved the manuscript.

PUBLICATION II: Wobbe, F. and K. Gohl, 2013. Continental deformation of Antarctica during Gondwana's breakup. In G. Lohmann, K. Grosfeld, D. Wolf-Gladrow, V. Unnithan, J. Notholt, and A. Wegner, editors, *Earth System Science: Bridging the Gaps between Disciplines—Perspectives from a Multi-Disciplinary Helmholtz Graduate Research School*, SpringerBriefs in Earth System Sciences, pp. 83–89. Springer, Berlin Heidelberg. ISBN 978-3-642-32234-1. doi:10.1007/978-3-642-32235-8_4.

The authors classify the continental deformation of the circum-Antarctic passive margins based on new data and a review of relevant published

data. The continental deformation of Antarctica prior to rifting lasted over 100 million years. The time span of deformation was sufficiently large and the rifting velocity low enough to extend the margin by up to 300–400 km. Accounting for continental margin deformation, a prerequisite for precise plate-tectonic reconstructions, the authors conclude that crustal thinning during breakup generates significant subsidence. Therefore, shallow water passages along the continental margins might already have developed during the rifting phase.

The principal author estimated the deformation of Antarctica's passive continental margins under the assumption of volume constancy, calculated stretching factors (β) from crustal thickness models, reconstructed the pre-rift suture, and wrote the manuscript. The co-author supervised the project and improved the manuscript.

PUBLICATION III: Gohl, K., A. Denk, G. Eagles, and F. Wobbe, 2013. Deciphering tectonic phases of the Amundsen Sea Embayment shelf, West Antarctica, from a magnetic anomaly grid. *Tectonophysics*, **585**(0), 113–123. doi:10.1016/j.tecto.2012.06.036.

The authors publish a vast magnetic dataset from helicopter- and ship-borne surveys on the shelf of the Amundsen Sea Embayment in 2006 and 2010. The magnetic anomaly map outlines the boundary zone between the sediment-covered middle to outer shelf and the inner shelf where basement rocks crop out. Distinct zones of anomaly patterns and lineaments can be associated with different tectonic phases. The authors conclude that the Amundsen Sea Embayment shelf is a zone of long-lived distributed crustal deformation.

The principal author wrote the manuscript based on the master's thesis of Astrid Denk. Astrid Denk processed the magnetic data, calculated the 2D models for the analysis of magnetic anomaly patterns, identified structural lineaments, characterized magnetic source bodies, and contributed to the manuscript. The author supervised the project and was chief scientist during R/V Polarstern cruises ANT-23/4 and ANT-26/3. Florian Wobbe compensated the ship-magnetic data for perturbations due to ship-induced magnetic fields and contributed to the data processing. Together with Graeme Eagles, he was in charge of the magnetic data acquisition during ANT-23/4 and ANT-26/3 respectively and improved the manuscript.

PUBLICATION IV: Wobbe, F., A. Lindeque, and K. Gohl, 2014. Anomalous South Pacific lithosphere dynamics derived from new total sediment thickness estimates off the West Antarctic margin. *Global Planet. Change*, **123**, 139–149. doi:10.1016/j.gloplacha.2014.09.006.

The authors present a total sediment thickness grid spanning the West Antarctic margin and combine this new grid with NGDC's original global 5 arc minute grid of ocean sediment thickness[1] (Whittaker et al. 2013). The

1 Available online at http://www.ngdc.noaa.gov/mgg/sedthick/

residual basement topography of the South Pacific has been derived from the sediment thickness. The authors conclude that present-day dynamic topography models disagree with the presented revised basement topography of the South Pacific and that paleotopographic reconstructions are still fairly uncertain.

The principal author calculated the sediment thickness, gridded the data, calculated the residual basement depth, undertook the analysis of the data, and wrote the manuscript. Ansa Lindeque contributed to the data processing and analysis, picked the acoustic basement and seafloor from seismic data needed to determine the total sediment thickness, and improved the manuscript. Karsten Gohl supervised the project.

PUBLICATION V: Wessel, P., W. H. F. Smith, R. Scharroo, J. Luis, and F. Wobbe, 2013. Generic Mapping Tools: Improved Version Released. *EOS Trans. AGU*, **94**(45), 409–410. doi:10.1002/2013EO450001. *Not included in this work.*

The authors release and present version 5 of the Generic Mapping Tools (GMT). This version of GMT provides many improvements, including a high-level Application Programming Interface (API), modularized GMT programs that use the API functions, access to Fast Fourier Transform (FFT) libraries, increased grid read/write performance, better integration with Geographical Information Systems (GIS), better uniformity of GMT options, and interactive program documentation.

The principal author is the lead application developer and wrote the manuscript. The co-authors contributed to the code base and improved the manuscript. Florian Wobbe took the lead in redesigning and rewriting GMT's build system using the CMake cross-platform build system generator, improved the grid processing, contributed to the FFT library integration, and redesigned the website.

4 | PUBLICATION I

Structure and breakup history of the rifted margin of West Antarctica in relation to Cretaceous separation from Zealandia and Bellingshausen plate motion

Florian Wobbe and Karsten Gohl[1]
Amandine Chambord and Rupert Sutherland[2]

ABSTRACT

Geophysical data acquired using R/V Polarstern constrain the structure and age of the rifted oceanic margin of West Antarctica. West of the Antipodes Fracture Zone, the 145 km wide continent–ocean transition zone (COTZ) of the Marie Byrd Land sector resembles a typical magma-poor margin. New gravity and seismic reflection data indicates initial continental crust of thickness 24 km, that was stretched 90 km. Farther east, the Bellingshausen sector is broad and complex with abundant evidence for volcanism, the COTZ is ~670 km wide, and the nature of crust within the COTZ is uncertain. Margin extension is estimated to be 106–304 km in this sector. Seafloor magnetic anomalies adjacent to Marie Byrd Land near the Pahemo Fracture Zone indicate full-spreading rates during c33–c31 (80–68 Myr) of 60 mm yr^{-1}, increasing to 74 mm yr^{-1} at c27 (62 Myr), and then dropping to 22 mm yr^{-1} by c22 (50 Myr). Spreading rates were lower to the west. Extrapolation towards the continental margin indicates initial oceanic crust formation at around c34y (84 Myr). Subsequent motion of the Bellingshausen plate relative to Antarctica (84–62 Myr) took place east of the Antipodes Fracture Zone at rates $<$40 mm yr^{-1}, typically 5–20 mm yr^{-1}. The high extension rate of 30–60 mm yr^{-1} during initial margin formation is consistent with steep and symmetrical margin morphology, but subsequent motion of the Bellingshausen plate was slow and complex, and modified rift morphology through migrating deformation and volcanic centres to create a broad and complex COTZ.

1 Alfred Wegener Institute for Polar and Marine Research, P.O. box 120161, 27515 Bremerhaven, Germany.
2 GNS Science, 1 Fairview Drive, Avalon, Lower Hutt 5040, New Zealand.

Keywords: continent–ocean transition zone; crustal thickness; magnetic spreading anomaly; plate reconstruction.

4.1 INTRODUCTION

The formation of continental passive margins by rifting is affected by the rate of rifting, the initial configuration of continental lithosphere, and the temperature and composition of the asthenosphere (White et al. 1992; van Wijk and Cloetingh 2002). The final breakup of Gondwana occurred during Late Cretaceous time as rifted continental crust of New Zealand separated from Antarctica at an intermediate-rate spreading ridge to produce typical oceanic crust (Molnar et al. 1975; Cande et al. 1995; Eagles et al. 2004a; Sutherland et al. 2010). Hence, the region presents an ideal opportunity to study classical conjugate rifted margins, but this outcome has been frustrated by extreme logistic difficulties associated with collecting data adjacent to Antarctica. We present a substantial new marine geophysical dataset collected using R/V Polarstern, which has general relevance for the study of continental margins, has substantial regional implications, and adds to the body of knowledge required to construct reliable global plate kinematic estimates. Of particular regional interest is the complication of a small and short-lived oceanic plate, the Bellingshausen plate, which was active after break-up adjacent to the Antarctic margin.

Geological samples, gravity data and receiver-function analysis of teleseismic earthquakes suggest that both West Antarctica (Llubes et al. 2003; Luyendyk et al. 2003; Winberry and Anandakrishnan 2004; Block et al. 2009) and the submarine plateaus surrounding New Zealand (Grobys et al. 2009, and references therein) consist of extended continental crust. Widespread continental extension is thought to have been largely complete before the continental margins were formed and Zealandia drifted from Antarctica. Breakup reconstructions of Zealandia from Antarctica consider a narrow continent–ocean transition zone (Larter et al. 2002; Eagles et al. 2004a).

In this study, we present new crustal thickness and density models of the Marie Byrd Land continental margin of Antarctica, and new magnetic anomaly interpretations from adjacent oceanic crust. The crustal thickness models provide a foundation for reconstructing the continent–ocean transition zone (COTZ), and hence better reconstructing the past positions of the conjugate continental fragments. Magnetic anomalies provide new constraints on the timing and rate of rifting during continental margin formation, and on subsequent plate motions.

4.2 DATA ACQUISITION AND PROCESSING

During the Polarstern cruises in 2006 (ANT-23/4) and 2010 (ANT-26/3), ship- and airborne magnetic and shipborne gravity data have been acquired. These data were combined with seismic reflection and refraction/wide-angle reflection surveys from the same cruises to constrain the COTZ of Marie Byrd Land. Regions where measured ship-data are unavailable were filled with public domain satellite-derived free-air gravity data (Andersen and Knudsen 2009), global seafloor topography data (Smith and Sandwell 1997, version 13.1, 2010), and ship-magnetic data from the GEODAS marine trackline geophysics database (NGDC 2007). Data acquisition and subsequent processing for each of the acquired datasets are described in the following sections.

4.2.1 Helicopter magnetics

In 2010, five thousand kilometers of aeromagnetic data were recorded at a sampling rate of 10 Hz during the North–South transit from New Zealand to the Amundsen Sea south of 69°S (Figures 4.1–4.3). A helicopter towed the optically pumped cesium-vapor magnetometer 30 m below its airframe to avoid magnetic disturbances. Flight lines were arranged perpendicular to the expected magnetic lineation of the seafloor at an average line spacing of 10–20 km, covering a profile distance of about 450 km at a flight elevation of 100 m above sea level. Geographic position, speed and altitude of the aircraft as well as time were recorded at a rate of 5 Hz (Gohl 2010).

The cesium-vapor magnetometer recorded data with a general heading error below 5 nT so that no calibration was necessary. Processing included removal of electromagnetic noise, resampling at 100 m intervals, and correction for the International Geomagnetic Reference Field using the IGRF-11 coefficients (Finlay et al. 2010). Measured magnetic anomaly amplitudes of 50–400 nT were greater than the daily variation of 20–30 nT, observed at the Eyrewell Geomagnetic Observatory in New Zealand. Local daily variations were therefore considered negligible.

4.2.2 Shipborne magnetics

Two three-component fluxgate vector magnetometers mounted on the crow's nest of R/V Polarstern measured shipborne magnetic data. The total magnetic field as well as the heading, roll, pitch, velocity, and position of the ship were logged at 1 Hz.

Calibration loops provide coefficients relating the ship orientation (heading, roll, pitch) and speed to the variations in magnetometer measurements. To compensate for perturbations due to ship-induced magnetic fields, we measured a total of 13 calibration loops, five of which are located in our study area (Figure 4.4). During a calibration loop, the ship follows an eight-

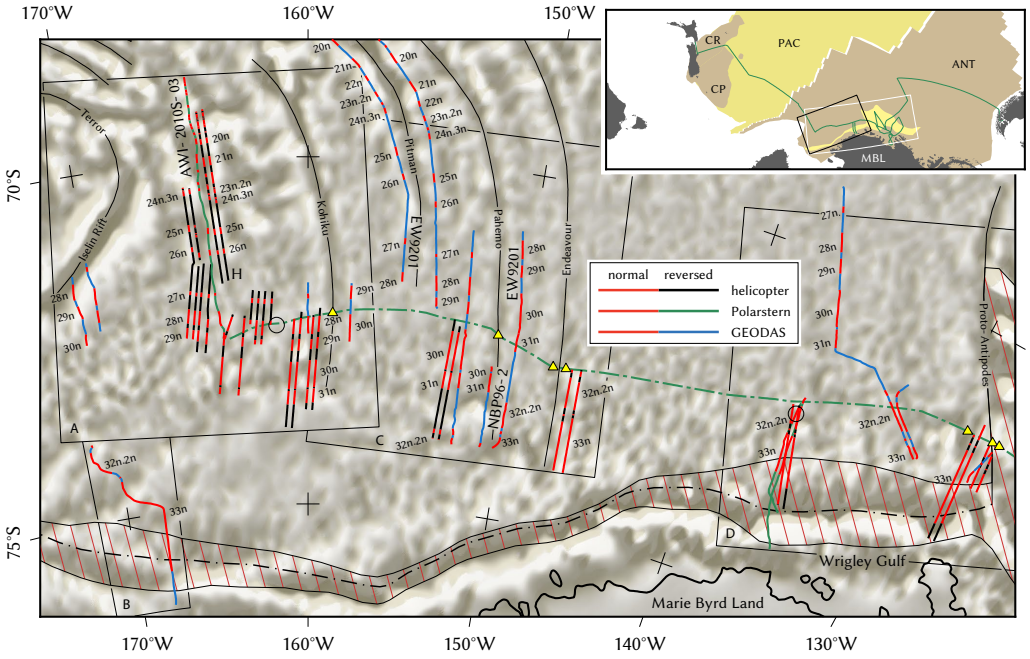

Figure 4.1. Identified magnetic spreading anomalies along helicopter- and ship-magnetic lines (R/V Polarstern lines AWI-2010S-00–AWI-2010S-03; GEODAS lines EW9201, NBP94-2, NBP96-2, NBP9702). Magnetic model of helicopter-magnetic line AWI-2010H-08-15-17 (H) and ship-magnetic line AWI-2010S-03 in Figure 4.16. Magnetic compensation loops during ANT-26/3 (circles); fracture zones (thin black lines); fracture zones evident in seismic lines AWI-20100110 and AWI-20100117 (yellow triangles); COTZ (striated area); and reconstructed pre-rift suture (dashed line). Black frames indicate locations of Figure 4.2. All features superimposed on DNSC08 satellite gravity map (Andersen and Knudsen 2009). Lambert conformal conic projection with central meridian 160°W and standard parallels 75°S and 69°S. Inset map: ship track of R/V Polarstern expedition ANT-26/3 (green line); location of maps in this figure and in Figure 4.4 (black and white frames); CP – Campbell Plateau; CR – Chatham Rise; ANT – West Antarctic plate; MBL – Marie Byrd Land; PAC – belonging to Pacific plate. Magnetic model of lines EW9201 and NBP96-2 in Figure 4.15.

shaped course of two consecutive turns of opposite veer with a radius of about 1.8 km (1 NM) and a velocity of 5–7 kn.

In the small area of a calibration loop, variations of the magnetic field due to crustal magnetization are considered negligible. In the larger area around the calibration loop, the shipborne magnetic measurements were corrected with the motion coefficients according to König (2006). The calibrated data have a maximum residual error of 20–30 nT under normal conditions at sea. Since the interference of the ship on the magnetic fields is larger than the daily magnetic variation, the daily variations were neglected in the determination of seafloor spreading anomalies.

The induced magnetic field of the ship is not static, but instead depends on the strength, inclination, and declination of the ambient magnetic field. Since the inclination and declination show a high local variance in the higher latitudes, calibration coefficients are only adequate to fully correct

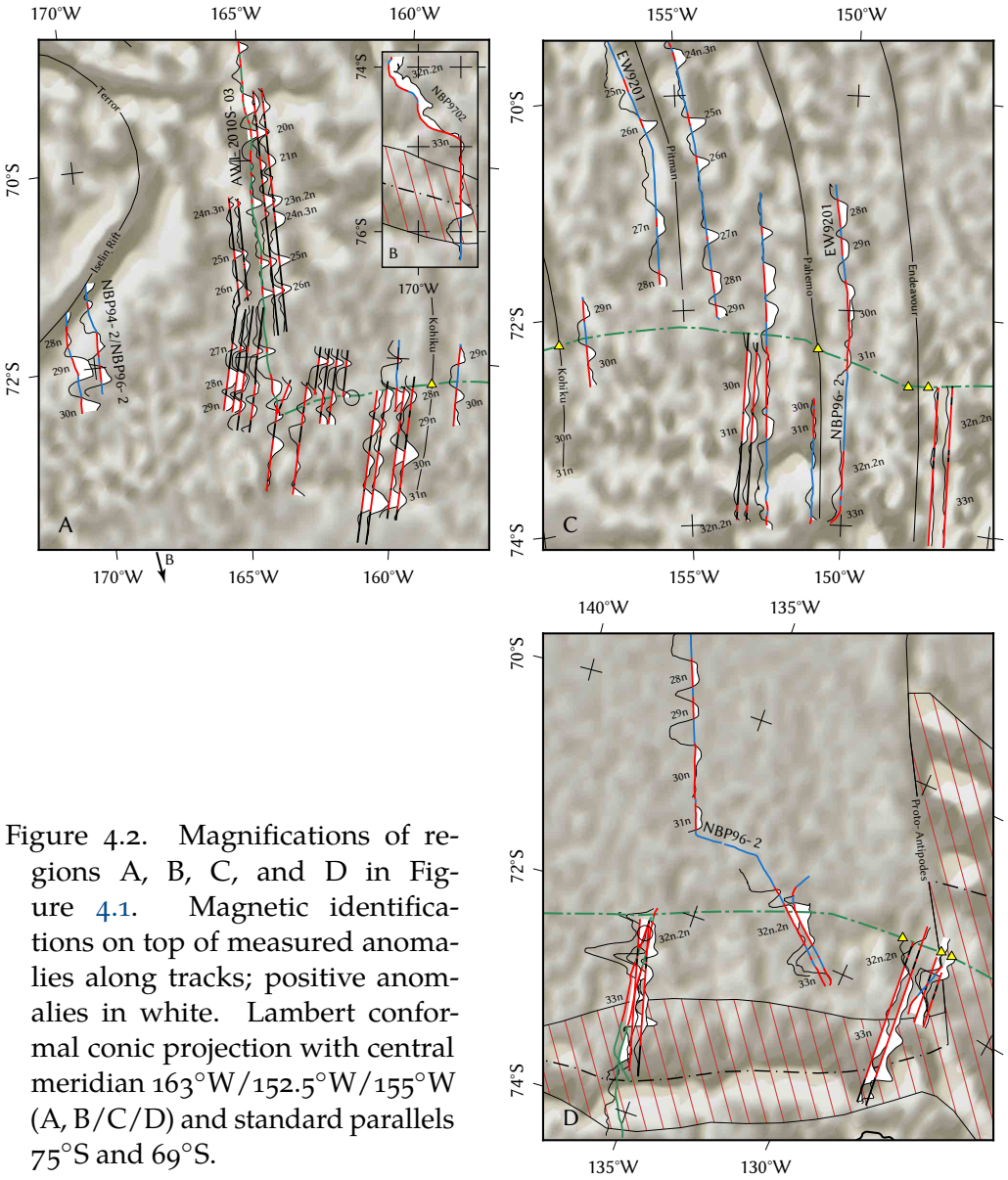

Figure 4.2. Magnifications of regions A, B, C, and D in Figure 4.1. Magnetic identifications on top of measured anomalies along tracks; positive anomalies in white. Lambert conformal conic projection with central meridian 163°W/152.5°W/155°W (A, B/C/D) and standard parallels 75°S and 69°S.

their influence when the vessel operates inside a radius of 500–1500 km around the location of the calibration loop.

The necessity for carrying out a new calibration loop was determined by comparing the calibrated data from the two separate magnetometer sensors. Once the difference between both increased steadily, the set of calibration coefficients was insufficient to compensate the magnetic readings (Gohl 2010).

Some magnetic profiles retained long wavelength residual anomalies after processing, possibly due to the high regional variation in the geomagnetic field and the large operating area. The long wavelength anomalies were removed by leveling the magnetic data of the ship to that measured by the air-borne magnetics. In areas without aeromagnetic profiles, a 500 km wide high-pass filter was applied.

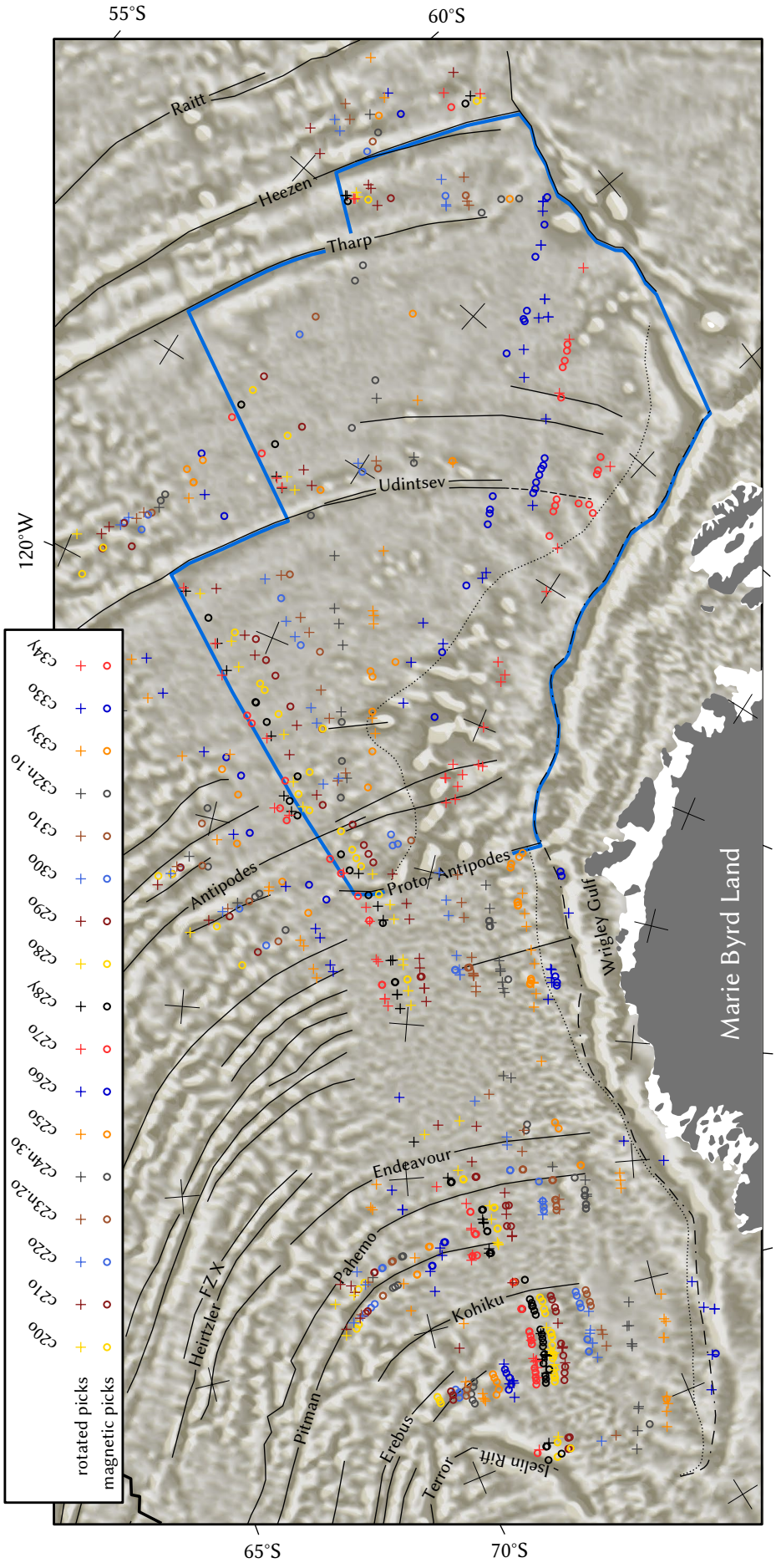

Figure 4.3. Compilation of magnetic picks on the West Antarctic and Bellingshausen plate, and rotated picks from the Pacific plate used for plate-tectonic reconstruction. Fracture zones (black lines); pre-rift suture (dashed line); COB (dotted line); and Bellingshausen plate (blue outline). Base map: DNSC08 satellite gravity (Andersen and Knudsen 2009), Lambert conformal conic projection with central meridian 145°W and standard parallels 72°S and 60°S.

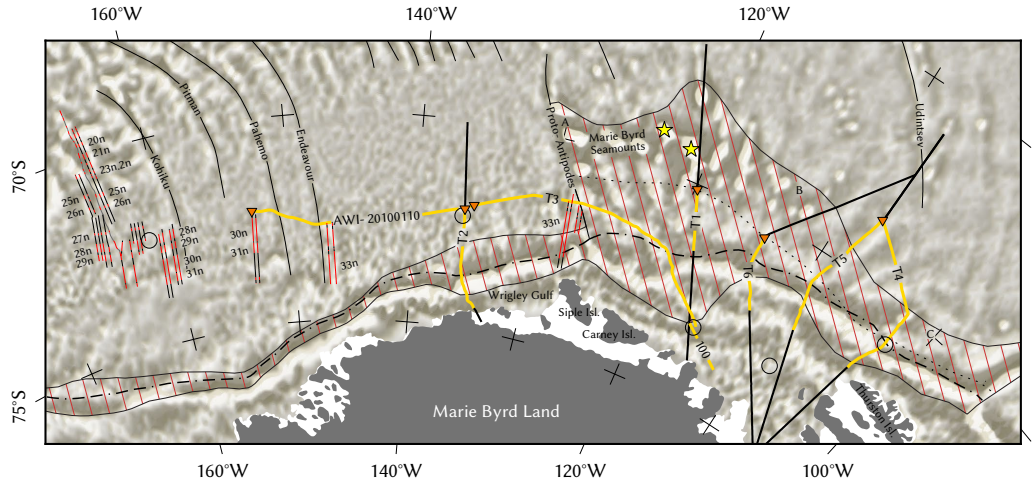

Figure 4.4. COTZ (striated) with reconstructed pre-rift suture (dashed line); calculated pre-rift suture, disregarding crustal addition (dotted line); seismic transects (thick yellow lines; 100 – AWI-20060100; T1 – AWI-20060200; T2 – AWI-20100111, AWI-20100112, AWI-20100113; T3 – AWI-20100117, AWI-20100118, AWI-20100119; T4 – AWI-20100126, AWI-20100129, AWI-20100130; T5 – AWI-20100131, AWI-20100132; T6 – AWI-20100139, AWI-20100140), and extensions (thick black lines); inverted triangles mark origin of each transect in Figure 4.5; identified magnetic spreading anomalies along ship profile ANT-2010S-03, and helicopter-magnetic lines (red – normal polarity, black – reversed); fracture zones (thin black lines); magnetic compensation loops (circles); A, B, C – see Figure 4.14; stars – locations of Haxby and Hubert Miller Seamount (from west to east). Base map: DNSC08 satellite gravity (Andersen and Knudsen 2009), Lambert conformal conic projection with central meridian 145°W and standard parallels 74°S and 66°S.

4.2.3 Shipborne gravity and seismic data

A gravity meter installed on-board measured the ambient gravitational field at 1 Hz during the ANT-23/4 and ANT-26/3 expeditions. The gravity readings were drift corrected via onshore reference measurements at the beginning of the cruise ANT-26/3 in Wellington Harbor, New Zealand, and at the end of the cruise in Punta Arenas, Chile (Gohl 2010). Gohl (2007) processed the gravity data of the cruise ANT-23/4 in the same manner. A median filter with a 5 km window size was applied to remove heave variability.

Deep crustal seismic refraction profiles, AWI-20060100 (Gohl et al. 2007b) and AWI-20060200 (Gohl 2007; Lindeque and Gohl 2010), acquired during the ANT-23/4 cruise in 2006, and a series of multichannel seismic reflection profiles, obtained during the ANT-26/3 cruise in 2010, lie within our study area (yellow lines in Figure 4.4). These seismic reflection profiles are currently being processed in-house (T. Kalberg, A. Lindeque, G. Uenzelmann-Neben, E. Weigelt, personal communication, 2011). The most relevant parameters for this study, basement depth, seafloor and total sediment thickness, were picked in two-way-travel time (TWT) from the preliminary single channel seismic data. The TWT values were converted

to depth (in km) using the sediment layer interval velocities from the finer AWI-20060200 P-wave refraction model (Lindeque and Gohl 2010), and velocities for the deeper crust were obtained from both the AWI-20060100 and AWI-20060200 models. The converted basement depths and total sediment thicknesses were incorporated in the gravity model.

4.3 MODELS

4.3.1 Magnetic modeling

The first step in our modeling was to identify the marine magnetic spreading anomalies along our profiles. This was done based on the methods and techniques of Vine and Matthews (1963). The synthetic spreading models were calculated using the open-source program MODMAG (Mendel et al. 2005), applying the geomagnetic polarity timescale of Gradstein et al. (2004). Two magnetic GEODAS profiles (Figure 4.1), EW9201 (R/V Maurice Ewing, 1992) and NBP96-2 (R/V Nathaniel B. Palmer, 1996), served as reference to tie the newly acquired aeromagnetic data to existing Pacific–Antarctic spreading models (Cande et al. 1995; Croon et al. 2008).

Helicopter- and ship-magnetic lines, obtained during the Polarstern cruise ANT-26/3, and GEODAS lines NBP94-2 and NBP9702, included in the existing model, increased the density of the magnetic spreading anomaly picks in the eastern Ross Sea and western Amundsen Sea. Figures 4.1–4.3 show the identified magnetic spreading anomalies from all available datasets (see electronic supplement for additional data).

4.3.2 Gravimetric modeling

Since refraction models in the area are sparsely distributed, gravity modeling was used to further estimate the crustal thickness, location of the continent–ocean boundary (COB) and width of the COTZ. We chose six transects from the continental shelf break to the abyssal plane, all approximately perpendicular to the continental shelf, so as to cross the potential COB and COTZ optimally (Figure 4.4). Lines reaching beyond the continental shelf were extended with satellite-derived gravity data (Andersen and Knudsen 2009), bathymetry data (Andersen and Knudsen 2009) and sediment thickness values (Scheuer et al. 2006a). The seafloor and basement depth, as well as total sediment thickness from the 2010 seismic reflection data, were imported in the gravity model as fixed layers. Where available, on-board gravity and echosound bathymetry data were used to supplement the seafloor picked in the single channel seismic data. The gravity response was then calculated by forward modeling using the method of Watts (1988); Watts and Fairhead (1999). We estimated densities of sedimentary rocks from P-wave velocities according to Gardner et al.

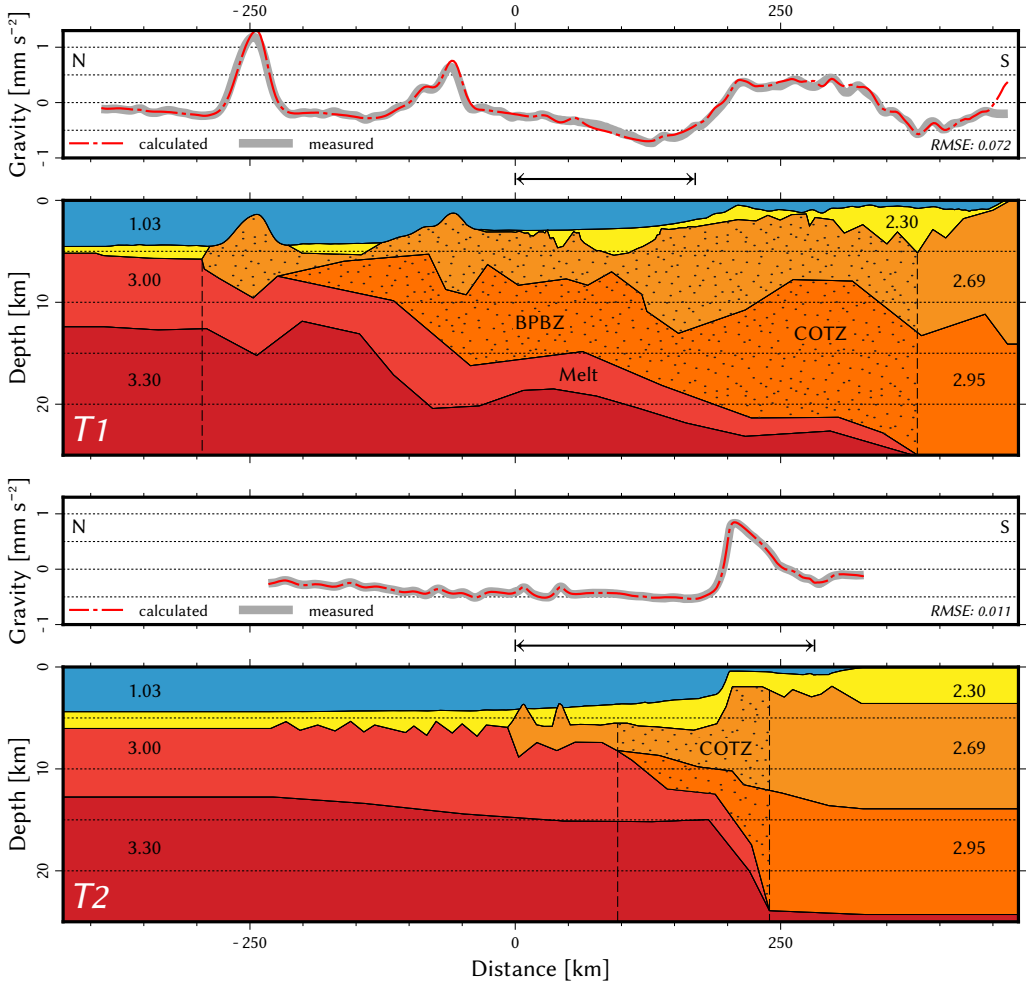

Figure 4.5. Crustal models along seismic transects T1 and T2 (locations on map in Figure 4.4). Numbers in the cross-section represent density (g cm^{-3}); stippled area indicates extended transitional crust/Bellingshausen Plate Boundary Zone (COTZ/BPBZ). Arrows indicate area covered by seismic transect. Transects T3 to T6 in electronic supplement.

(1974) and assumed uniform densities for the upper crust, the lower crust and the mantle on all transects to obtain crustal models. Then we created a start model that is similar to the deep crustal profile (T1) and tried to fit the measured gravity by altering the structure of the crust as little as possible. When the thickness of the sediments overlying the basement is known from seismics we did not change them. Fortunately, the geometry of the sediments and water column have the biggest influence on the gravity signal, so there is less freedom for fitting the underlying crust in the model.

The resulting gravity models (examples T1 and T2 in Figure 4.5) constrained the pre- and post-rift crustal thickness well, allowing us to assess the amount of continental deformation involved during the initial rifting process and subsequent Zealandia–Antarctica breakup.

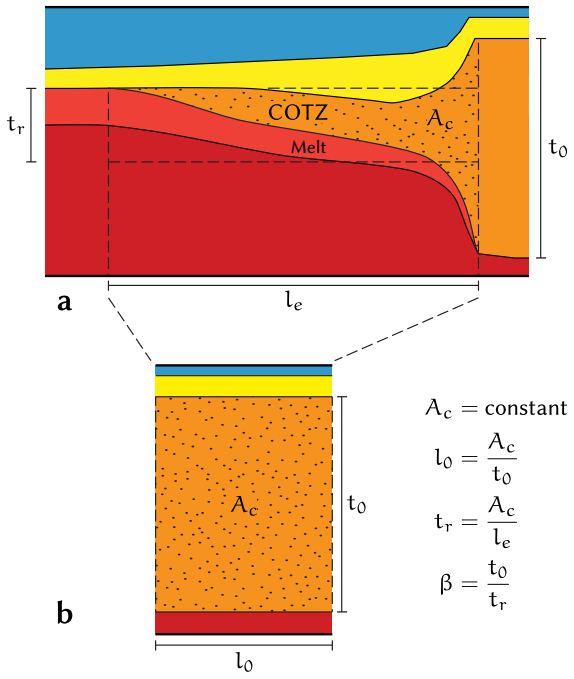

Figure 4.6. Determination of the COTZ width prior to rifting. (a) Extended transitional crust (stippled area) on passive continental margin from gravity inversion model (Figure 4.5). (b) Reconstruction of the stippled area in (a) before rifting. β – stretching factor; A_c/l_e – COTZ area/width; l_0 – pre-rift width of COTZ; t_0/t_r – initial/extended crustal thickness.

4.3.3 Continental deformation model

Our model considers deformation that is located in the COTZ (stippled area in Figure 4.6), an area, where the origin of the crust cannot be classified unequivocally as either continental or oceanic. In this zone, oceanic crust can be interleaved with segments of transitional crust, but the crustal thickness generally increases from its outer edge to the inner bound. Contrary, the amount of generated melt increases towards the outer edge, where the thickness of the oceanic crust equals the melt thickness.

In order to reconstruct the pre-rift shape of the Marie Byrd Land margin, we determined the width of the COTZ, l_e, and the crustal thickness prior to its extension, t_0, within each of the six seismic transects T1 to T6. We assumed volume constancy of the continental crust during deformation, and—reduced to a 2D profile—a continuous cross section area, A_c.

The aforementioned parameters permitted the calculation of the pre-rift width of the COTZ, l_0, the mean thickness of the extended crust, t_r, and the stretching factor, β, according to the equations in Figure 4.6. Both, t_r and β, are independent from the obliquity of the 2D section with respect to the COTZ, when a three-dimensional continuation of the geological units to either side of the 2D section is presumed. The areal extent of the COTZ, depicted in Figures 4.1 and 4.4, was estimated by interpolation between the seismic transects.

4.3.4 Plate-tectonic reconstruction

Visual fitting of picks of the magnetic spreading anomalies from Cande et al. (1995), Eagles et al. (2004b), and this study as well as fracture zone

traces using GPlates (Boyden et al. 2011) yielded new finite rotations (Figures 4.3 and 4.11, Table 4.2 in the supplement).

Occasionally, ambiguities in the magnetic identifications allowed for multiple rotation solutions. In these cases, we regarded the position of flow lines and fracture zones to be more trustworthy than the location of modeled magnetic isochrons and preferred a better fit of flow lines over that of magnetic isochrons. Fracture zones were digitized from seismic lines and satellite gravity data. Lateral shifts of magnetic identifications in adjacent profiles further constrained fracture zone traces that are not apparent as flow lines in the gravity data.

Whenever magnetic data were unavailable due to the Cretaceous Normal Superchron (84–125 Myr) or tectonic/magmatic overprinting, we attempted to determine the finite rotation pole by extrapolating spreading rates from the oldest distinguishable chron back to the margin. For this we assumed that spreading rates were constant during the Cretaceous Normal Superchron and resembled the rate that was determined at c34y (84 Myr). In some cases, it was possible to estimate the spreading rate directly from existing spreading anomalies on the conjugate margin assuming identical half-spreading rates. The pre-rift reconstruction of Marie Byrd Land, Chatham Rise, and Campbell Plateau originated from the fit of the pre-rift sutures of the continental margins at 90 Myr.

4.4 DATA ANALYSIS AND DISCUSSION

4.4.1 Crustal model

The crustal models (Figure 4.5), obtained from gravity inversion along seismic transects T1 to T6 (Figure 4.4), image an uneven basement, covered by sediments up to 2.8 km thick. If we compare the top-of-basement of Grobys et al. (2009) with our crustal models, we observe a 1 km elevation difference between Zealandia and Marie Byrd Land, consistent with the findings of Sutherland et al. (2010). The Moho depth varies around 24 km, and the lower crust is generally 10 km thick.

Two representative crustal models along the seismic transects T1 and T2 are displayed in Figure 4.5. The models consist of five layers—sedimentary cover (2.3 g cm^{-3}), upper crust (2.69 g cm^{-3}), lower crust (2.95 g cm^{-3}), melt addition/oceanic crust (3.0 g cm^{-3}), and mantle (3.3 g cm^{-3})—whose densities and thicknesses were obtained from the velocity–depth model.

Apart from slight deviations, the gravity-derived crustal model of transect T1 reflects the observations from the velocity–depth model: Crust with a low density, but anomalously large thickness extends seaward of the continental slope. The Moho and the boundary between upper and lower crust rise gradually towards the shelf, and the gravity anomaly describes the rugged topography of the upper crust and the Marie Byrd

Seamounts. The upper part of the submarine volcanoes consists of material with approximately equal density as the upper crust. Subsidence of the transitional crust and subsequent formation of small sediment basins increase the distance of the denser material to the surface and generate negative gravity anomalies.

By contrast, transect T2, which lies west of the Marie Byrd Seamounts, displays an elongated positive free-air gravity anomaly aligned with the Moho step. This anomaly is caused by gravimetric superposition of the Moho step with the bathymetric step of the steep continental slope and some minor sedimentary effect. The gravity high is followed by a less pronounced landward low close to the shelf that trends subparallel to shelf edge. Comparable elongate gravity anomalies are considered commonly associated with Atlantic-type passive continental margins (Watts 1988; Watts and Fairhead 1999). Unlike T1, the transition from thick continental crust to thin oceanic crust is abrupt with the Moho raising about 8 km. The sedimentary cover reaches thicknesses of up to 4 km.

Transects T3 to T6 (see electronic supplement) are more similar to transect T1 than to T2. The former transects feature an equally thick low-density crust extending far from the slope. The free-air anomaly, also similar to that in the transect T1, indicates the same rugged crust topography and sedimentary cover. Compared to the cross sections further west, transects T4 and T5 are characterized by increased amounts of sediments (3–4 km) on the slope. We observed a small but distinct increase of the upper crust thickness, where transect T3 crosses the Proto-Antipodes Fracture Zone.

Except for the central part of transect T1, which is covered by the velocity–depth model, the gravity models are based only on reflection seismic data. This leads to lower confidence on sediment thickness estimates due to poorly constrained interval velocity, as well as a lack of information about basement properties. However, variations of sediment and basement properties within commonly-accepted bounds would not be enough to explain the gravity field differences between the transects. Hence, we expect the effects of these uncertainties on the determination of the crustal thickness, COTZ, and β-factors to be small.

We can distinguish between the Marie Byrd Land sector with a sharp transition in the free-air anomaly and a narrow COTZ, and the extremely wide Bellingshausen Plate Boundary Zone (BPBZ). The Marie Byrd Land margin best compares to magma-poor passive continental margins in the central South Atlantic, e.g., the Brazilian Espírito Santo margin and conjugate North Angolan margin (Blaich et al. 2011; Huismans and Beaumont 2011). Despite the uncertainties in the crustal models, several features support this classification: There are no indications of syn-rift magmatism like oceanic seaward dipping reflectors or anomalously high P-wave velocities within the transitional crust. Instead, seismic velocities of the lower crust (Gohl et al. 2007b; Gohl 2007; Lindeque and Gohl 2010) are consistent with magmatic underplating. Throughout the entire Marie Byrd Land margin, we observed a wide region of thinned transitional crust of low

density. Sedimentation patterns in the seismic image of line AWI-20100110 reveal sedimentation patterns of a type similar to those observed off the southeastern Brazil–Angola margin (A. Lindeque, personal communication, 2011). Unlike the Marie Byrd Land sector, the Bellingshausen sector is unique in that it was subject to ongoing deformation and volcanism after breakup. This is further discussed in Section 4.4.5.3.

Close to the Antarctic shelf—where thick sediment layers attenuate the gravity signal of the basement—flow lines, indicating fracture zones, cannot be traced anymore. On the seismic image of line AWI-20100110, the basement reflectors are discontinuous and show a vertical offset of 0.2–0.3 s TWT. These features are interpreted as spatially coincident fracture zones, which are also evident in the bathymetry [*Lindeque*, 2011, personal communication], and correspond to the magnetic anomaly signatures in our study (Figure 4.4). The seismic transect and observed shifts in the magnetic pattern between parallel magnetic profiles along the Kohiku Fracture Zone support the proposed position and extend the fracture zone interpretation further south. We further constrained the locations of Pahemo and Endeavour Fracture Zones at their southern tips from seismics and magnetic spreading anomalies (Figure 4.1).

4.4.2 Continental extension of Marie Byrd Land

We identified domains of transitional crust, illustrated as stippled areas in the cross-sections in Figure 4.5, along each of the six crustal models T1 to T6. Consequently, the area representing the present-day COTZ was determined by interpolation between the transects (striped area in Figure 4.4). We derived the parameters A_c, t_o, t_r and l_e from the cross-sections and calculated the (along-profile) pre-rift width of the COTZ, the pre-rift suture as well as the amount of continental stretching and the associated stretching factors (β) according to the scheme in Figure 4.6. The results, summarized in Table 4.1 and Figure 4.4, indicate a strong regional variation of the COTZ width. The width of the COTZ steps from 50–130 km west of the Proto-Antipodes Fracture Zone to more than 650 km east of that fracture zone. By contrast, the stretching factors remain low to moderate (1.8–3.5) on the entire Marie Byrd Land margin.

We determined the amount of generated melt along the transects to obtain unbiased β-factors by fitting the gravity anomalies with an extra underplate layer. This layer gradually increases in thickness from its inner (continental) bound to the outer (oceanic) side, where it eventually transforms into oceanic crust. There is not much room for big melt thickness and initial crustal volume variability in fitting transect T2 so that we can assume a constant volume of the deformed crust. The estimation of added material due to volcanism in the Marie Byrd Seamount province remains speculative with the available data. Therefore, fitting Chatham

Table 4.1. COTZ properties of the Marie Byrd Seamount province along seismic transects (Figure 4.4).

No.	β-Factor	COTZ width	Cont. stretching
T1	1.83	670 km	304 km
T2	2.62	145 km	90 km
T3	—	—	—
T4	1.89	225 km	106 km
T5	3.55	220 km	158 km
T6	3.12	345 km	234 km

Rise to Marie Byrd Land can only be attempted via the plate circuit West Antarctica–Campbell Plateau–Chatham Rise–Bellingshausen plate.

The initial crustal thickness of 20–24 km for Marie Byrd Land is equivalent to the thickness of the submarine plateaus of Zealandia (Grobys et al. 2009, and references therein). Further, the crustal thickness model of Grobys et al. (2008) suggests a mean COTZ width of 100 km for the Campbell Plateau and Chatham Rise. Although these widths are similar to those on the western Marie Byrd Land margin, they differ much from those of the eastern part of Marie Byrd Land, which raises the question whether extensive continental stretching was associated with rifting only (see Section 4.4.5.3).

4.4.3 Age and spreading model

We identified magnetic spreading anomalies along 44 helicopter- and ship-magnetic profiles in the eastern Ross Sea (Figures 4.1–4.3). Both data sources show clearly identifiable seafloor spreading anomalies with similar amplitudes (Figure 4.16), even though the shipborne data are preprocessed more aggressively.

The oldest identified magnetic spreading anomaly, c33n (73.6–79.5 Myr), occurs in several locations in the Ross Sea, the Wrigley Gulf and to the west of the Marie Byrd Seamounts/Proto-Antipodes Fracture Zone (Figure 4.1). A reversed magnetic anomaly occurs south of c33n. Based on its proximity and location within the COTZ, it is more likely to be of continental origin than a c33r magnetic seafloor spreading anomaly.

The spreading model in Figure 4.15 suggests a half-spreading rate of about 30 mm yr^{-1} along the Pahemo Fracture Zone during c32n.2n (72 Myr). Later, the spreading rate increased up to 37 mm yr^{-1}, where it peaked around chron c27n, and steadily decreased to 11 mm yr^{-1} between chrons c26n and c22n. Further west, the spreading rate was slower by about 10 mm yr^{-1} (Figure 4.16).

4.4.4 Fitting fracture zones

Fracture zones and flow lines in the South Pacific (Figures 4.3 and 4.11) are essential constraints for the lateral alignment of conjugate plates in the plate-tectonic reconstruction (Figures 4.7 and 4.12). Although fracture zones prior to 43 Myr are explained well by synthetic flow lines derived from the models of Cande et al. (1995); Larter et al. (2002); Eagles et al. (2004a), the fit of older fracture zones of conjugate plates is not ideal. There are particularly large model differences during the initial rifting phase between Zealandia and Marie Byrd Land. We suspect this to be due to fitting unreliable or not well constrained magnetic isochrons using the Hellinger (1981) criteria (Cande et al. 1995; Larter et al. 2002). In this study, we improved the plate-tectonic reconstruction by visually fitting magnetic picks and fracture zones while ensuring that the model would be geologically sound (Figures 4.3 and 4.12).

Fracture zones, as observed in satellite gravity, are generally 10 km wide and have clearly defined boundaries in the gravity signal. We assume that we can achieve an accuracy of about 2 km if we take care to digitize the same boundary or the centerline on both conjugate plates. As there are many parallel fracture zones along the margin, these errors average out in the end. We determined the offsets between conjugate fracture zone segments in the Ross Sea sector using the rotation poles of Eagles et al. (2004a), and compared these results to the offsets in our model. We obtained a general misfit of considerably less than 5 km, whereas offsets as large as 60 km occur in the former model.

4.4.5 Plate-tectonic reconstruction

In Figure 4.7, we present the key frames of the improved plate-tectonic reconstruction of the conjugate Marie Byrd Land and Zealandia margins. Croon et al. (2008) refined the Pacific–Antarctic plate rotations of previous studies by Cande et al. (1995); Cande and Stock (2004); Eagles et al. (2004a), however, their model does not include rotations prior to c200 (43 Myr). Here, we focus on the evolution of Marie Byrd Land and Zealandia beyond that point. An animated video included in the electronic supplement shows the deduced plate movements, which could be divided into the following major phases of plate reorganizations:

90–84 Myr (c34n) Onset of continental extension; Chatham Rise separated from Marie Byrd Land as a fragment of Zealandia with a velocity of 30–40 mm yr^{-1}. Rifting started in the Amundsen Sea, where the oldest seafloor spreading anomalies (c34y) are observed, and then propagated west.

84–80 Myr (c33r) Zealandia and Marie Byrd Land initially rotated about a pole located in Wilkes Land; spreading propagates into the Ross Sea.

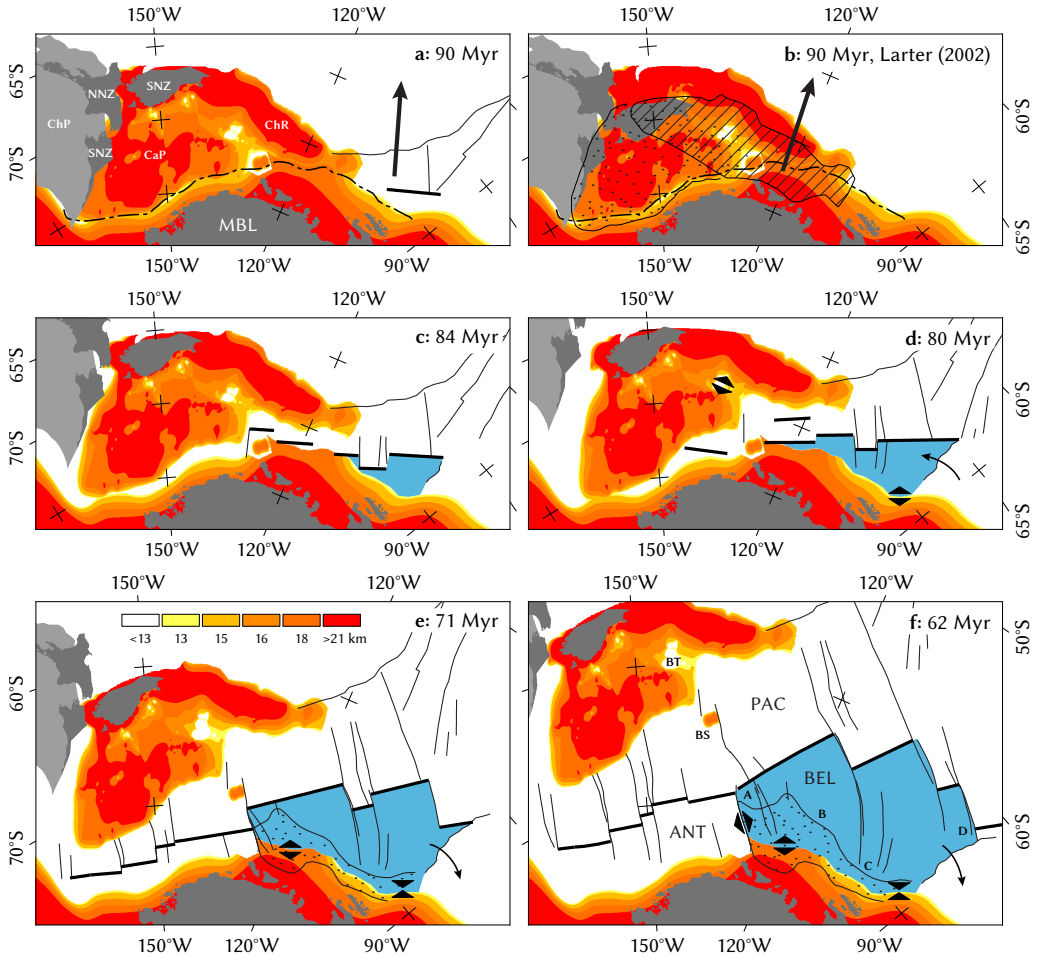

Figure 4.7. Pre-rift reconstruction models of Marie Byrd Land, Chatham Rise, and Campbell Plateau using finite rotations of this study and from Grobys et al. (2008) (a, c–f), and using rotation parameters from Larter et al. (2002); Eagles et al. (2004a) (b). Chatham Rise (striated), Campbell Plateau (stippled), and Marie Byrd Land overlap the pre-rift suture (dashed line) from this study. Arrows indicate initial plate motion direction of Pacific plate/Chatham Rise. Plate-tectonic reconstruction models of Zealandia, Marie Byrd Land, and Bellingshausen plate (c–f) at magnetic chrons c34y (84 Myr), c33o (80 Myr), c32n.1o (71 Myr), and c27o (62 Myr). The Bellingshausen plate (blue) moved independently from the Antarctic plate between c34y and c27o (small arrows). Oceanic crust formed along the southern Bellingshausen plate margin (c/d) was later deformed (BPBZ, stippled area, e/f). The tectonic regime in the BPBZ and Bounty Trough is illustrated by arrowheads pointing towards (convergent) and away (divergent) from each other. The Bollons Seamount was transferred from the West Antarctic to the Pacific plate around c33o. The rotation between Chatham Rise and Campbell Plateau occurred during chron c33n. Parallel spreading centers at 120°W (d) represent ridge jumps. Thin black lines – fracture zones, thick black lines – mid-ocean ridge segments; ANT – West Antarctic plate, BEL – Bellingshausen plate, BS – Bollons Seamount, BT – Bounty Trough, CaP – Campbell Plateau, ChP – Challenger Plateau, ChR – Chatham Rise, MBL – Marie Byrd Land, NNZ – North Island of New Zealand, PAC – Pacific plate, SNZ – South Island; A, B, C, D – see Figure 4.14. Base map: crustal thickness of Zealandia (Grobys et al. 2008) and Antarctica, Lambert conformal conic projection with central meridian 145°W and standard parallels 72°S and 60°S.

84–62 Myr (c33r–c27r) The Bellingshausen plate moved as an independent plate for about 22 Myr. During this time, the southern plate boundary was subject to extensive transtension located in an up to 670 km wide deformation zone.

80–74 Myr (c33n) The Campbell Plateau and Chatham Rise rotated against each other and the Bounty Trough was opened. The Bollons Seamount was transferred to the southeastern plate boundary of the Campbell Plateau. The lateral displacement between Marie Byrd Land, Campbell Plateau and Chatham Rise was shifted from the Bollons transform fault west of Bollons Seamount to the Proto-Antipodes Fracture Zone. Plate motion velocities between Marie Byrd Land and Zealandia ranged from 50 (west of the Proto-Antipodes Fracture Zone) to 80 mm yr^{-1} (east of the Proto-Antipodes Fracture Zone). The tectonic regime in the Ross Sea changed from transtension to extension, and first fracture zones were formed.

74–62 Myr (c32r.2r–c27r) The rotation between Campbell Plateau and Chatham Rise ceased, and the Pacific–Antarctic separation velocity decreased to 55–70 mm yr^{-1}. The rotation of the Bellingshausen plate shifted from counterclockwise to clockwise (Figure 4.14), causing a characteristic curve in the trace of the Udintsev Fracture Zone and the Eltanin Fault System. Eventually, the independent motion of the Bellingshausen plate stopped around 62 Myr, and the plate became fixed to the West Antarctic plate.

71–69 Myr (c31r) The traces of the Pahemo, Endeavour, and Kohiku Fracture Zones begin to bend left in direction from the Ross Sea towards the spreading center, indicating a slight shift of the Pacific plate motion direction. The Bollons Seamount passed the northern tip of the Proto-Antipodes Fracture Zone during the same time, and the overall spreading velocity decreased by about 10 mm yr^{-1}.

62–45 Myr (c26r–c21n) Following the end of the independent Bellingshausen plate movement, full-spreading rates constantly decreased from 60–70 mm yr^{-1} to 30–40 mm yr^{-1}.

45–42 Myr (c20r–c20n) For a short period, the rotation pole between the West Antarctic and Pacific plates moved into the Ross Sea (163° 49.8'W, 71°17.4'S) and initiated a 3.5° counterclockwise rotation of the Pacific plate relative to West Antarctica in only 3.8 Myr.

4.4.5.1 Estimation of breakup time

The time of onset of the COTZ formation is not constrained by our observations, but we interpret the margin west of the Proto-Antipodes Fracture Zone as forming during c33r and the end of c33n (79.5 Myr). Supporting

our interpretation, Siddoway et al. (2004) relate a rapid cooling event during 80–71 Myr—recorded by apatite fission-track ages of samples from the Cape Colbeck region in the Eastern Ross Sea—to denudation associated with the breakup of Campbell Plateau from Marie Byrd Land.

Breakup time estimates in the range of 105–81 Myr in earlier works (e.g., Molnar et al. 1975; Cande et al. 1995; Luyendyk 1995; Larter et al. 2002; Stock and Cande 2002; Cande and Stock 2004; Eagles et al. 2004a) are based on paleomagnetic data or extrapolation of spreading rates back into the Cretaceous Normal Superchron (c34n). Without the benefit of dated samples from the margin or magnetic anomalies of the appropriate age, the onset of COTZ formation and the initial rate of COTZ deformation are basically unknown, but likely fall within a certain range of possibilities.

The new magnetic data we collected in vicinity of the Proto-Antipodes Fracture Zone indicates that Chatham Rise and Campbell Plateau separated from Marie Byrd Land with a velocity of 30–40 mm yr^{-1} during chron c33r (79.5–84 Myr). These velocities also match spreading rates based upon extrapolation beyond the oldest chrons detected along the margin west of the Proto-Antipodes Fracture Zone. Taking into account the continental deformation (~90 km extension along the margin of Campbell Plateau and Marie Byrd Land) during breakup and assuming a constant spreading rate during chrons c33r and c34n, a close fit of the modeled pre-rift suture between Zealandia and West Antarctica is reached at about 89 Myr. Subduction of the Hikurangi Plateau beneath the Chatham Rise stopped around 96 Myr (Davy et al. 2008). Aside from maybe back-arc extension before that time, we consider this to be the earliest possible onset of the Zealandia–Antarctic rifting with an implied minimal plate motion velocity of 14 mm yr^{-1} during the rifting phase.

Numeric lithosphere extension models suggest that the rifting time—before continental breakup occurs—is a function of extension velocity (van Wijk and Cloetingh 2002). For rapid breakup times (in this case 5–12 Myr with an initial extension between 96 and 89 Myr), their models predict extension rates of more than 30 mm yr^{-1}. Although the crustal thickness of the modeled crust is greater than that of the Marie Byrd Land margin and the rheology of the latter is unknown, which could alter the relationship between rifting time and extension velocity, we nevertheless attempted to estimate the breakup time based on the data of van Wijk and Cloetingh (2002). In our reconstruction, a late extension (starting at 90 Myr and with a separation velocity of >30 mm yr^{-1}) as opposed to an earlier extension (at 96 Myr with a slower velocity of about 14 mm yr^{-1}) fits the van Wijk and Cloetingh (2002) model better.

4.4.5.2 Early breakup and opening of Bounty Trough

New evaluation of continental extension on the Marie Byrd Land margin in this study and the crustal thickness model of Grobys et al. (2008) have enabled numerous improvements to the reconstruction of the early

Zealandia–Marie Byrd Land breakup history. Also they provided answers to open questions and voids of previous studies that originated from a lack of constraints regarding the dynamics of the plate margins.

Unresolved issues remaining in previous reconstructions include:

- The rotation of Chatham Rise with respect to Campbell Plateau by Larter et al. (2002) causes a 350 km wide overlap because the extend of the COTZ on both margins was underestimated. This close fit reconstruction of Marie Byrd Land and Chatham Rise introduces an overlap of the latter with the continental shelf of Marie Byrd Land as far as Siple and Camey Islands (Figure 4.7b). Further, the Bollons Seamount is traversed by Chatham Rise, and the southwest margin of Campbell Plateau overlaps the continental shelf of the West Antarctic Plate by about 100 km. A compression of this dimension cannot be explained by our continental deformation model, since the transitional crust of the continental shelf of Marie Byrd Land, the crust of the Bounty Trough, and its adjacent plateaus (Grobys et al. 2008) is relatively thick (low β-factors).

- Davy et al. (2008) interpreted the cessation of subduction of the Hikurangi Plateau beneath the Chatham Rise at about 96 Myr, followed by a switch in the tectonic regime in New Zealand from northeast to northwest directed extension, which Davy et al. (2008) construed to be parallel to the breakup orientation. The southern branches of Udintsev and adjacent Fracture Zones further east (Figures 4.3 and 4.11) strike northwest–southeast, thus confirming a northwest directed separation of Chatham Rise from Marie Byrd Land. Larter et al. (2002); Eagles et al. (2004a) suggest a north by west directed initial movement of Chatham Rise (90–84 Myr, arrow in Figure 4.13 and supporting animation) which is oblique to the fracture zones and contradicts the interpretation of Davy et al. (2008).

Our updated plate reconstruction, based on the location of the pre-rift suture between Marie Byrd Land, Chatham Rise, and Campbell Plateau, ensures that there are no or only minor overlaps between Marie Byrd Land and Zealandia as well as Chatham Rise and Campbell Plateau. Further drawbacks of previous reconstructions were circumvented in this study by first rotating Zealandia with respect to Marie Byrd Land and then rotating Chatham Rise with respect to Campbell Plateau in a separate step, after the Bollons Seamount was transferred to the margin of the Campbell Plateau at about 80 Myr. This allowed a fit of the conjugate ends of the Udintsev Fracture Zone as well as adjacent fracture zones further east and guaranteed a northwest directed extension in New Zealand.

The plate-tectonic reconstruction of Zealandia (Grobys et al. 2008) does not constrain the time and duration of the rotation between Chatham Rise and Campbell Plateau. However, a rotation is not possible prior to chron c33n without introducing a cycle of rapid extension followed by

compression along the southern boundary of the Bellingshausen plate (see animations in electronic supplement). Furthermore, the reliability of the c34y identifications in the Bounty Trough area is questionable (Davy 2006). Rifting on the northern Campbell Plateau was complete by 84 Myr (Cook et al. 1999), but the age of cessation of rifting is unconstrained for the Bounty Platform or southern Campbell Plateau. Sutherland (1999) suggests that a ridge may have existed during c33n in the outer part of the Bounty Trough and then jumped southward. By initiating the rotation between Chatham Rise and Campbell Plateau during chron c33n (as opposed to c34n, Larter et al. 2002), we can fit c33o south of Bollons Seamount while minimizing the Bellingshausen plate motion relative to Marie Byrd Land at the same time. This implies that until c33y, when the Chatham Rise vs. Campbell Plateau rotation ceased, the Proto-Antipodes Fracture Zone separated two independent spreading centers (Antarctic–Pacific and Antarctic–Campbell Plateau).

4.4.5.3 Transitional crust of the Bellingshausen plate

In Section 4.4.2, we concluded that pre-rift crustal thicknesses of Marie Byrd Land, Campbell Plateau, and Chatham Rise were alike. Moreover, the width of the COTZ of west Marie Byrd Land, Campbell Plateau, and Chatham Rise were uniform, whereas the BPBZ is three to five times wider (Figures 4.4 and 4.5; Table 4.1). Because the opening of the Amundsen Sea and Ross Sea propagated from east to west, leading to lower spreading velocities in the west and increasing the potential of basin propagation (van Wijk and Cloetingh 2002), we should expect a widening of the COTZ towards the Ross Sea. By contrast, we observed a narrow COTZ west of the Bellingshausen sector.

There are several indicators implying that the extensive continental stretching between Chatham Rise and east Marie Byrd Land was not associated with the initial rifting alone, but instead developed partly after their separation:

- Alkali basalt samples, dredged from Haxby Seamount and Hubert Miller Seamount (Figure 4.4) yield $^{40}Ar/^{39}Ar$ ages ranging from 64.73 ± 0.84 to 55.72 ± 0.63 Myr (Kipf et al. 2008, 2013). This dating clearly marks the end of the independent Bellingshausen plate movement and is too young to be associated with the rifting between Zealandia and Marie Byrd Land.

- We determined an extension velocity of >30 mm yr^{-1} (Section 4.4.5.1) associated with a short rifting time. Continental deformation along the Campbell Plateau and western Marie Byrd Land margin ceased in less than 10 Myr, and lithosphere extension models (van Wijk and Cloetingh 2002) suggest that deformation should have stopped in eastern Marie Byrd Land as well.

- Magnetic spreading anomalies c34n, c33r, and partly c33n cannot be detected on the central Marie Byrd Land margin (Figure 4.3), although they exist on the conjugate margin (Chatham Rise). It is likely that oceanic crust formed on the Marie Byrd Land side as well and transformed later on.

We propose that the complete Marie Byrd Land margin developed similar to the conjugate margin of Zealandia during the initial separation. Rifting between Chatham Rise and Marie Byrd Land stopped before c34y (84 Myr), and, consequently, oceanic crust formed in the Amundsen Sea. Most of this oceanic crust, generated on the Bellingshausen plate margin until the end of chron c33r, was either magmatically altered or tectonically interleaved with transitional crust at a 1:1 ratio.

The Bellingshausen plate moved independently of the West Antarctic plate for about 22 Myr since c34y. Its plate motion trajectories indicate an overall plate drift to the northeast with respect to Marie Byrd Land and a velocity varying from 3 to 36 mm yr^{-1} with a peak around 9 mm yr^{-1} (Figure 4.14). The southern and western border of the Bellingshausen plate were subject to a 8–14 mm yr^{-1} dextral motion relative to Marie Byrd Land and subparallel to its plate boundary.

First counterclockwise, then clockwise rotation of the Bellingshausen plate caused a tectonic regime of alternating convergence and extension west of the balance point B (Figures 4.7 and 4.14) and vice versa east of it. This is supported by previous studies by Cunningham et al. (2002); Larter et al. (2002); Eagles et al. (2004b), who interpreted the Bellingshausen Gravity Anomaly (southeast of point C) and the continental margin off Thurston Island as zone of accommodated convergent motion between the Bellingshausen and West Antarctic plates. Seamounts occur en echelon along the southern plate boundary of the Bellingshausen plate near point A. Their strike is approximately northeast–southwest directed and perpendicular to the motion path of A during the second half of the existence of the autonomous Bellingshausen plate. The clockwise rotation, the strike of the seamount chains and the dated sample from Hubert Miller Seamount are indicators that the seamounts formed during the end of the independent Bellingshausen plate movement (65–55 Myr).

Traditionally, the chemistry signal (Kipf et al. 2008, 2013), increased crustal thickness (Figure 4.5), local highs in the gravity field, and disrupted magnetic signature were used as indicators to suggest intraplate volcanism as a simple solution to account for the transitional crust in the Bellingshausen plate (e.g., Storey et al. 1999). Our data, the geochemical signature, and the age of the Marie Byrd Seamounts (Kipf et al. 2008, 2013) indicate that the Bellingshausen plate motion preceded intraplate volcanism. The tectonic setting at the time the seamounts formed indicates an enriched mantle source (Halliday et al. 1995; Pilet et al. 2008), which released melts through fissures created by lithospheric extension on the southern Bellingshausen plate margin. Fertilization of the mantle could

either be explained by Mesozoic subduction beneath the Gondwana convergent margin or by metasomatism of the lithospheric mantle through fractures in the weakened Bellingshausen plate.

Especially during chron c33r (79.5–84 Myr) and at the end of the existence of the plate, there was very little movement relative to Marie Byrd Land. Lithosphere extension models show that rifting velocities lower than 8 mm yr^{-1} do not lead to seafloor spreading because the lithosphere in the formed basin cools and becomes stronger than in the surrounding regions (van Wijk and Cloetingh 2002). Consequently, the deformation zone migrates and the process repeats itself, forming a wide COTZ. We assume, a similar process, combined with oscillating transpression and transtension along the Bellingshausen plate margin, lead to the formation of an up to 670 km wide zone of transitional crust interleaved with segments of oceanic crust (BPBZ, in Figure 4.5). The deformation was intense enough to annihilate signs of oceanic crust such as magnetic seafloor spreading anomalies.

4.5 SUMMARY

We present and analyse an extensive new dataset of air- and shipborne geophysical measurements acquired during R/V Polarstern cruises in 2006 (ANT-23/4) and 2010 (ANT-26/3) at the rifted oceanic margin of Antarctica in the eastern Ross Sea and Bellingshausen Sea. We construct models of seafloor magnetic anomalies to interpret oceanic age, and models of the continental margin crust that are constrained by active-source seismic reflection and refraction data as well as gravity data. We subdivide the continental margin into two sectors divided by the Proto-Antipodes Fracture Zone (Figure 4.4).

The western sector of the continental margin, the Marie Byrd Land sector, has a relatively narrow steep slope and resembles a typical magma-poor margin. The width of the COTZ on our modeled transect is 145 km, which we interpret—based on our crustal model—to represent an initial continental crust of thickness 24 km and width 55 km. It was stretched 90 km and intruded at its base by melt, eventually transitioning to normal-thickness oceanic crust (~7 km, White et al. 1992) at its seaward limit.

The eastern sector of the continental margin, the Bellingshausen sector, is broad and complex with abundant morphologic evidence for later volcanism, confirmed by dredging (Kipf et al. 2008). The widths of the COTZ/BPBZ on our modeled transects are up to 670 km, and substantial uncertainty remains as to the nature of the crust within the COTZ/BPBZ because we have little control on crustal thickness or density. Our preferred interpretation is that some stretched continental crust is present throughout this zone, but that it has been substantially added to by basaltic

igneous rocks (density 3.0±0.1 g cm^{-3}). The extension estimates fall in the range of 106–304 km for the COTZ/BPBZ (Table 4.1).

We identify seafloor magnetic anomalies c33n (79.5 Myr) to c20n (42 Myr) on a number of transects adjacent to the Marie Byrd Land sector (Figures 4.1–4.3). The Bellingshausen sector is too complex and sparsely sampled for us to reliably interpret magnetic anomalies as isochrons. At the longitude of the Pahemo Fracture Zone, in the central part of the Marie Byrd Land sector, the full-spreading rate during chrons 33–31 (80–68 Myr) was 60 mm yr^{-1}, increasing to a maximum of 74 mm yr^{-1} at chron 27, and then dropping to 22 mm yr^{-1} by chron 22. Spreading rates generally decrease westward. Based upon extrapolation towards the continental margin, we estimate that initial oceanic crust formation in the Bellingshausen sector was at approximately chron 34y (84 Myr) and that it formed rapidly. West of the Proto-Antipodes Fracture Zone, seafloor spreading initiated at chron 33n (79.5 Myr). At rates of 30–60 mm yr^{-1}, the 90 km of inferred extension could be achieved in 1.5 to 3.0 Myr.

We construct an improved set of plate reconstructions utilizing our updated analysis of the Antarctic continental margin to place our local interpretations of Antarctica in context. From these we make inferences regarding the general sequence of events during inception of seafloor spreading, and calculate the subsequent motion history of the Bellingshausen plate, which is the oceanic plate adjacent to the Bellingshausen sector of the continental margin (see supplement). Our preferred interpretation is that the tipline of the spreading ridge and hence initial seafloor formation propagated westward between ~89 and 84 Myr. Subsequent motion of the Bellingshausen plate relative to Antarctica was at rates <40 mm yr^{-1} and was most commonly 5–20 mm yr^{-1}. Although we have not attempted a quantitative uncertainty analysis, our predictions that motion direction and rate varied spatially and temporally and involved both local compression and extension are supported by local geology and geophysics (e.g., Cunningham et al. 2002; Larter et al. 2002; Gohl et al. 2011; Gohl 2012).

Our new data and interpretations are generally consistent with previous analyses that indicate Gondwana breakup along this part of the margin was at ~84 Myr, and there was subsequent formation of the Bellingshausen plate east of the Proto-Antipodes Fracture Zone (Molnar et al. 1975; Stock and Molnar 1987; Cande et al. 1995; Larter et al. 2002; Stock and Cande 2002; Cande and Stock 2004; Eagles et al. 2004a, b). The relatively high rifting rate of 30–60 mm yr^{-1} during initial margin formation is consistent with the relatively sharp and symmetrical morphology of the margin, and confirms predictions from numerical models (van Wijk and Cloetingh 2002). By contrast, subsequent motion of the Bellingshausen plate relative to Antarctica has been slow and complex, and has modified the initial rift morphology to create a broad deformed BPBZ that was strongly affected by migrating patterns of deformation and volcanism.

ACKNOWLEDGMENTS

This project is funded by the Earth System Sciences Research School (ESSReS), an initiative of the Helmholtz Association of German research centres (HGF) at the Alfred Wegener Institute for Polar and Marine Research (AWI). We thank the master, crew and scientists of R/V Polarstern and especially the pilots and technicians of HeliService international for their support and assistance. We are grateful to Graeme Eagles for his constructive review, and two other reviewers, who chose to remain anonymous, as well as the numerous people who commented on earlier drafts of the manuscript. All of the figures in this paper but Figures 4.6, 4.15, and 4.16 were created using GMT (Generic Mapping Tools by Wessel and Smith 1991). We especially thank Paul Wessel for coding extra features into GMT5 overnight.

4.6 SUPPLEMENT

4.6.1 Additional figures

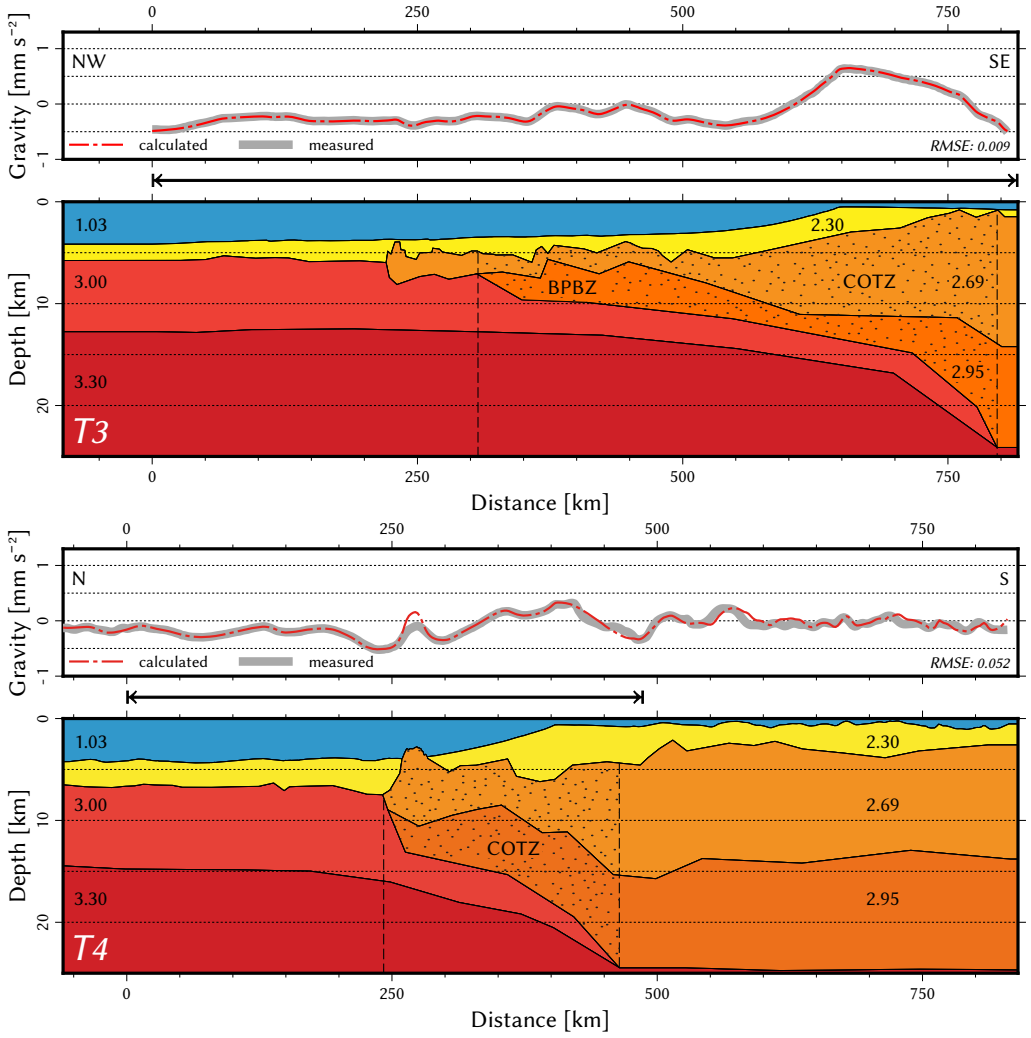

Figure 4.8. Crustal models along transects T3 and T4. Numbers in the cross-section represent density (g cm^{-3}); stippled area indicates extended transitional crust/Bellingshausen Plate Boundary Zone (COTZ/BPBZ). Arrows indicate area covered by seismics.

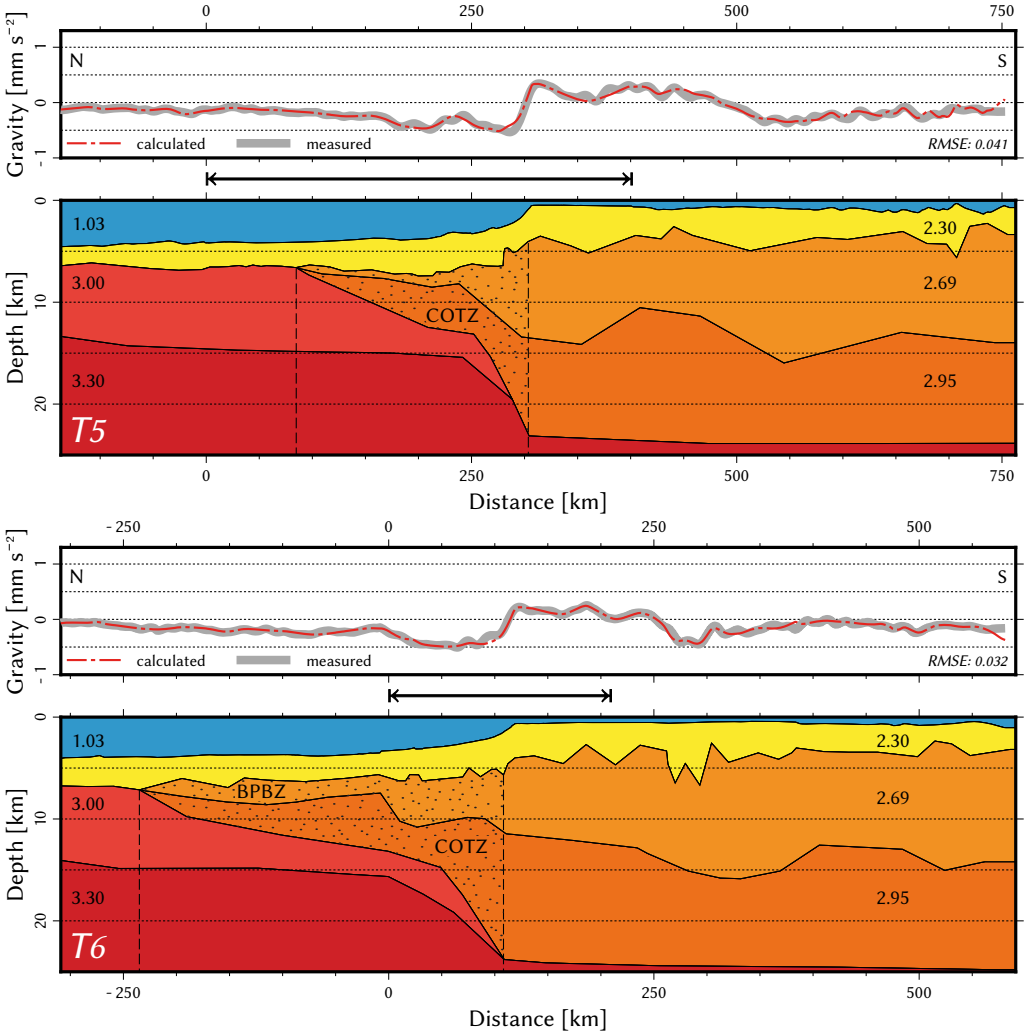

Figure 4.9. Crustal models along transects T5 and T6. Numbers in the cross-section represent density (g cm^{-3}); stippled area indicates extended transitional crust/Bellingshausen Plate Boundary Zone (COTZ/BPBZ). Arrows indicate area covered by seismics.

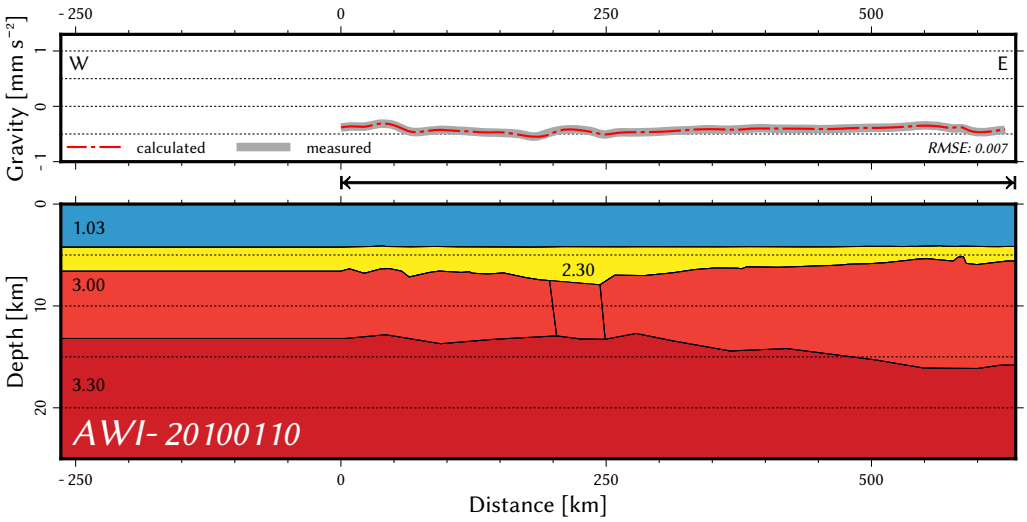

Figure 4.10. Crustal model along transect AWI-20100110. Numbers in the cross-section represent density (g cm^{-3}). Arrow indicates area covered by seismics.

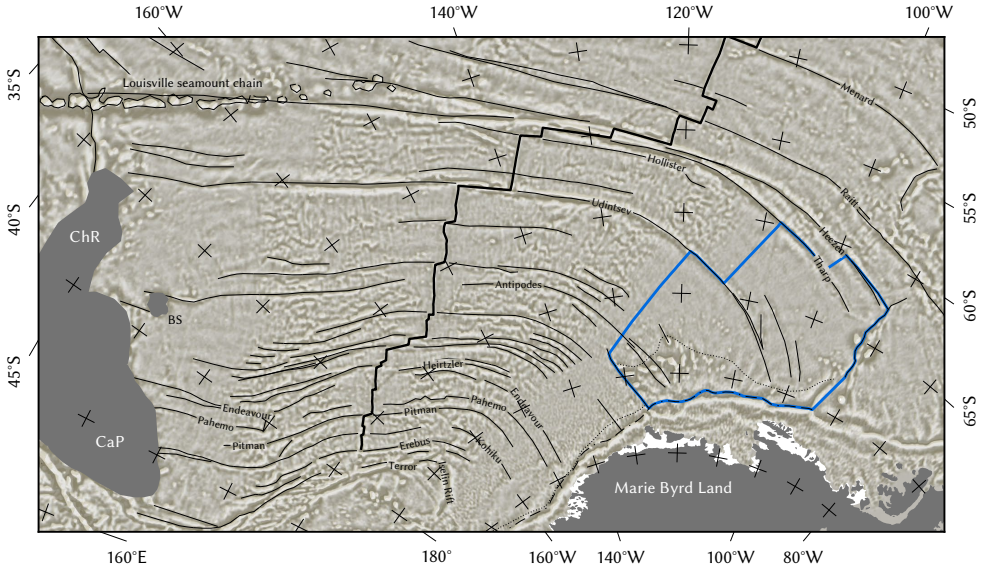

Figure 4.11. Fracture zone and flow line traces used for plate-tectonic reconstruction with pre-rift suture (dashed line), COB (dotted line), and Bellingshausen plate (blue outline). BS – Bollons Seamount; CaP – Campbell Plateau; ChR – Chatham Rise. Base map: DNSC08 satellite gravity (Andersen and Knudsen 2009), oblique Mercator projection with coordinates 170°E/50°S and 110°W/72.5°S on the oblique equator.

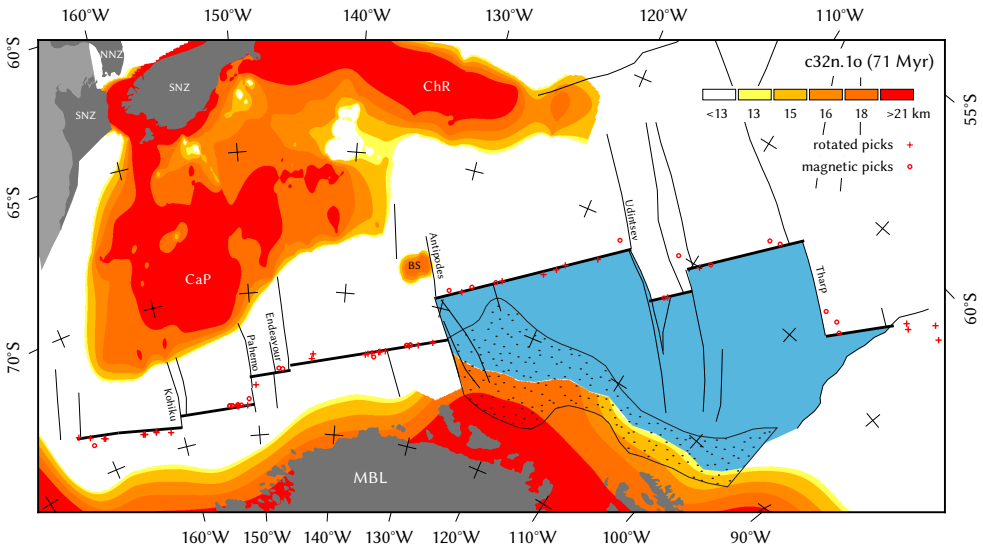

Figure 4.12. Plate-tectonic reconstruction model of Zealandia, Marie Byrd Land, and Bellingshausen plate (blue polygon) at magnetic chron c32n.1o (71 Myr) with magnetic picks on the West Antarctic and Bellingshausen plate, and rotated picks from the Pacific plate. The snapshot illustrates how Kohiku, Pahemo, Endeavour, Antipodes and Udintsev Fracture Zones fit. Thin black lines – fracture zones; thick black lines – mid-ocean ridge segments; stippled area – Bellingshausen Plate Boundary Zone; BS – Bollons Seamount; CaP – Campbell Plateau; ChP – Challenger Plateau; ChR – Chatham Rise; MBL – Marie Byrd Land; NNZ – North Island of New Zealand; SNZ – South Island. Base map: crustal thickness of Zealandia (Grobys et al. 2008) and Antarctica, Lambert conformal conic projection with central meridian 145°W and standard parallels 72°S and 60°S.

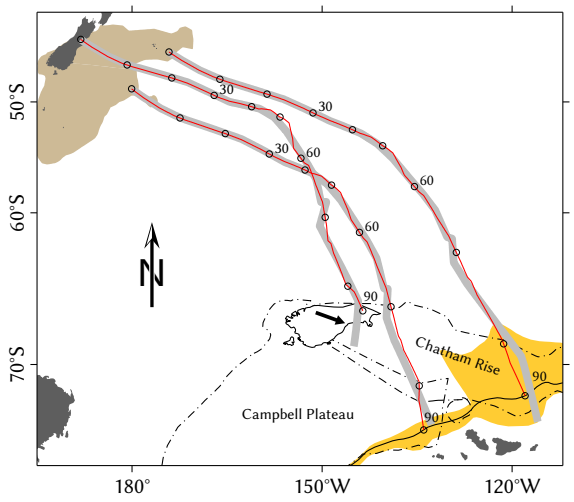

Figure 4.13. Plate motion paths of selected locations from the South Island of New Zealand, Campbell Plateau, and Chatham Rise. Gray lines – paths from Cande et al. (1995) and Eagles et al. (2004a); red – paths from Croon et al. (2008) and this study; yellow – COTZ of Marie Byrd Land; solid black line – estimated pre-rift suture; dashed lines – reconstruction of Zealandia at 90 Myr. Arrow indicates opening of the Bounty Trough after Larter et al. (2002). Mercator projection.

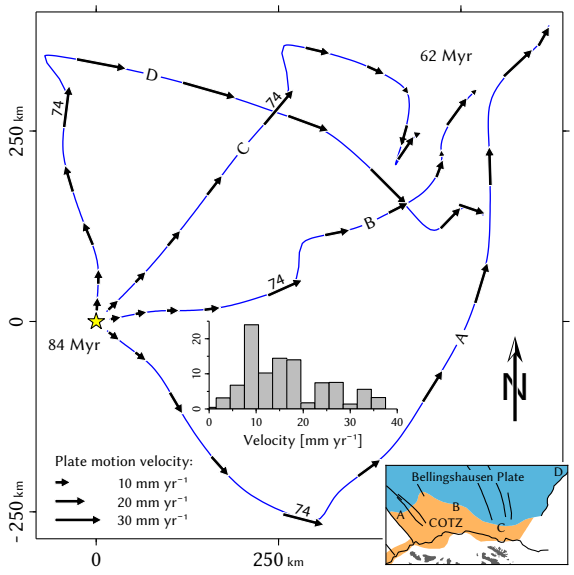

Figure 4.14. Plate motion paths of selected locations A–D from the southern and eastern border of the Bellingshausen plate between c34y and c27o (84–62 Myr, arrows every 2 Myr). Velocities are relative to Marie Byrd Land. Mercator projection; origin of each motion path shifted to a common point (star). Histogram shows distribution of Bellingshausen plate motion velocity along the paths A–D during c34y–c27o; units in frequency percent. For example, point A first moved to the southeast with increasing speed for 10 Myr and then changed direction to the northeast. Throughout one third of the time of the independent Bellingshausen plate motion, velocities are lower than 10 mm yr^{-1}.

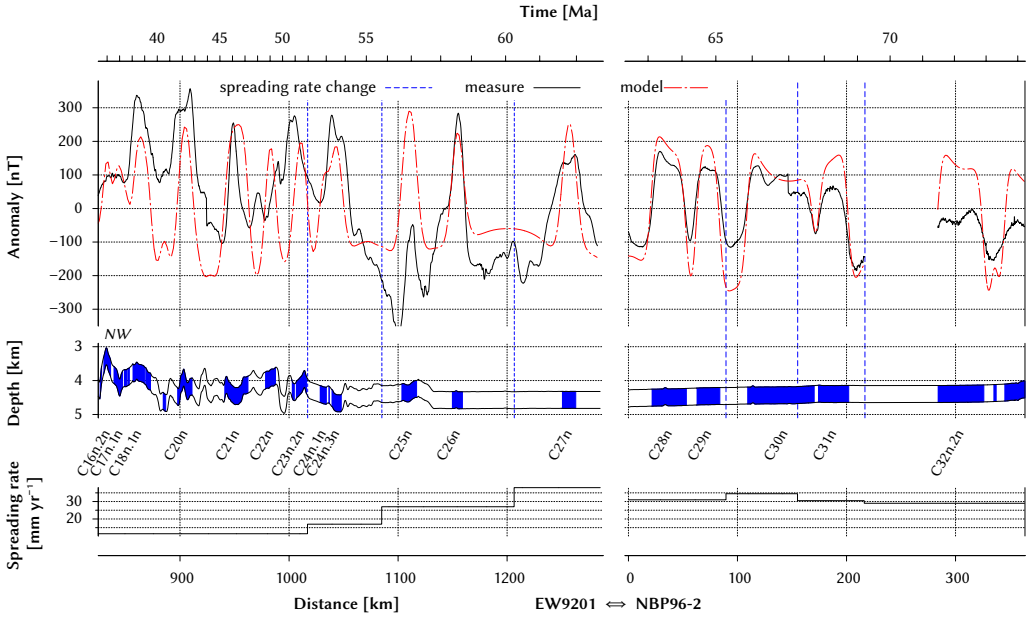

Figure 4.15. Magnetic data along NGDC lines EW9201 and NBP96-2. Spreading models based on geomagnetic polarity timescale of Gradstein et al. (2004). Velocities are half-spreading rates. Data of these and other lines in electronic supplement.

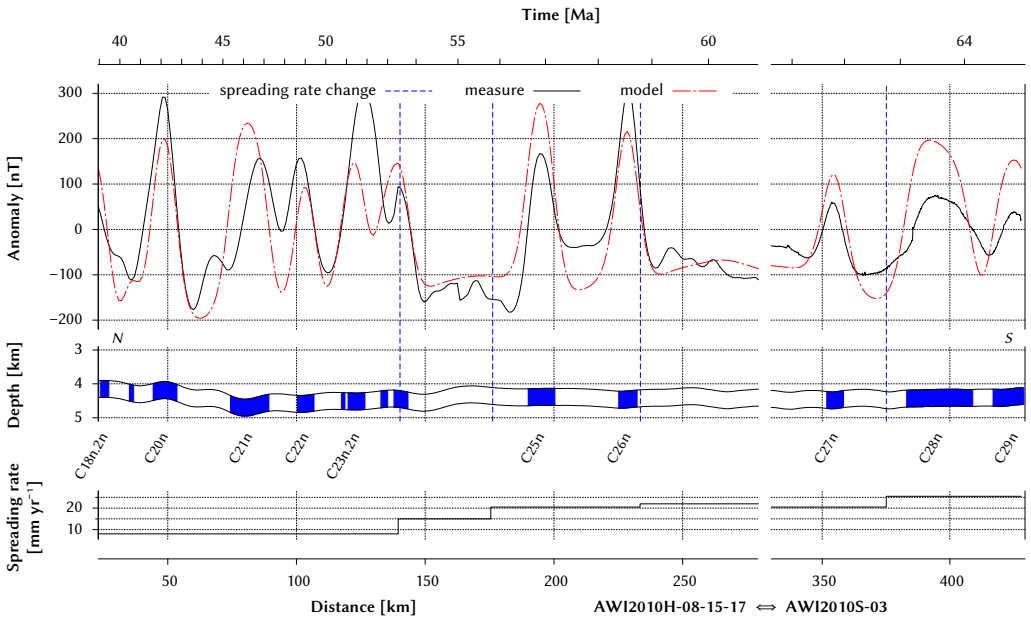

Figure 4.16. Spreading model and magnetic data along helicopter-magnetic line AWI2010H-08-15-17 and ship-magnetic line AWI2010S-03. Velocities are half-spreading rates.

4.6.2 Additional table

Table 4.2. Finite rotations used for plate tectonic reconstruction (Figure 4.7). Intermediate rotation at 75 Myr interpolated between c33o and c33y.

Chron	Time	Lat	Long	ω
Pacific plate relative to West Antarctic plate				
c20o	42.77	74.92	−49.86	35.11
c21o	47.24	74.8	−45.52	38.32
c22o	49.43	74.58	−45.89	39.32
c23n.2o	51.9	74.49	−45.0	40.48
c24n.3o	53.81	74.3	−45.12	41.53
c25o	57.18	73.1	−52.49	41.58
c26o	58.74	72.23	−56.53	41.36
c27o	61.98	71.35	−54.61	45.34
c28o	64.13	70.54	−55.29	46.67
c29o	65.12	70.05	−55.64	47.45
c30o	67.7	69.02	−56.18	49.49
c31o	68.73	68.52	−56.61	50.03
c32n.1o	71.23	67.56	−57.3	51.23
c33y	73.58	66.65	−57.49	52.95
—	75.0	66.35	−55.79	54.85
c33o	79.54	65.68	−52.38	60.56
c34y	84.0	66.11	−45.65	66.68
—	90.0	65.92	−42.81	71.46
Bellingshausen plate relative to Pacific plate				
c27o	61.98	−70.77	121.21	43.42
c28y	63.1	−70.93	123.01	45.08
c28o	64.13	−70.58	122.4	45.71
c29o	65.12	−70.49	122.51	46.91
c30o	67.7	−71.36	131.05	53.17
c32n.1o	71.23	−71.59	137.5	59.75
c33y	73.58	−71.15	138.42	62.74
c33o	79.54	−68.74	133.95	66.21
c34y	84.0	−68.58	138.46	71.18

Continued...

Chron	Time	Lat	Long	ω
Bellingshausen plate relative to Marie Byrd Land				
c27o	0–61.98	−76.2	−39.07	0.0
c34y	84.0–90.0	−76.2	−39.07	5.59
Campbell Plateau relative to Chatham Rise (rotation according to Grobys et al. 2008)				
c33y	0–73.58	−47.5	166.0	0.0
c33o	79.54–90.0	−47.5	166.0	6.25
Bollons Seamount relative to West Antactic plate (Campbell Plateau–Marie Byrd Land cross over)				
c33o	79.54	65.04	−59.96	54.87

5 PUBLICATION II

Continental Deformation of Antarctica During Gondwana's Breakup

Florian Wobbe and Karsten Gohl[1]

ABSTRACT

Geophysical data acquired along the Antarctic passive margins constrain the structure and geometry of the deformed continental crust. Crustal thickness estimates range between 7 and 50 km and the Antarctic continent–ocean transition zone (COTZ) extends up to 100–670 km towards the ocean. Continental deformation prior to rifting over a c. 100 million years long time span resulted in crustal stretching factors varying between 1.8 and 5.9. The time span of deformation was sufficiently large and the rifting velocity low enough to extend the margin by up to 300–400 km. Crustal thinning generates a significant subsidence and shallow water passages might already have developed during the rifting phase along the margin. Accounting for accurate continental margin deformation has also consequences for plate-tectonic reconstructions.

Keywords: Antarctica; plate-tectonics; continental deformation; crustal thickness; stretching factor; plate reconstruction; continent–ocean transition zone; magnetic sea floor spreading anomalies.

5.1 INTRODUCTION

Plate-tectonic reconstructions are based on the existence of magnetic anomalies induced by sea floor magnetization parallel to mid-ocean spreading ridges (Cox 1973). Already in 1963 Vine and Matthews proposed that lava, erupted on the sea floor, preserves the polarity of the Earth's magnetic field upon solidification. As the Earth's magnetic field reverses and sea floor spreading along the ridge continues, a set of magnetic stripes with opposite magnetic polarity develops parallel to the spreading ridge (Figure 5.1a). Anomalies of the same age—so-called isochrons—are identified

1 Alfred Wegener Institute for Polar and Marine Research, P.O. box 120161, 27515 Bremerhaven, Germany.

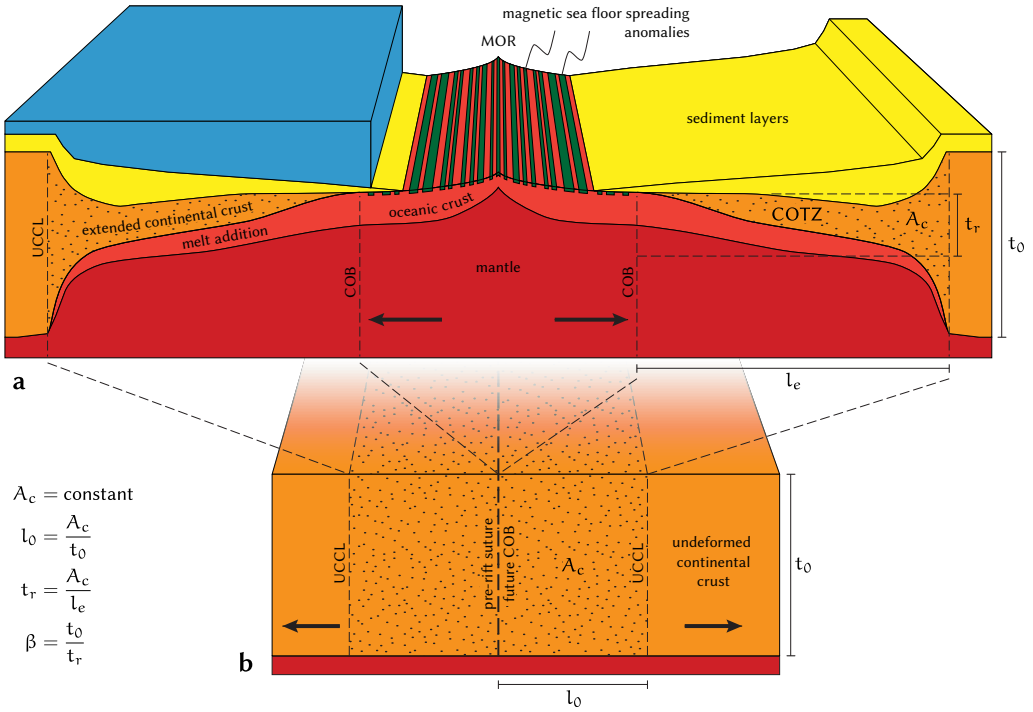

Figure 5.1. Simplified model of a rifted passive continental margin (a) and reconstructed geometry prior to rifting (b). COB – continent–ocean boundary; COTZ – continent–ocean transition zone; MOR – mid-ocean spreading ridge; UCCL – unstretched continental crust limit; β – stretching factor; A_c/l_e – COTZ area/width; l_0 – pre-rift width of COTZ; t_0/t_r – initial/extended crustal thickness.

on both sides of the ridge and fitting these isochrons provides the relative motion of the two diverging plates.

Magnetic sea floor spreading anomalies are only observed in oceanic crust. Magnetic anomalies originating from deformed continental or transitional crust of passive margins cannot be interpreted as spreading anomalies. Therefore, the initial rifting times and extension rates of diverging plates need to be determined by different means. Usually, geological markers—e.g., volcanic material erupted during rift initiation—can be dated and allow estimating the onset of continental rifting. Intra-plate deformation associated with the breakup process prior to the formation of oceanic crust is predominantly located in the continent–ocean transition zone (COTZ). The zone of extended continental and transitional crust is bounded by the landward unstretched continental crust limit (UCCL) and the seaward continent–ocean boundary (COB, Figure 5.1a). The width of the COTZ and its crustal thickness give indications on the extension rates and the amount of continental extension during the rifting phase (van Wijk and Cloetingh 2002).

Geological samples, gravity data and seismic tomography models suggest that most, if not all, of Antarctica's rifted passive margins consist of extended continental crust (Totterdell et al. 2000; Luyendyk et al. 2003; Winberry and Anandakrishnan 2004; Stagg et al. 2005; König and Jokat

2006; Gohl 2008; Jokat et al. 2010; Whittaker et al. 2010; Leinweber and Jokat 2012; Wobbe et al. 2012). Hence, the region presents an ideal opportunity to study conjugate rifted margins, but this outcome has been hampered by logistic difficulties associated with collecting data adjacent to Antarctica.

For the first time, this study classifies the continental deformation of the circum-Antarctic passive margins based on new data and a review of relevant published data. It also discusses the implications of the margin properties for plate-tectonic and paleobathymetric reconstructions.

5.2 METHOD AND DATA

The motion of a rigid tectonic plate on the Earth's surface may be described by a rotation about a virtual axis through the center of the Earth. Cox and Hart (1986) refer to such rotations as finite rotations and to the intersection of the axis with the Earth's surface as finite pole of rotation. Hence, motion paths of points on a tectonic plate as well as transform faults and flow lines of the generated oceanic crust lie on small circles about this rotation pole. Likewise, the extension during rift initiation is directed parallel to small circles about a finite rotation pole.

If the volume—or cross section area, A_c—of the deformed transitional crust is constant throughout time and the amount of added material (e.g., melt addition) is known, then a reconstruction of the pre-rift suture is possible (Figure 5.1b). A_c is determined by integrating the crustal thickness over the width, l_e, of the COTZ along each small circle and the crustal thickness prior to its extension, t_0, is measured at the UCCL. The aforementioned parameters permit the calculation of the pre-rift width of the COTZ, l_0, the mean thickness of the extended crust, t_r, and the stretching factor, β, according to the equations in Figure 5.1. Both, t_r, and β, are independent from the obliquity of the 2D section with respect to the COTZ, when a three-dimensional continuation of the geological units to either side of the 2D section is presumed (Wobbe et al. 2012).

Crustal thicknesses of the Antarctic passive margins are obtained from teleseismic, seismic and gravity data. Bayer et al. (2009), Reading (2006), and Winberry and Anandakrishnan (2004) estimated crustal thicknesses by using teleseismic earthquakes in Dronning Maud Land, in the Lambert Glacier region, and Marie Byrd Land (Figure 5.2). Deep crustal seismic data are available in the Weddell Sea, the Lazarev Sea (Jokat et al. 2004), between the Kerguelen Plateau and Prydz Bay (Gohl et al. 2007a), and in the Amundsen Sea (Gohl et al. 2007b; Wobbe et al. 2012). Further potential field crustal models from Stagg et al. (2005) and Wobbe et al. (2012) off Enderby Land, Wilkes Land, and Marie Byrd Land were used to esti-mate stretching factors and margin extension.

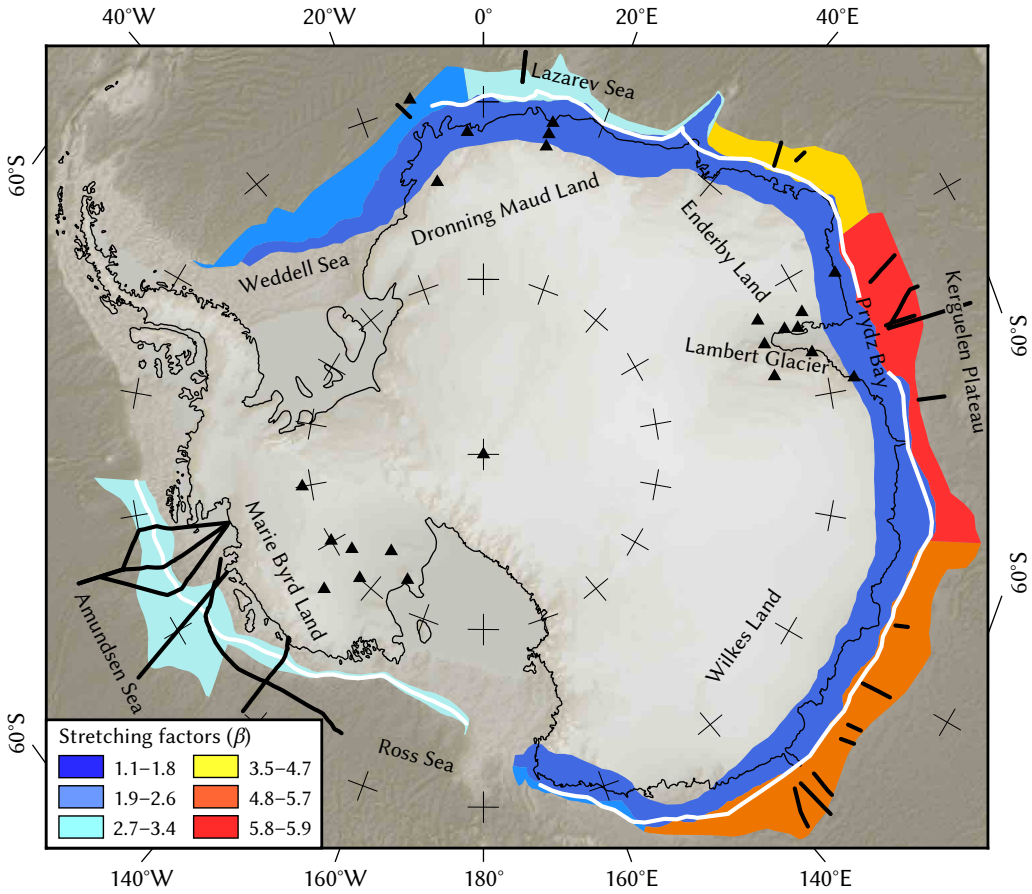

Figure 5.2. Transitional crust of Antarctica and associated stretching factor (β). Black profiles and triangles – location of known crustal thickness; white line – reconstructed pre-rift suture. Polar stereographic projection.

5.3 RESULTS

Crustal thickness estimates of Antarctica's passive continental margins range from 7 to 50 km. Winberry and Anandakrishnan (2004) as well as Wobbe et al. (2012) estimate the continental crust of West Antarctica to be at most 24 km thick, whereas values of less than 50 km are typical in Dronning Maud Land (Jokat et al. 2004; Bayer et al. 2009). In the Lambert Glacier region and off Prydz Bay the crust is thinner than 44 km (Reading 2006; Gohl et al. 2007a). Distal potential field crustal models off Enderby Land and Wilkes Land from Stagg et al. (2005) suggest thicknesses of less than 18 km.

Stretching factors were derived from the crustal thickness models for the five extensional domains of Antarctica that represent the conjugate to South America, Africa, India, Australia, and Zealandia respectively (Table 5.1). Figure 5.2 illustrates the geographical extent of the transitional crust and the associated stretching factors. This and other recent studies demonstrate that the Antarctic COTZ is generally wider than previously assumed and can extend up to 100–670 km oceanward from the UCCL (Gohl 2008; Jokat et al. 2010; Whittaker et al. 2010; Leinweber and Jokat 2012; Wobbe et al.

Table 5.1. Rate and lapse of continental deformation of Antarctica's passive continental margins.

Domain (conjugate margin)	β-Factor	Period [Myr]
Weddell Sea (South America)	1.9–2.6	167–147[a] (20)
Dronning Maud Land (Africa)	1.9–3.4	183–154[b] (29)
Enderby Land (India)	3.5–5.9	>118–84[c] (>34)
Wilkes Land (Australia)	4.8–5.9	160–84[d] (76)
Marie Byrd Land (Zealandia)	1.8–3.5[e]	90–(84)62[e] (28)

[a] König and Jokat (2006); [b] Leinweber and Jokat (2012); [c] Jokat et al. (2010); [d] Totterdell et al. (2000); [e] Wobbe et al. (2012)

2012). The wide COTZ reflects the c. 100 million years long timespan of intracontinental deformation that led to the final breakup of Gondwana. The obtained stretching factors roughly correlate with the deformation duration and COTZ width as predicted by numeric lithosphere extension models (van Wijk and Cloetingh 2002).

5.4 DISCUSSION AND SUMMARY

The separation of South America, Africa, India, Australia and Zealandia from Antarctica was a complex process that stretched over a timespan of c. 100 million years. The breakup and rifting of the continents caused intraplate deformation during which the continental crust was stretched by up to 300–400 km with stretching factors of 1.8–5.9. Such large deformation zones develop over prolonged periods (>20 Myr) at low spreading rates (<8 mm/yr), causing the formation of a series of failed rifts that migrate oceanward, referred to as basin migration (van Wijk and Cloetingh 2002). Rifting along Antarctica's margins initiated at different times with varying velocities, generating heterogeneous margin geometries and leading to distinct reconstructions of the pre-rift suture and COTZ. In Marie Byrd Land for instance, pre-rift suture and present-day COB lie as close as 90 km (Wobbe et al. 2012), whereas both are c. 400 km apart in Wilkes Land.

The implications of continental deformation on local plate-tectonic reconstructions are substantial: wrong estimation of the pre-rift suture or the neglect of deformation altogether can result in inaccurate reconstructions and large overlaps as illustrated in Figure 5.3. Apart from the restored plate geometry, the paleotopography is particularly important for paleobathymetry models that describe the history of seafloor topography. Crustal thinning along the Antarctic margins over large periods might have been responsible for subsidence long before the breakup of the continents. Hence, shallow water passages already could have existed during the rifting phase—much earlier than previously assumed.

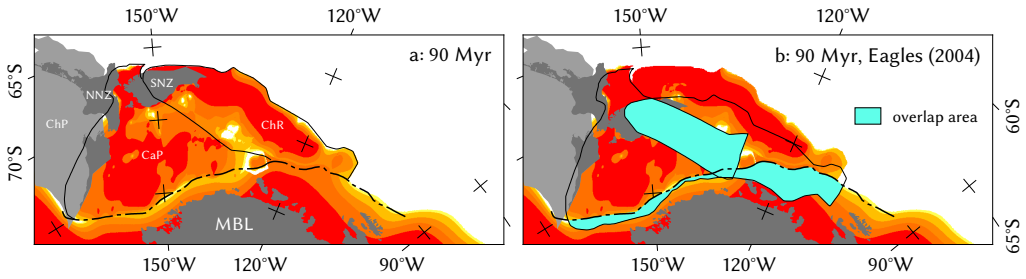

Figure 5.3. Pre-rift reconstruction models of Marie Byrd Land, Chatham Rise and Campbell plateau considering continental deformation and using finite rotations from (a) Wobbe et al. (2012), and model neglecting continental deformation using rotation parameters from (b) Eagles et al. (2004a). CaP – Campbell Plateau, ChP – Challenger Plateau, ChR – Chatham Rise, MBL – Marie Byrd Land, NNZ – North Island of New Zealand, SNZ – South Island; black lines – oceanic plateaus; dashed line – pre-rift suture. Base map: crustal thickness of Zealandia and Antarctica, lambert conformal conic projection with central meridian 145°W and standard parallels 72°S and 60°S.

ACKNOWLEDGEMENTS

Many thanks go to Klaus Grosfeld, the editors, and an anonymous reviewer, whose comments helped to improve the publication.

6 PUBLICATION III

Deciphering tectonic phases of the Amundsen Sea Embayment shelf, West Antarctica, from a magnetic anomaly grid

Karsten Gohl[1], Astrid Denk[2],
Graeme Eagles[3], and Florian Wobbe[1]

ABSTRACT

The Amundsen Sea Embayment (ASE), with Pine Island Bay (PIB) in the eastern embayment, is a key location to understanding tectonic processes of the Pacific margin of West Antarctica. PIB has for a long time been suggested to contain the crustal boundary between the Thurston Island block and the Marie Byrd Land block. Plate tectonic reconstructions have shown that the initial rifting and breakup of New Zealand from West Antarctica occurred between Chatham Rise and the eastern Marie Byrd Land at the ASE. Recent concepts have discussed the possibility of PIB being the site of one of the eastern branches of the West Antarctic Rift System (WARS). About 30,000 km of aeromagnetic data—collected opportunistically by ship-based helicopter flights—and tracks of ship-borne magnetics were recorded over the ASE shelf during two R/V *Polarstern* expeditions in 2006 and 2010. Grid processing, Euler deconvolution and 2D modelling were applied for the analysis of magnetic anomaly patterns, identification of structural lineaments and characterisation of magnetic source bodies. The grid clearly outlines the boundary zone between the inner shelf with outcropping basement rocks and the sedimentary basins of the middle to outer shelf. Distinct zones of anomaly patterns and lineaments can be associated with at least three tectonic phases from (1) magmatic emplacement zones of Cretaceous rifting and breakup (100–85 Ma), to (2) a southern distributed plate boundary zone of the Bellingshausen Plate (80–61 Ma) and (3) activities of the WARS indicated by NNE–SSW trending

1 Alfred Wegener Institute for Polar and Marine Research, Am Alten Hafen 26, 27568 Bremerhaven, Germany
2 Institute of Geophysics and Meteorology, University of Cologne, Zülpicher Straße 49a, 50674 Köln, Germany; present address: Dept. of Geosciences, University of Tübingen, Hölderlinstr. 12, 72074 Tübingen, Germany
3 Dept. of Earth Sciences, Royal Holloway University of London, Egham TW20 0EX, UK

lineaments (55–30 Ma?). The analysis and interpretation is also used for constraining the directions of some of the flow paths of past grounded ice streams across the shelf.

KEYWORDS: Aeromagnetics; Data processing; Pine Island Bay; Gondwana breakup; Bellingshausen Plate; West Antarctic Rift System.

6.1 INTRODUCTION

The Amundsen Sea Embayment contains one of the largest continental shelves of the Pacific margin of West Antarctica. Pine Island Bay, in the eastern part of the embayment, has for a long time been suggested to contain the crustal boundary between the Thurston Island block and the Marie Byrd Land block (e.g., Dalziel and Elliot 1982; Grunow et al. 1991; Storey 1991). Plate tectonic reconstructions suggest that this region was a key area for the initiation of continental breakup, that it was the location of a possible plate boundary, and that it may have been, or still is, an active branch of the West Antarctic Rift System (Larter et al. 2002; Eagles et al. 2004a; Dalziel 2006; Gohl et al. 2007b; Jordan et al. 2010; Wobbe et al. 2012). In spite of all this, little is known about the tectonic evolution and architecture of the embayment from direct study there.

Tectonically induced displacements of the crust are the underlying processes controlling the development of landscapes upon which climate processes play out. This context is of particular importance for reconstructing continental ice sheet evolution. In the Amundsen Sea Embayment, the Pine Island, Thwaites, Smith and Kohler glacier systems are thinning at rapid rates, and some of them have also started to flow at dramatically increased rates (e.g Rignot et al. 2008; Pritchard et al. 2009). If these glaciers were to drain their catchment area, the volume of ice lost to the ocean could potentially lead to 1.5 m of sea-level rise (Vaughan et al. 2006). Modelling results (Pollard and DeConto 2009) suggest that the ice sheet in the Amundsen Sea Embayment may have retreated with similar dynamics several times since the Pliocene. Identifying tectonic lineaments and understanding the tectonic architecture of the shelf of the Amundsen Sea Embayment may thus not only help explaining the geodynamic and kinematic processes of continental rifting in this West Antarctic realm, but also provide valuable constraints on flow paths and subglacial substrate of basement for paleo-ice sheet modellers.

An extensive ship-borne and helicopter-borne magnetic dataset was collected for the first time in the Amundsen Sea Embayment and Pine Island Bay by the Alfred Wegener Institute during R/V *Polarstern* expeditions ANT-XXIII/4 in 2006 and ANT-XXVI/3 in 2010. The distribution and spacing of the survey tracks are suitable to allow spatial gridding and 3D field analysis for delineating crustal and basement features. In this paper, we describe the workflow from magnetic data acquisition to processing

and modelling and put forward a model for the tectonic architecture of the offshore Amundsen Sea Embayment.

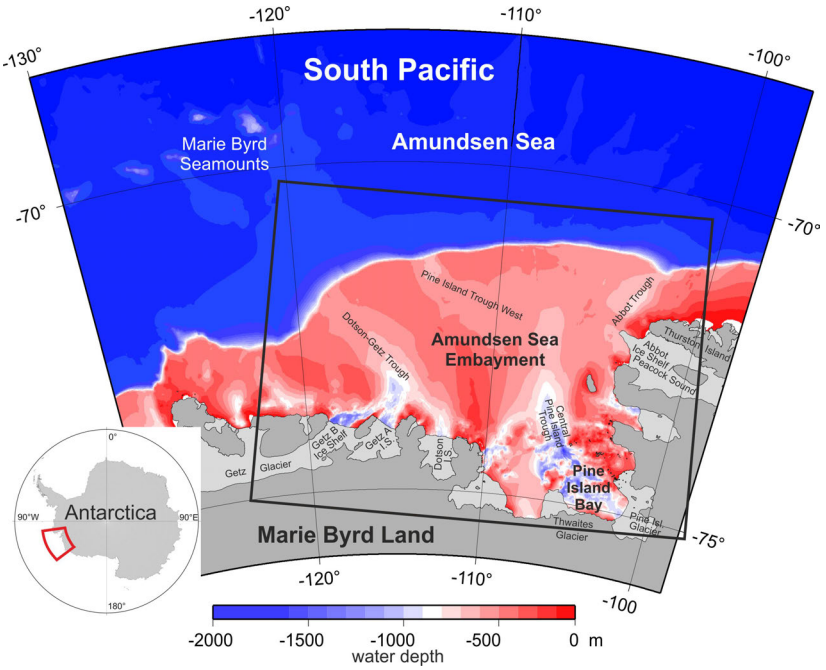

Figure 6.1. Overview map of the Pacific margin of West Antarctica with the Amundsen Sea Embayment and Pine Island Bay. The bathymetry was compiled by Nitsche et al. (2007) and illustrates the glacially eroded deep troughs on the continental shelf. Middle grey areas are land regions with grounded ice, and light grey areas mark ice shelves. The black box marks the area of the magnetic survey shown and discussed in this paper.

6.2 GEOLOGICAL AND GEOPHYSICAL BACKGROUND

Fig. 6.2 summarizes the main stages in the tectonic development of the Pacific margin of West Antarctica. At least three distinct phases since Late Cretaceous have been discussed in recent literature.

The extension, and subsequent separation, of New Zealand and West Antarctica dominate the tectonic signature of the Amundsen Sea Embayment. This early divergence of the Pacific and Antarctic plates led first to rifting and crustal extension between Chatham Rise and the Amundsen Sea Embayment off easternmost Marie Byrd Land as early as 90 Ma (Larter et al. 2002; Eagles et al. 2004a; Wobbe et al. 2012). Rifting possibly continued within the Great South Basin between the Campbell Plateau and the South Island of New Zealand until its abandonment in favour of a new extensional locus to the south, forming the earliest oceanic crust between Campbell Plateau and Marie Byrd Land by 84–83 Ma.

From about 79 Ma, the Bellingshausen Plate moved independently of the Pacific and Antarctic Ridge on the southern flank of the Pacific–Antarctic Ridge until about 61 Ma, when a major plate reorganisation occurred in

the South Pacific (e.g., Larter et al. 2002; Eagles et al. 2004a, b). This small plate's western boundary passed through the region of the Marie Byrd Seamounts, north of the Amundsen Sea Embayment. Its eastern transpressional boundary lies along the Bellingshausen Gravity Anomaly lineament in the western Bellingshausen Sea (Gohl et al. 1997; Eagles et al. 2004a). Although a discrete southern plate boundary has been depicted running from the seamounts onto the shelf and mainland, its true nature is poorly known (Eagles et al. 2004a, b) and it may be a more distributed feature.

The location of Pine Island Bay has led several researchers to suggest that it hosts a major crustal boundary between the Marie Byrd Land block to the west and the Thurston Island/Ellsworth Land blocks to the east. These blocks are suggested to have moved with respect to each other during the Late Cretaceous New Zealand–Antarctic separation and perhaps also in early Mesozoic or Paleozoic times (e.g., Dalziel and Elliot 1982; Grunow et al. 1991; Storey 1991). However, direct evidence of the presence of such a boundary is still missing. Conceptual models also suggest that Pine Island Bay and the eastern Amundsen Sea Embayment hosted basins of the West Antarctic Rift System. Jordan et al. (2010) invert airborne gravity data to reveal an extremely thin crust and low lithospheric rigidity beneath the onshore Pine Island Rift. Müller et al. (2007) and Eagles et al. (2009) considered how, at times between chrons 21 and 8 (48–26 Ma), the West Antarctic Rift System east of the Ross Sea operated in either dextral strike-slip or extensional motion through the region to the south and east of the Amundsen Sea Embayment connecting eventually to a Pacific–Phoenix–East Antarctic triple junction via the Byrd Subglacial Basin and the Bentley Subglacial Trench. There are indications for an early West Antarctic Rift System extension in western Marie Byrd Land in the mid-Cretaceous (e.g., McFadden et al. 2010), but its eastern continuation is less well understood. It is possible that in the north-south striking zone of thinned crust in Pine Island Bay was an eastern arm of this early manifestation of the West Antarctic Rift System (Dalziel 2006; Ferraccioli et al. 2007; Gohl et al. 2007b; Jordan et al. 2010)

6.3 MAGNETIC SURVEYS AND DATA PROCESSING

The Amundsen Sea was the target area for geoscientific, oceanographic and biological studies during the R/V *Polarstern* expeditions ANT-XXIII/4 in 2006 and ANT-XXVI/3 in 2010. Ship-borne magnetic data were continuously recorded with two 3-component fluxgate magnetometer sensors, which are permanently installed on the crow's nest. One of the two BO-105 helicopters on board was equipped with a cesium-vapor magnetometer sensor towed by a 30 m long cable. Helicopter-borne magnetic data were

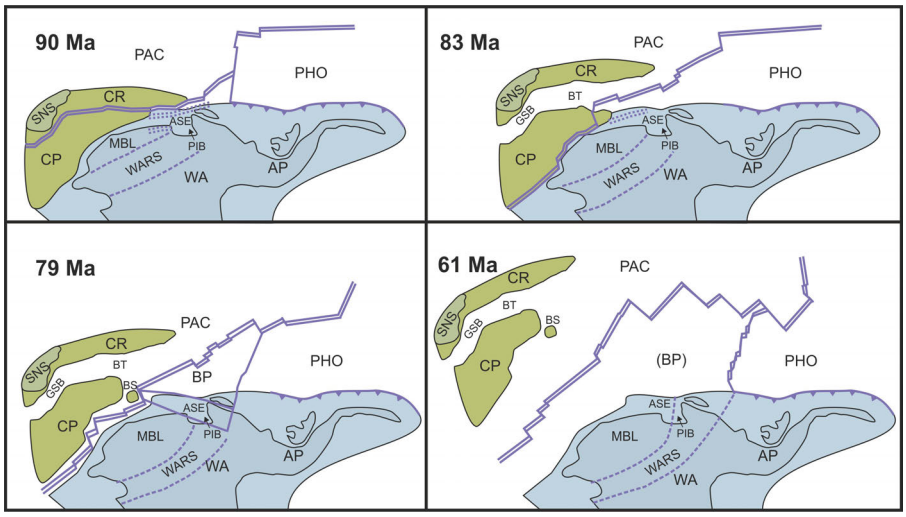

Figure 6.2. Plate tectonic reconstruction of the tectonic development in the Amundsen Sea area from 90 to 61 Ma. The plates are rotated according to rotation parameters compiled and derived by Eagles et al. (2004a). The outline of the West Antarctic Rift System (WARS) faults or boundaries is an approximate estimation, because an accurate geometry of the rift system has not been identified yet. Abbreviations are: AP Antarctic Peninsula, ASE Amundsen Sea Embayment, BP Bellingshausen Plate, BT Bounty Trough, BS Bollons Seamount, CP Campbell Plateau, CR Chatham Rise, GSB Great South Basin, MBL Marie Byrd Land, PAC Pacific plate, PHO Phoenix Plate, PIB Pine Island Bay, SNS South Island New Zealand, and WA West Antarctica. Modified from Gohl (2012).

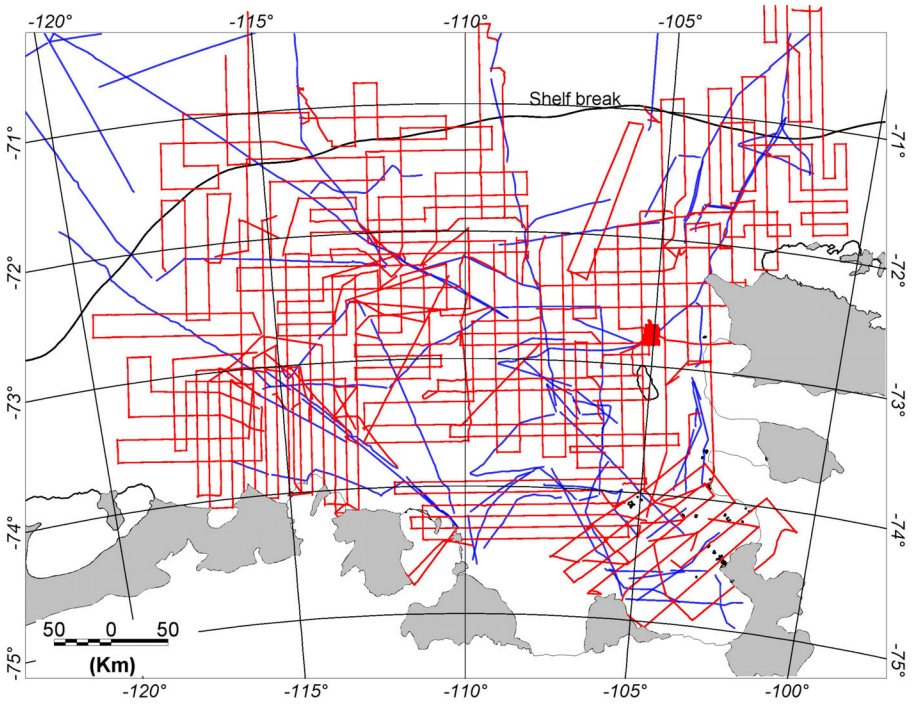

Figure 6.3. Map with combined helicopter-borne (red lines) and ship-borne (blue lines) magnetic tracks of both R/V Polarstern expeditions in 2006 and 2010, which are included in the preparation of the magnetic anomaly grids. The irregular line geometry is due to opportunistic surveying.

collected opportunistically along track lines as far as possible within a predetermined survey pattern, but subject to the constraints of the vessel's primary marine geoscientific and oceanographic tasks. Each survey flight covered 350–450 km in 2 to 2.5 h at a nominal 100 m flight height with a sampling interval of 3–5 m. Up to 3 or 4 flights were conducted on days with good flight conditions and no other transport tasks. With this survey approach, the Amundsen Sea Embayment shelf was effectively covered with patches of survey lines that total about 30,000 km of data (Fig. 6.3). The survey line spacing varies between 5 and 25 km and—although a regular flight grid could not be maintained—allows spatial gridding and 3D field analysis for delineating regional crustal and basement features.

Before merging into the processing stream with the helicopter-magnetic data, the 3-component ship-borne magnetic data had to be pre-processed to compensate for interactions between the ship's ferrous body and the variable geomagnetic field. To facilitate this, a number of figure-eight shaped magnetic compensation loops were completed during the cruises from which compensation coefficients for all headings were calculated. Corrections were applied using these coefficients according to the methods and descriptions of König (2006) and Wobbe et al. (2012). The main contribution to an erroneous shift of the measured magnetic data comes from the ship's heading (Nogi and Kaminuma 1999). For instance, a one degree change of the ship's heading causes about 300 nT of variation in the horizontal components. The vertical component is less affected by the ship's heading but shows noise due to roll and pitch. In order to avoid noise in the total intensity field, the data acquired during and immediately after substantial heading changes were excluded from further processing.

The total magnetic field data of helicopter-borne cesium-vapor sensor turned out to be rather unaffected by the helicopter's heading, except for major turns at flight line change. Such data were also removed from further processing. In general, the helicopter-magnetic records appeared to be less noisy than the ship-borne data.

After this initial pre-processing, both ship-borne and helicopter-borne data went through the same principal processing steps (Table 6.1) using *Geosoft Oasis montaj™* software for most applications:

REMOVAL OF INTERNATIONAL GEOMAGNETIC REFERENCE FIELD (IGRF) We removed the IGRFs of 2005 and 2010 from the data of 2006 and 2010, respectively. We used the mean date for each survey.

EDITING AND FILTERING Visual editing of obvious erroneous data improved the overall data quality of the datasets of both expeditions. For instance, data affected by tilts in loops of the helicopter's flight tracks were removed. Large numbers of data were removed in particular from the ship-borne records, owing to noise induced during ship manoeuvres, heading changes and crane movements. A band-pass filter removed spikes and other short-wavelength noise from all datasets. As it was not possible to set up a magnetic base station in the coastal area of the

Table 6.1. Magnetic data processing and analysis flow.

Removal of IGRF
⇓
Editing and filtering
⇓
Upward field continuation of ship-borne data to 150 m
⇓
Cross-point analysis and levelling
⇓
Gridding and micro-levelling
⇓
Derivatives, field continuations, high-pass filtering, analytical signal
⇓
Power spectra, Euler deconvolution
⇓
2-D forward modelling

Amundsen Sea Embayment for the duration of both cruises, the data may still be affected by diurnal variations of the geomagnetic field.

LEVELLING This process is required to the data in order to minimise the differences at cross-points before any gridding is applied. The plane tolerance of crossing survey line points was chosen to be 0.0005° (~50 m). As the helicopter data have shown to provide more reliable results than the ship-borne data, the two datasets were treated separately. The differences at cross-points within the dataset were minimised using an iterative approach to their mean values. We divided the intersection points of the helicopter lines into reliable intersection points (differences vary less then ±10 nT) and less reliable intersections points (all other intersection points). In the first step, these lines were levelled separately: Lines with reliable intersection points were levelled using an 'iterative levelling' algorithm. Lines with less reliable intersections were levelled using 'full levelling' algorithm. 'Iterative levelling' calculates a least-squares trend line through the error data to derive a linear trend error curve, which is then added to the data to be levelled. These steps are repeated for crossing lines until a convergence is reached. 'Full levelling' adjusts the values of an input channel by adding a correction defined in an error channel. In a second step, an iterative levelling algorithm was again applied, this time simultaneously to all profiles from both platforms. In this step, we levelled the ship-borne data into the levelled framework of helicopter data after splitting the ship-borne data into straight segments and generating an intersection table with points of ship-borne data crossing helicopter survey lines. Intersection points within the ship-borne

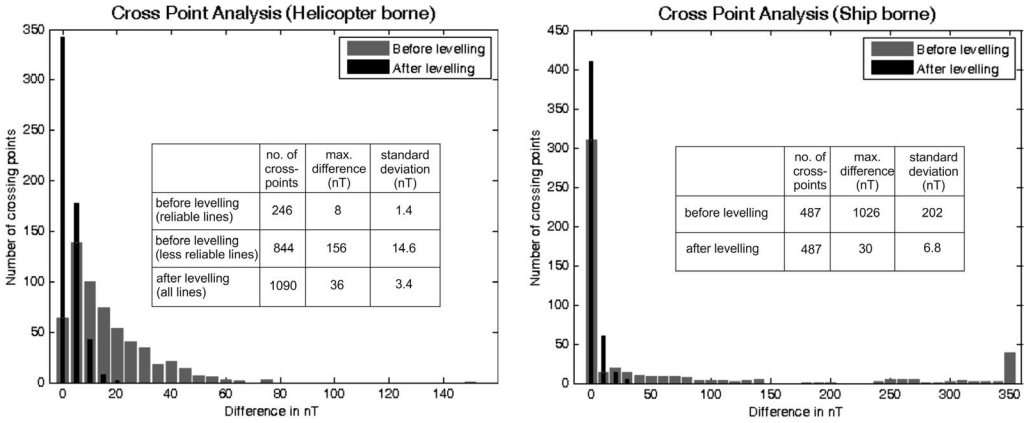

Figure 6.4. Results of the cross-point analysis for the helicopter-borne and ship-borne survey lines before and after levelling.

dataset were ignored. The cross-point histograms and tables (Fig. 6.4) show the large reduction in intersection misfits brought about by the levelling. It is noteworthy that the levelling process removes the large errors (~350 nT) at ship-line cross-points in south-eastern Pine Island Bay, which are a long distance from the nearest compensation loop.

GRIDDING AND MICRO-LEVELLING Particular care was taken in gridding the data because of the irregular line spacing and orientation. We applied a minimum curvature approach between less sampled areas and those areas with good coverage. Initially, a coarse grid with a large grid cell size is used. Nodes represent either the real data, which is found within a specific radius, or an average of all data points of the grid. Iteratively, the grid is adjusted to the real data nearest to the grid nodes. If an acceptable misfit between real data and coarse grid node is achieved, the cell size is divided by two and the procedure starts again. The gridded data still show some noise resulting from residual levelling and gridding errors. Although these errors are small in comparison to the measured anomalies, they account considerably for noise in further processing. Removing these errors by the application of a low-pass filter to smooth derivative grids is a process known as micro-levelling (Green 1983; Ferraccioli et al. 1998). As the screening of the line data indicated, the shelf is partitioned into two magnetic anomaly domains characterised by different wavelengths. We found that micro-levelled grids of 5 and 2 km cell size best represent both domains with a minimum of artefacts (Fig. 6.5A, B). A further decrease of the cell size to 1 km in combination with a 30-km high-pass filter (Fig. 6.5C) shows clearly the wave-field distinction between the inner shelf domain and the middle to outer shelf but also creates numerous artificial anomalies.

FURTHER ANALYTICAL FIELD ANALYSIS We applied a wide spectrum of standard wave-field processing methods to the grid in order to constrain directional trends and the shapes and edges of magnetic anomaly units. These methods included the calculation and application of (1) horizontal,

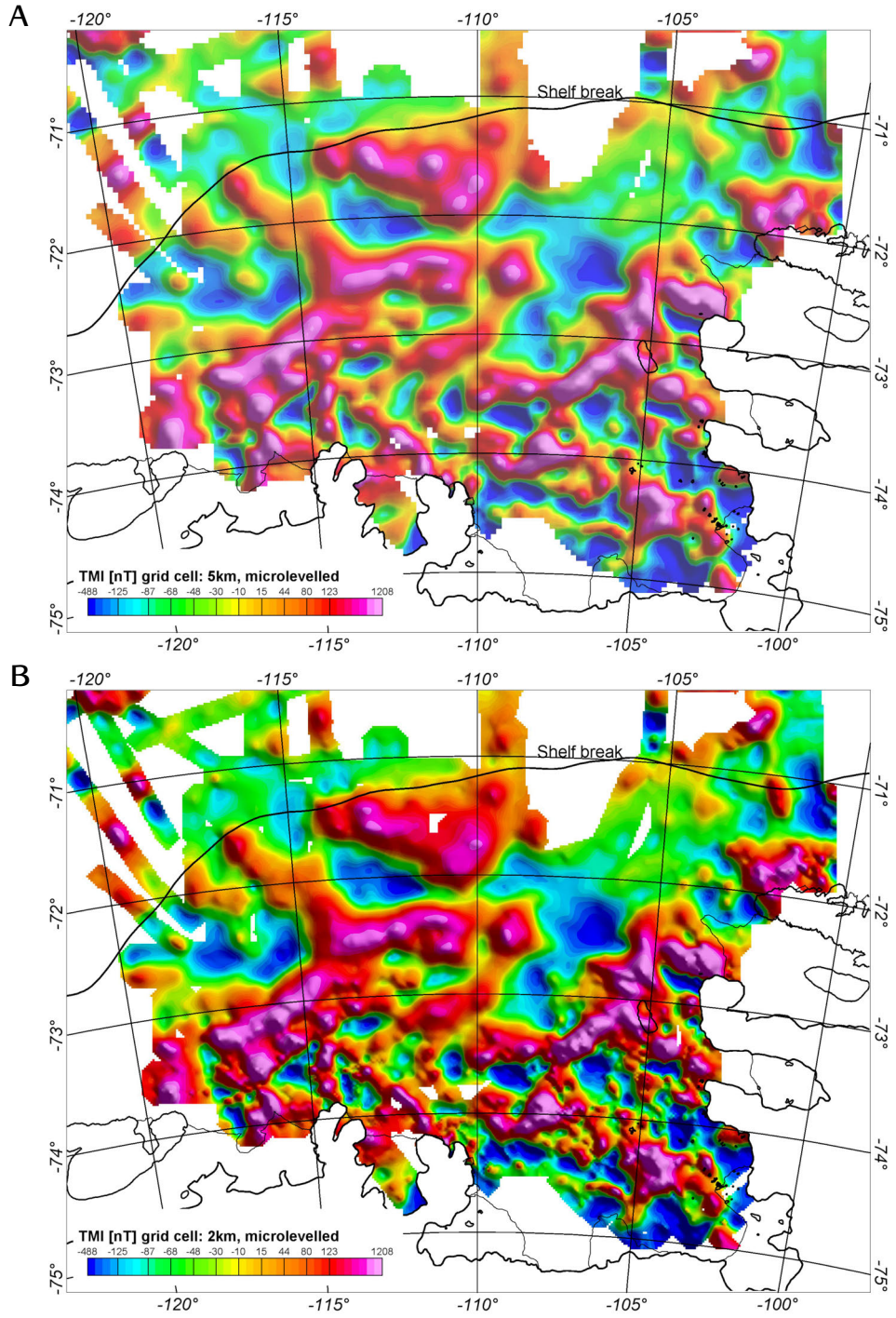

Figure 6.5. Processed magnetic anomaly grids with grid cell sizes of (A) 5 km, (B) 2 km, and (C) 2 km with a 30-km cut-off high-pass filter. Fig. 6.5C also shows the boundary (white line) between the outcropping basement of the inner shelf in the south and the sediment basin in the north, and an estimated 3-km-depth marker (hashed black line) to which the top of basement dips northward from this boundary.

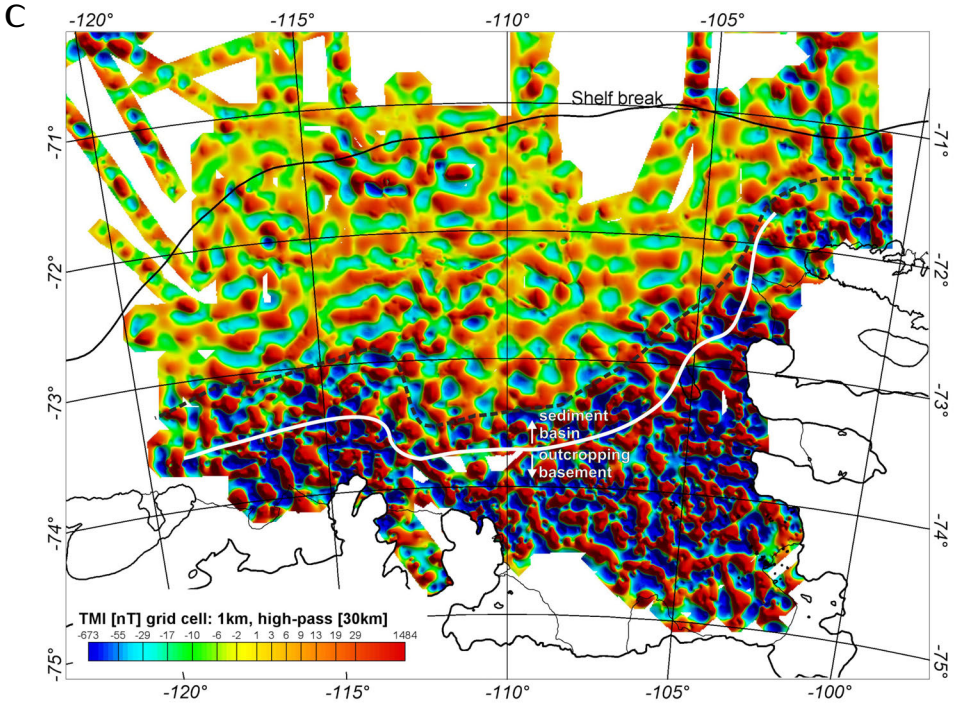

Figure 6.5. (Continued)

vertical and tilt derivatives, (2) upward field continuations, (3) high-pass filters, (4) pseudo gravity and (5) analytical signal. At moderate wavelengths, these methods serve to highlight the magnetic bodies and tectonic lineation trends that can be coarsely interpreted from the regular anomaly grids. High-pass filtering, in particular, much more readily delineates the boundary zone between outcropping basement of the inner shelf and the sedimentary cover of the middle and outer shelf (Fig. 6.5C).

6.4 DEPTH ESTIMATES

In addition to standard power spectra analyses for estimating the depths of magnetic anomaly sources, we applied the Euler deconvolution method to the grid in an attempt to better delineate the spatial distribution and extent of the tops and edges of source bodies. We used the approach of Thompson (1982) and Reid et al. (1990) in which the depth solution is related to a chosen structural index *SI* (0 for a planar contact, 1 for a dike or sill, 2 for a vertical pipe, 3 for a sphere). A square window is defined within the grid, which contains at least 3×3 grid cells. For each grid cell, the deconvolution is calculated. Hence, a 3×3 cell window results in 9 equations, which are solved via a least-squares inversion. The window is then shifted across the grid and the same procedure is applied. It is obvious that the solution is dependent on the chosen window size. If the window size is so large that neighbouring anomalies intrude into it, the inversion

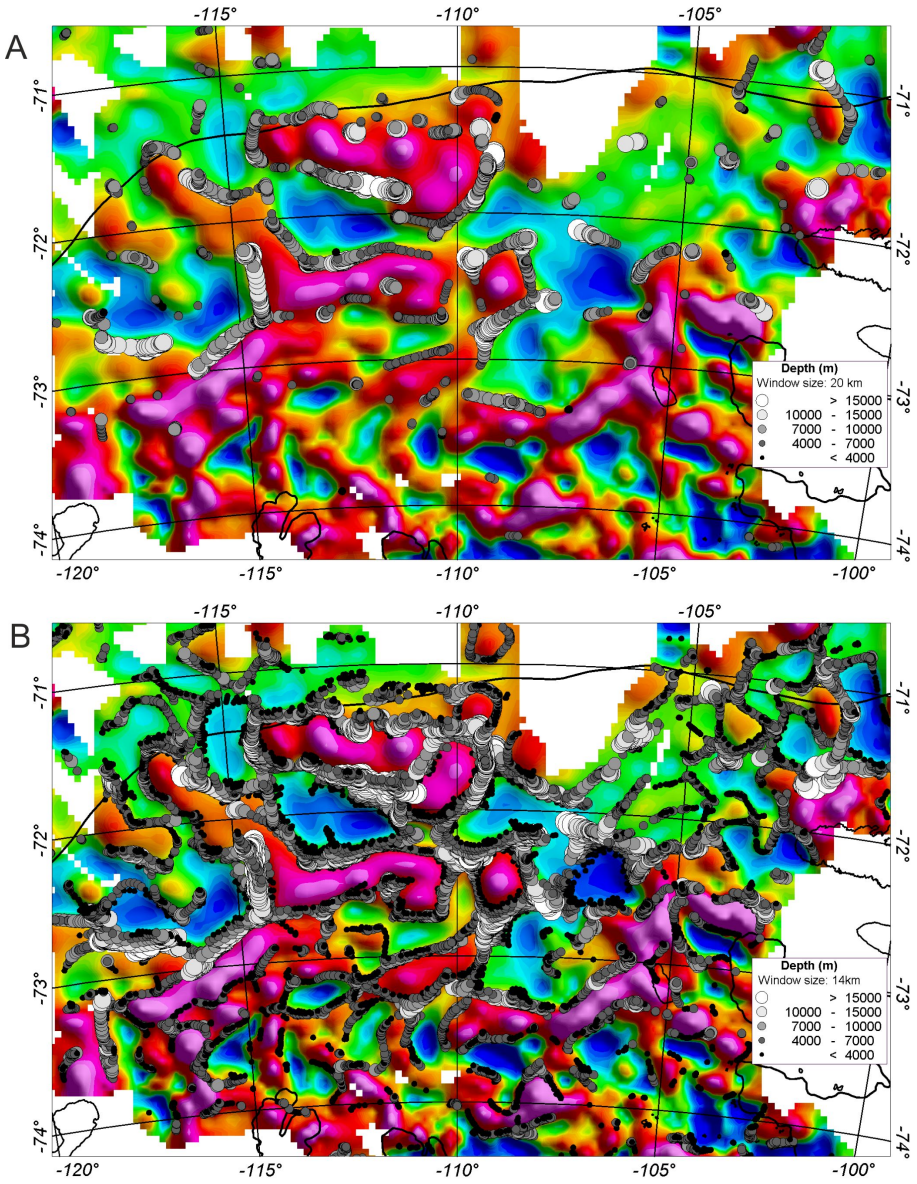

Figure 6.6. Anomaly grids (grid cell size of 2 km, micro-levelled) of the central embayment with top of magnetic source depth estimates from Euler deconvolution using the same structural index of SI = 0, but different window sizes of (A) 20 km and (B) 14 km.

can fail and its solutions are rejected. This is the case for distinct anomalies on the inner shelf in the south (Fig. 6.6A). On the other hand, if a window size is too small, then anomalies from deep-seated sources may not be adequately represented in the inversion, interfering with the solutions for shallower sources and resulting in artificially shallow source solutions. Fig. 6.6B shows that smaller window sizes generate more solutions and that long-wavelength anomalies yield shallower depth solutions than when a larger window is used.

Our two examples of Euler deconvolution solutions use different window sizes of 14 and 20 km but the same structural index (Fig. 6.6). The solutions provide estimates of a dense distribution of source tops at depths below

7 km over the middle to outer shelf, while further south, below the inner shelf, source tops are typically located at depths shallower than 7 km.

6.5 TECTONIC LINEAMENTS AND 2D MODELLING

One of the most striking observations in the magnetic anomaly grid is the domination of the inner shelf by relatively short-wavelength anomalies and the middle and outer shelf by middle to long wavelength anomalies (Fig. 6.5A, B). The boundary between the two domains is abrupt and clearly shown in the high-pass filtered wavefield (Fig. 6.5C). This boundary is the northern limit of a coastal and inner shelf domain in which basement crops out or exists in shallow subcrop, as suggested by the rugged topography (Fig. 6.1). It can be assumed that most of this basement is composed of crystalline rocks similar in type to the granitoids and porphyritic dykes observed from coastal and island outcrops of the embayment (e.g., Kipf et al. 2012; Pankhurst et al. 1993). Conversely, the longer wavelength signals over the middle and outer shelf are consistent with the presence of a thick drape of sediments overlying the basement (Lowe and Anderson 2002; Weigelt et al. 2009). Depth estimates from Euler deconvolution help identify a boundary zone across which the basement drops downwards to the north to about 3 km depth (Fig. 6.5C), which is consistent with observations from seismic data across this boundary (Graham et al. 2009; Lowe and Anderson 2002; Uenzelmann-Neben et al. 2007; Weigelt et al. 2009).

One of the objectives of the magnetic surveys was to identify crustal features for delineating tectonic events in the history of the crustal formation in the Amundsen Sea Embayment (Fig. 6.7). The middle and outer shelf show fundamentally different preferential anomaly strikes. While a major set of long-wavelength anomalies strike WSW–ENE along the middle shelf, the outer shelf west of 107°W exhibits mainly NW–SE striking anomalies which may continue on the inner shelf of the eastern embayment. A third directional trend is observed for positive anomalies on the inner and middle shelf striking NNE–SSW. These are less pronounced but seem to border a broad magnetic zone of low amplitude negative anomalies on the middle shelf at 106–109°W.

We selected two 2D modelling transects crossing the Amundsen Sea Embayment shelf from north to south and NW to SE across the major observed magnetic anomaly lineaments and proposed source bodies (Fig. 6.7). The data along the transects were taken from the magnetic anomaly grid at 5 km cell size. *Encom ModelVision™* was used as modelling software. The depth estimates from Euler deconvolution solutions provided some constraints for the parameterisation of these magnetic susceptibility models. Other constraints on crustal properties, such as crustal thickness, sediment thickness and the approximate locations of mafic (high density,

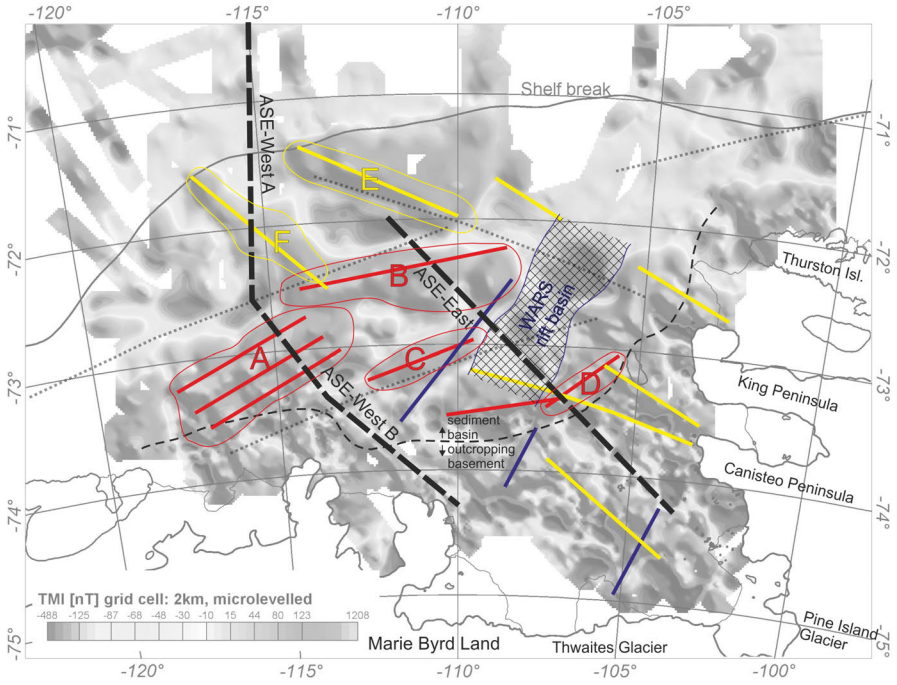

Figure 6.7. Map with major directional anomaly trends and tectonic features identified in the magnetic anomaly grid. The grid is shown slightly subdued and in grey scale with superposed trends of major satellite-derived gravity anomalies (thin dotted grey lines; from Gohl et al. 2007b). The outcropping basement–sediment boundary is marked with a thin, hashed black line. NW–SE trending anomalies are marked in yellow lines and fields; ENE–WSW trends are in red; NNE–SSW trends are in blue. The largest anomalies or anomaly groups with directional trends are encircled with a thin line in the respective colour and annotated from A to F. Thick, hashed black lines show the modelled profiles of Fig. 6.8. The WARS rift basin is interpreted as a branch of the West Antarctic Rift System.

high susceptibility) bodies, were implemented from seismic reflection data (Weigelt et al. 2009), a deep crustal seismic refraction model and a gravity anomaly inversion of the Amundsen Sea shelf region with crustal thicknesses of 20–25 km (Gohl et al. 2007b). Water depths were taken from the bathymetry compilation of Nitsche et al. (2007).

We chose a modelling procedure in which we parameterised the model starting with thick layers and large bodies from the lower crust for long-wavelength signals and moving on to small-size layers and bodies of the upper crust to generate short-wavelength signals. The responses were iteratively calculated for a range of susceptibilities and body sizes such that the root-mean-square (rms) misfit between observed and calculated total intensities could be minimised. Due to the different wave-field characteristics of transects ASE-West A, ASE-West B and ASE-East, each model was treated independently of the others. Although various studies show that the ranges of susceptibilities of individual rock types can span several orders of magnitude, it is possible to distinguish domains of sedimentary, felsic and mafic composition on the basis of susceptibilities. Most pub-

lished susceptibilities of intrusive felsic rocks range from 0.0001 to 0.02 SI unit (average 0.0012 SI), while those of intrusive rocks of mafic composition have values of 0.0001 to 0.13 SI (average 0.012 SI, e.g. Sanger and Glen 2003). We applied a constant susceptibility of 0.000005 SI for sediments and of 0.001 SI for the bulk of the continental crust in all models and started modelling with the average values of intrusive bodies by Sanger and Glen (2003). By adjusting the susceptibilities of these bodies, we stayed within the above given ranges.

The model transect ASE-West A (Fig. 6.8A) covers the continental slope and the outer shelf and includes two high-susceptibility bodies embedded into the upper crust of the continental rise. Much of the upper surface of the large high-susceptibility body 3 beneath the slope and outer shelf is located beneath 5 km depth, with shallower peaks at 2–3 km depth, producing the long-wavelength high with superposed short-wavelength fluctuations seen in the data. Similar high-susceptibility bodies were required to fit the anomalies of the middle and inner shelf model transects ASE-West B (Fig. 6.8B) and ASE-East (Fig. 6.8C). In both models, we inserted shallow, small-sized bodies of high susceptibilities to fit the shortest wavelength anomalies. On the inner shelf, where basement crops out, we topped most of the source bodies at the seafloor.

6.6 SUPERPOSED TECTONIC EVENTS

The modelled properties of the dominant ENE–WSW trending magnetic anomalies A, B, C and D (Fig. 6.7) indicate that they are caused by major elongated and deep-seated features of predominantly mafic composition. They parallel the initial spreading centre's azimuth between Chatham Rise and West Antarctica and can thus be related to rift processes occurring before breakup as early as 100 Ma and during breakup between 90 and 85 Ma (Eagles et al. 2004a; Larter et al. 2002; Wobbe et al. 2012). With their seaward-dipping outer edges, bodies of anomalies A and B might be interpreted as thick wedges of basaltic lava and mafic intrusions of the kind known from volcanic extended continental margins such as the Vøring margin or Afar Rift (Planke and Eldholm 1994; Wolfenden et al. 2005). The body modelled for anomaly A reaches near the seafloor at its southern limit which correlates with the steep northern flank of the inner Dotson-Getz Trough (Graham et al. 2009; Larter et al. 2009). The trough coming from the Getz B Ice Shelf strikes nearly in east–west direction on the inner shelf before merging with the outflow troughs originating from the Getz A and Dotson Ice Shelves and turning northwards on the middle shelf and to the northwest on the outer shelf (Fig. 6.1). We suggest that this intrusive body is more resistant to pre-glacial and glacial erosion and caused an east to northeastward deviation of grounded ice streams from the eastern Getz Glacier.

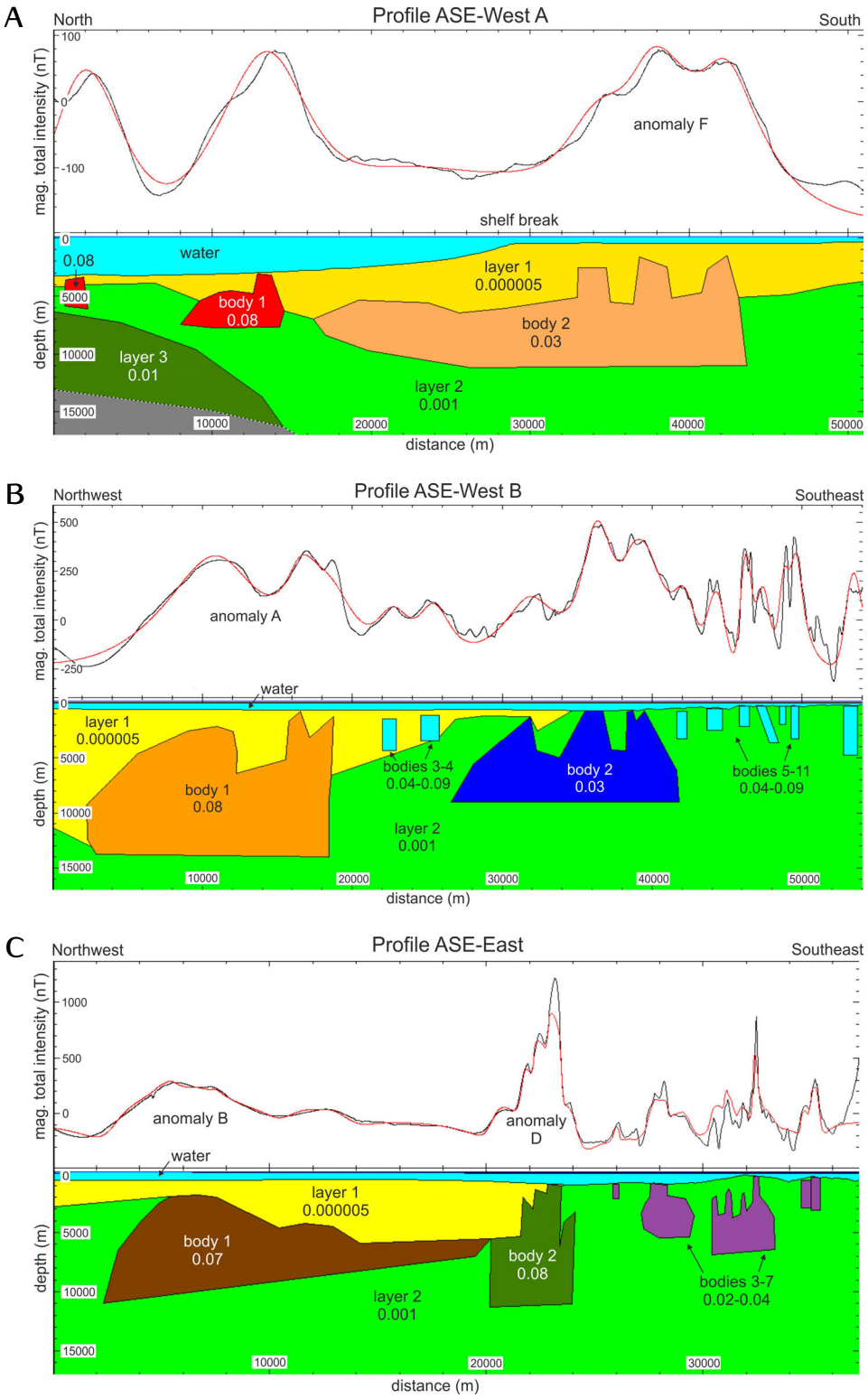

Figure 6.8. Results of magnetic 2D forward modelling along profiles (A) ASE-West A, (B) ASE-West B and (C) ASE-East. Black lines mark the measured anomaly data, and red lines represent the calculated model response, respectively. Model bodies are annotated with their respective magnetic susceptibility values in SI units. Profile locations are marked in the map of Fig. 6.7.

The NW–SE trending set of magnetic anomalies (including E and F of Fig. 6.7) is parallel to the so-called Peacock Gravity Anomaly northwest of Peacock Sound (Eagles et al. 2004a; Larter et al. 2002) which has been modelled with an underlying high-density body (Gohl et al. 2007b). It is interpreted as a magmatic zone, which interferes with the ENE–WSW trending rift structure (causing anomalies A to D). Modelling along transect ASE-West A indicates that the magnetic anomalies in this zone are caused by elongated bodies of similar depth, dimension and susceptibility as those causing the ENE–WSW trending anomalies. Consistent with the plate tectonic process described for the Bellingshausen Plate (Eagles et al. 2004a, b; Wobbe et al. 2012) we infer that these features represent mafic intrusions emplaced when the southern Bellingshausen Plate boundary was active between 80 and 61 Ma, giving rise to a distributed pattern of compressional, extensional and translateral movements at various stages of the activity of this boundary. The location of these magmatic units over a long time period in a very wide continent–ocean transition zone (Wobbe et al. 2012) suggests the Amundsen Sea Embayment may be the product of a long-lived zone of distributed crustal deformation, and that it may host multiple failed rifts and rift accommodation zones.

The third set of magnetic anomaly lineaments runs NNE–SSW, is rather subtle in amplitude, and more spatially limited than the other anomaly sets (Fig. 6.7). The broad magnetic anomaly low indicates the presence of a sedimentary sub-basin within the middle shelf. The margins of this low are asymmetrical; its southeastern margin is characterised by greater amplitudes and shorter wavelength anomalies than its northwestern margin. The basin, therefore, might be interpreted as having a half-graben geometry, with a bounding basement-involved normal fault zone on its southeastern edge, and a downthrown floor characterised by broad flexure northwestward away from the fault zone. The Paleogene plate tectonic model of Müller et al. (2007) predicts that a crustal boundary with this orientation would have responded to West Antarctica–East Antarctica relative motion along the WARS in right-lateral strike-slip motion. They suggest that this boundary extended from the Bentley Subglacial Trough and Byrd Subglacial Basin across western Ellsworth Land and the Thurston Island block, where it continues into the area of the dominant north-trending gravity anomaly lineaments of the Bellingshausen Sea. More consistent with the interpretation of a NNE-trending basin, however, the alternative plate tectonic model of Cande et al. (2000) predicts a strongly oblique right-lateral extension. In any case, the orientation of the identified sub-basin on the eastern ASE shelf (annotated as 'WARS rift basin' in Fig. 6.7) infers that it may be related to eastern WARS motion, possibly active as early as 55 Ma and lasting until at least 30 Ma before the zone of translateral deformation migrated or jumped eastward to join the triple junction at the spreading ridge colliding with the convergent margin of the southern Antarctic Peninsula as postulated by Müller et al. (2007). Somewhat more speculative, but not unrealistic, is a correlation of the sub-basin with

the dextral transtensional strain in western Marie Byrd Land observed by Siddoway (2008), who interprets this strain as an expression of an early WARS activity in the Late Cretaceous.

The shallow, small-sized bodies of very high susceptibilities between 0.02 and 0.09 SI unit on the inner shelf (Fig. 6.8B, C), are interpreted to be caused by a mafic dyke field related to the Cenozoic volcanic province of eastern Marie Byrd Land and western Ellsworth Land (e.g., LeMasurier 1990; Paulsen and Wilson 2010). Due to the presence of the nearby volcanic Hudson Mountains, one might expect volcanic, ~5 km radius cone-like features on the shelf as well, but the line spacing of the survey does not allow for the unequivocal identification or clear resolution of such features.

6.7 CONCLUSIONS

Newly acquired magnetic datasets from helicopter-borne and ship-borne surveys in 2006 and 2010 were used to generate levelled anomaly grids from the shelf of the Amundsen Sea Embayment. We applied grid processing, Euler deconvolution and 2D modelling for the analysis of magnetic anomaly patterns, identification of structural lineaments, and characterisation of magnetic source bodies.

The magnetic anomaly grid clearly outlines the boundary zone between the inner shelf where basement rocks crop out and a more thickly-sedimented middle to outer shelf. This sedimentation can be related to a long history of distributed extension inferred from the regional plate tectonic setting and from the presence of distinct zones of anomaly patterns and lineaments that can be associated with at least three tectonic phases in that history.

The first of these phases was the establishment of magmatic emplacement zones during Cretaceous New Zealand–Antarctic rifting and breakup (100–85 Ma). The second phase involved further magmatism in a distributed plate boundary zone between the Bellingshausen and Antarctic plates (80–61 Ma). Finally, the West Antarctic Rift System may have caused further extension in the region at later times (55–30 Ma?), focussed within a possible half-graben basin system bounded by NNE–SSW trending tectonic lineaments. Mafic dykes cross the inner shelf of the embayment and Pine Island Bay and may be associated with Cenozoic volcanism observed on land. They possibly relate to activities of one of the eastern branches of the West Antarctic Rift System.

Our magnetic data and the analysis show for the first time an identification of at least three sets of superposed tectonic lineaments in the Amundsen Sea Embayment shelf. The correlation of this observation to plate tectonic motion and associated magmatic emplacement in the West Antarctic realm suggests that the wide shelf of the Amundsen Sea Embayment may be the product of a long-lived zone of distributed crustal

deformation, and that it may host multiple failed rifts and rift accommodation zones.

By an example of a modelled intrusive body, this study also shows that such emplacement of resistive material acted as an obstacle for past ice flows across the inner shelf.

ACKNOWLEDGEMENTS

Many thanks to the ship crews, the helicopter pilots of Heli-Service GmbH and the geophysical teams for their support of acquiring the magnetic data during R/V *Polarstern* expeditions ANT-XXIII/4 (2006) and ANT-XXVI/3 (2010). We, in particular, thank Volker Leinweber, Sonja Suckro and Christina Mayr for their engagement in the helicopter-magnetic team of 2006. The collaboration with Prof. B. Tezkan of University of Cologne in co-supervising A. Denk's Diploma/MSc thesis, of which parts contributed to this paper, is gratefully acknowledged. This project is entirely supported by institutional funds of the Alfred Wegener Institute.

7 PUBLICATION IV

Anomalous South Pacific lithosphere dynamics derived from new total sediment thickness estimates off the West Antarctic margin

Florian Wobbe[1], Ansa Lindeque[2], and Karsten Gohl[1]

ABSTRACT

Paleotopographic models of the West Antarctic margin, which are essential for robust simulations of paleoclimate scenarios, lack information on sediment thickness and geodynamic conditions, resulting in large uncertainties. A new total sediment thickness grid spanning the Ross Sea–Amundsen Sea–Bellingshausen Sea basins is presented and is based on all the available seismic reflection, borehole, and gravity modeling data offshore West Antarctica. This grid was combined with NGDC's global 5 arc minute grid of ocean sediment thickness (Whittaker et al. 2013) and extends the NGDC grid further to the south. Sediment thickness along the West Antarctic margin tends to be 3–4 km larger than previously assumed. The sediment volume in the Bellingshausen, Amundsen, and Ross Sea basins amounts to 3.61, 3.58, and 2.78 million cubic kilometers respectively. The residual basement topography of the South Pacific has been revised and the new data show an asymmetric trend over the Pacific–Antarctic Ridge. Values are anomalously high south of the spreading ridge and in the Ross Sea area, where the topography seems to be affected by persistent mantle processes. In contrast, the basement topography offshore Marie Byrd Land cannot be attributed to dynamic topography, but rather to crustal thickening due to intraplate volcanism. Present-day dynamic topography models disagree with the presented revised basement topography of the South Pacific, rendering paleotopographic reconstructions with such a limited dataset still fairly uncertain.

Keywords: sediment isopach map; sediment thickness grid; sediment volume; residual basement depth; dynamic topography; paleotopography.

1 Alfred Wegener Institute, Helmholtz Centre for Polar and Marine Research, Am Alten Hafen 26, 27568 Bremerhaven, Germany
2 TGS Geophysical Company (UK) Limited, 1 The Crescent, Surbiton, Surrey, KT6 4BN, United Kingdom

7.1 INTRODUCTION

The accurate reconstruction of paleotopography is the main prerequisite for robust simulations of paleoclimate scenarios. Current paleotopographic models contain large uncertainties due to absent or sparse sediment thickness data and constraints on geodynamic conditions. Since the Southern Ocean plays an important role in global climate processes, we assess the sedimentary and geodynamic conditions of the Southern Pacific to ascertain these essential factors for modern paleotopographic reconstructions.

We present an improved sediment thickness grid for the West Antarctic margin, which is now based on all the available seismic reflection, borehole, and gravity modeling data. This new grid spans the Antarctic Peninsula, Bellingshausen Sea, Amundsen Sea, and Ross Sea and links to Whittaker et al.'s (2013) data off Victoria Land. In the first part of this publication, we compare our results to previous work and discuss possible implications for paleotopography and paleoclimate reconstructions of Antarctica.

In the second part, we analyze and re-evaluate the Late Cretaceous to present lithosphere dynamics of the South Pacific after the final breakup of Gondwana. The rifted continental margins of New Zealand and West Antarctica experienced different tectonic histories: As New Zealand drifted away from Antarctica it was subjected to excess tectonic subsidence of 500–900 m, with a maximum during the interval 70–40 Myr (Spasojevic et al. 2010; Sutherland et al. 2010). The conjugate Marie Byrd Land margin, by contrast, was deformed by movement of the Bellingshausen plate relative to Antarctica (Wobbe et al. 2012), affected by intraplate volcanism (Kipf et al. 2013), and covered by large amounts of glacial sediments (e.g., Rebesco et al. 1997; Scheuer et al. 2006a). The West Antarctic margin and its adjacent seafloor is currently more than 1000 m shallower than the conjugate New Zealand margin. It has been suggested that mantle upwelling following the Gondwana subduction cessation could have caused this anomalously high topography (e.g., Storey et al. 1999; Sieminski et al. 2003; Winberry and Anandakrishnan 2004; Finn et al. 2005; Spasojevic et al. 2010; Sutherland et al. 2010). In order to test this hypothesis with new data, we determined the sediment-corrected basement topography for the South Pacific and compared it to (i) an empirical sediment-corrected depth model from the North Pacific (Crosby et al. 2006), (ii) various dynamic topography models (e.g., Ricard et al. 1993; Steinberger 2007; Conrad and Husson 2009; Spasojevic and Gurnis 2012; Flament et al. 2013), and (iii) a current mantle shear wave velocity model (Schaeffer and Lebedev 2013). The differences between the dynamic topography models are discussed and the implications for reconstructing the South Pacific paleobathymetry and paleotopography are highlighted.

7.2 SEDIMENT THICKNESS GRIDS OF THE WEST ANTARCTIC MARGIN

We derived new 5 km and 5 arc minute resolution sediment thickness grids from seismic reflection and refraction data, from gravity models, and from data of selected drill sites on the West Antarctic margin of the Pacific (Ross Sea–Amundsen Sea–Bellingshausen Sea–Antarctic Peninsula).

7.2.1 Sediment thickness calculation

Total sediment thickness estimates of the continental margin and the deep ocean floor are largely based on multichannel seismic reflection surveys (Figure 7.1). We used the two-way travel times (TWT) between the seafloor and the acoustic basement reflections along seismic reflection transects available from the Antarctic Seismic Data Library System (SDLS, Wardell et al. 2007, Table 7.1 in the supplement) and along recently acquired and processed seismic profiles (e.g., ANT-18/5a, ANT-23/4, and ANT-26/3: Scheuer et al. 2006a, b; Lindeque and Gohl 2010; Uenzelmann-Neben and Gohl 2012; Wobbe et al. 2012; Gohl et al. 2013b; Kalberg and Gohl 2014).

The TWT values, 2T in s, were converted to depth, Z in km, using Carlson et al.'s (1986) empirical relation $Z = 3.03\ln(1 - 0.52T)$. This method has been applied to seismic data acquired along the Antarctic Peninsula in past work (Rebesco et al. 1997; Scheuer et al. 2006a, b). Carlson et al.'s (1986) TWT–depth relationship is calibrated for sediments up to 1.4 km thick (~1.4 s TWT) only and the sediment thickness is considerably overestimated for TWTs larger than 2.8 s. This affects <5 % of the data points, mainly located on the continental rise–slope transition. Due to the lack of area-wide seismic velocity models or downhole velocity measurements at drilling sites, we have to assume the acoustic velocity of sediments thicker than 2.8 s TWT.

P-wave velocities of 5–6 km thick sediments on the continental rise in polar regions typically range from 1800 to 4000 m s^{-1} (e.g., West Greenland, Chian et al. 1995; Suckro et al. 2012) or even 4200 m s^{-1} (e.g., East Greenland, Voss and Jokat 2007). On the Amundsen Sea continental rise, sediment layer interval velocities from a P-wave refraction model (Lindeque and Gohl 2010; Kalberg and Gohl 2014) and from stacking velocities (Gohl et al. 2007b; Uenzelmann-Neben and Gohl 2012; Gohl et al. 2013b) range from 1600 to 4200 m s^{-1}. We determined the best fitting average acoustic velocity of sediments thicker than 2.8 s TWT to be 2818 m s^{-1} and converted all TWT values greater than 2.8 s to depth using this velocity.

The seismic data coverage of the Amundsen Sea Embayment shelf (Gohl et al. 2013b) is better than what the profiles used for this publication imply (Figure 7.1). However, only few seismic lines reveal the top of basement, and those which do not were excluded. The limit of the sedimentary cover

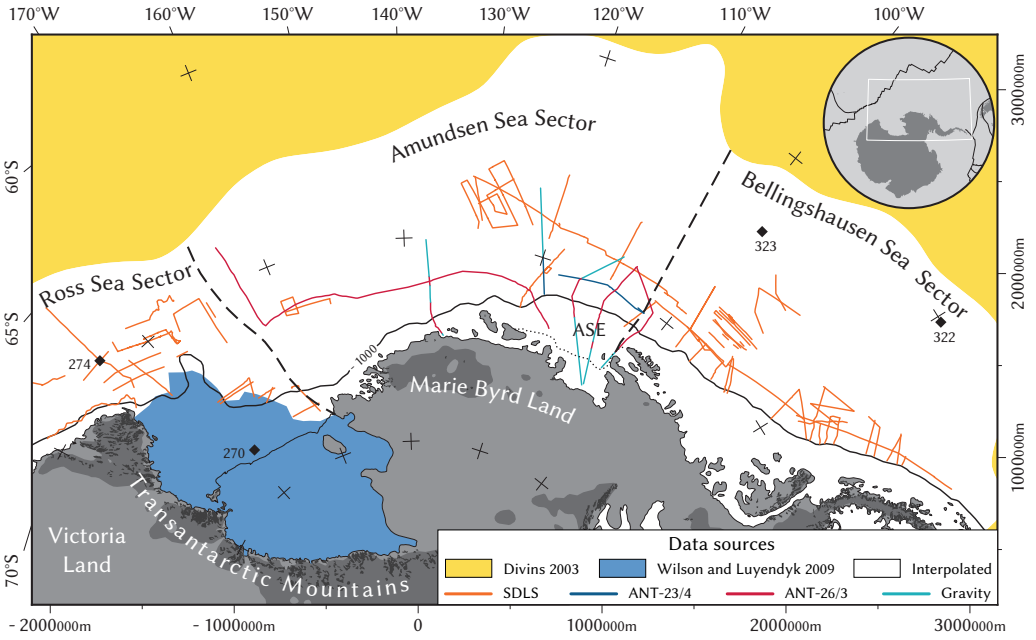

Figure 7.1. Data sources used for compiling total sediment thickness and estimating sediment volumes. Areas based on gridded external data sources filled with solid colors (Divins 2003; Wilson and Luyendyk 2009). Data collected on transects are mostly multichannel seismic-reflection data available from the Antarctic Seismic Data Library System (SDLS, Wardell et al. 2007) and recent publications (ANT-23/4 and ANT-26/3: Scheuer et al. 2006a; Lindeque and Gohl 2010; Uenzelmann-Neben and Gohl 2012; Wobbe et al. 2012; Gohl et al. 2013b; Kalberg and Gohl 2014). Some sediment thickness estimates in the Amundsen Sea sector are based on 2D gravity models (Wobbe et al. 2012). Dotted line outlines limit of sedimentary cover on inner Amundsen Sea Embayment (ASE) shelf (Gohl et al. 2013b). Polar stereographic projection with central meridian of 138°W and latitude of true scale at 71°S referenced to WGS84.

approaching the inner shelf is well documented (e.g., Gohl et al. 2013a, b, dotted line in Figure 7.1).

7.2.2 Data merging and gridding

In order to extend data coverage of the mapped basement horizons from multichannel seismic data (Figure 7.1) to the Ross Sea region, we incorporated total sediment thickness above the acoustic basement from Cooper et al. (1991). Wilson and Luyendyk (2009), whose data we included as well, estimated sediment thickness under the Ross Ice Shelf by extrapolating thickness trends in the Ross Sea from gravity anomalies. Four Deep Sea Drilling Project (DSDP) boreholes in the area of interest reach the basement. Their borehole depth measurements complement the sediment thickness data from the Ross Sea (sites 270 and 274, Hayes et al. 1975) and fill in the gaps of the most distal areas along the Antarctic Peninsula (sites 322 and 323, Hollister et al. 1976). Data from other DSDP, Ocean Drilling Project (ODP), and Antarctic Drilling (ANDRILL) drill sites along the West

Antarctic margin were discarded because these boreholes do not yield the basement. Some sediment thickness estimates in the Amundsen Sea sector are based on a P-wave refraction model (Lindeque and Gohl 2010; Kalberg and Gohl 2014) and two-dimensional gravity models from Wobbe et al. (2012). The latter provide sediment thickness estimates along the axial extensions of adjacent seismic lines (light blue lines in Figure 7.1). The limit of the sedimentary cover on the Amundsen Sea Embayment shelf was extrapolated east onto the Bellingshausen Sea shelf guided by gravity anomalies. We allocated values from the original ocean sediment thickness grid of the National Geophysical Data Center (NGDC, Divins 2003) to areas further north and distant from the constrained data sources. These areas are roughly defined by the 100 m sediment isopach in the NGDC sediment thickness grid.

The compiled total sediment thickness point-based data (cf. Figure 7.11 in the supplement) were pruned by calculating 10 by 10 km block medians to remove short wavelengths and to avoid spatial aliasing during gridding. To fill the gaps between the points (white area in Figure 7.1), the dataset was gridded using Smith and Wessel's (1990) continuous curvature splines algorithm with a tension factor of 0.2 to suppress local maxima and minima. Although data along the coastline were tapered to zero, we had to introduce about 150 further estimates of total sediment thickness to maintain a sensible appearance of the grid in areas remote from constrained sediment thickness. This is mostly the case, where the acoustic basement could not be identified on seismic profiles crossing the continental shelf. Our estimates are either plausible assumptions based on local geomorphology or inferred from the nearest constrained value.

Short range variations from the sediment thickness grid were removed by a second-order Butterworth low-pass filter with a cutoff wavelength of 100 km. We chose the Butterworth filter because it has no ripple in the passband at the expense of a relatively wide roll-off (Oppenheim and Schafer 2009). The final grid was further resampled by bicubic interpolation to 5 km resolution. This new total sediment thickness grid is available in Antarctic Polar Stereographic Projection with a latitude of true scale at 71°S, referenced to WGS84 (Figure 7.2).

The new regional Southern Pacific total sediment thickness grid was combined with the recently updated global sediment thickness grid of NGDC (Divins 2003; Whittaker et al. 2013) to create an updated 5 by 5 minute global grid of ocean sediment thickness. The blending of the datasets was done by interpolating a 40 km buffer between the global and our smaller, regional grid, using continuous curvature splines with a tension factor of 0.2. The new total sediment thickness grids are available from PANGAEA (Wobbe et al. 2014b).

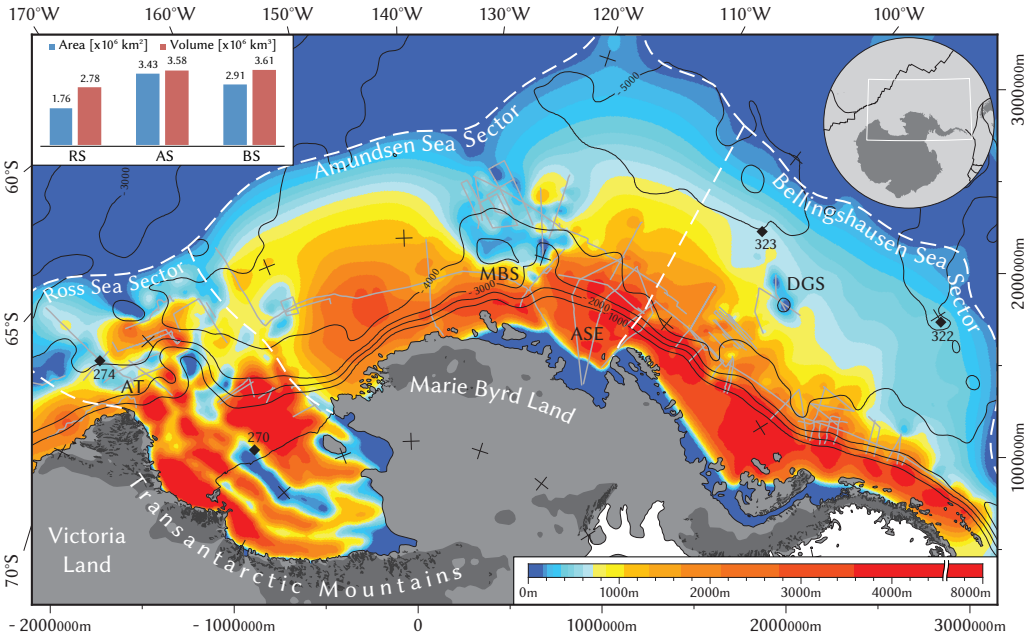

Figure 7.2. The new total sediment thickness map of the Pacific margin of West Antarctica. Isopachs are color coded, contour lines indicate water depth in meter. White dashed lines delineate sediment catchment areas for the Ross Sea (RS), Amundsen Sea (AS) and Bellingshausen Sea (BS) basins. Compacted sediment volume estimates for these regions are illustrated in the top left corner. Black diamonds indicate locations of DSDP sites taken into account. Darker gray shading inland shows topography above 500 m. Rock outcrops from SCAR Antarctic Digital Database. AT – Adare Trough, DGS – De Gerlache Seamounts, MBS – Marie Byrd Seamounts. Polar stereographic projection with central meridian 138°W and true scale at 71°S.

7.2.3 Comparison to previous work and uncertainties

The presented total sediment thickness grid (Figure 7.2) covers an area of more than 8 million square kilometers and reveals major differences when compared to the sediment thickness compilation of Divins (2003). Divins' (2003) original NGDC global sediment thickness grid has recently been updated for the Australian–Antarctic region (Whittaker et al. 2013), as it became apparent that sediment thickness along the continental margins has been underestimated by more than 2000 m. The current NGDC grid, which excludes areas south of 70°S, largely underestimates sediment thickness off the Antarctic Peninsula and off Marie Byrd Land while slightly overestimating total sediment thickness around the De Gerlache Seamounts and the Marie Byrd Seamounts (cf. Figures 7.12 and 7.13 in the supplement). Sediments in West Antarctic waters are approximately 4–4.8 km thick around the continental slope (approximately −1000 m contour in Figure 7.2), which is about 3 km thicker than what Divins' (2003) NGDC compilation indicates. Sediments reach a maximum thickness of 6–8 km in glacial troughs on the Ross Sea shelf but taper off to less than 2 km further north. Total sediment thickness is estimated as larger than 4 km off the Antarctic Peninsula but less than 2–2.5 km off the coast of

Marie Byrd Land and Victoria Land (west of DSDP site 274), and is maintained farther west (cf. Whittaker et al. 2013). Data from several proprietary seismic profiles (R/V Tangaroa, TAN0207 survey for the New Zealand UNCLOS program) off Chatham Rise indicate that Divins' (2003) sediment thickness estimates of West Antarctica's conjugate margin are accurate and do not compromise our residual basement depth calculation south of New Zealand in Section 7.3.

The mean West Antarctic sediment thickness (volume per deposition area ratio) varies slightly. It is largest in the Ross Sea and Bellingshausen Sea sectors (1.6 and 1.2 km), consistent with the very large flux associated with glacial sediment transport, and decreases to about 1.0 km in the Amundsen Sea sector. The total sediment volume amounts to 10 million cubic kilometers of which approximately 70 % is equally distributed between the Amundsen and Bellingshausen Sea sectors (3.58 resp. 3.61×10^6 km^3), and the remaining 30 % is spread across the Ross Sea sector (2.78×10^6 km^3).

Neglecting any margin parallel sediment transport, our calculations indicate that most of the terrigenous sediment influx from the West Antarctic originates from the smallest source area—the Antarctic Peninsula (15 % of all area draining into the South Pacific). To illustrate this we determined the hypothetical minimum height of a sediment pile that would cover West Antarctica if all sediments were returned to their source areas by applying Wilson et al.'s (2012) estimates for in situ sediment density (1.95–2.1 g cm^3) and source rock density (2.6 g cm^3). DSDP and ODP boreholes around Antarctica yield a maximum pelagic fraction of 15 %, which is not restored to the continent in this calculation. The terrigenous sediment source areas, draining into our three West Antarctic sectors, were determined from Zwally et al.'s (2012) present-day drainage system divides within the grounding line and west of the Transantarctic Mountains. Assuming these drainage system divides and their areas did not change with time, our calculations predict that sediments from the Ross Sea sector would pile up to a thickness of 2.9 km (or 640 m if source areas of East Antarctica are considered as well). Sediments from the Amundsen Sea sector would accumulate to a thickness of 3.8 km, and those from the Bellingshausen Sea sector would reach a height of 11 km. The very large value for the Bellingshausen drainage area can be explained by West Antarctica's high paleotopography (Wilson et al. 2012) which led to more erosion during the glacial. Earlier, subduction tectonics adjacent to the Antarctic Peninsula (e.g., Larter et al. 2002) may also have fostered an increased sediment influx into the basin.

Wilson and Luyendyk (2009) estimated a sediment volume of 2.0×10^6 km^3 above the oldest Ross Sea unconformity (RSU6, Oligocene and younger, e.g., Cooper et al. 1991). Our calculation takes into account a c. 30 % larger Ross Sea deposition area and additional sediment thickness estimates along SDLS seismic reflection transects. Even though, the new sediment volume estimates above RSU6, 2.08×10^6 km^3, are not signifi-

cantly larger, because the added distal deposition areas contain much less sediment than the ones in the central and western Ross Sea.

Although Scheuer et al.'s (2006a) sediment thickness grid of the Bellingshausen Sea and eastern Amundsen Sea shows east–west directed low frequency oscillation artifacts and occasionally large local minima and maxima, it compares reasonably well to our results in that the total sediment volume deviates by about 0.35×10^6 km^3 (cf. Figures 7.12 and 7.13 in the supplement). This similarity can be attributed to the common database constraining the sediment thickness along seismic profiles, whereas the deviation is likely caused by a varied degree of data pruning and low-pass filtering.

The accuracy of the presented total sediment thickness grid varies proportionally to the distribution and abundance of seismic data offshore West Antarctica (Figure 7.1). To a lesser degree, the sediment thickness data is affected by the TWT to depth conversion uncertainties rooted in the lack of seismic velocity models and drilling sites with key constraining downhole velocity data. The Ross Sea area is exceptionally well surveyed with a densely distributed seismic profile network and two basement yielding DSDP sites provide good calibration. The continental rise and slope within all sectors, except the westernmost and deeper Amundsen Sea are well mapped. In other places, where total sediment thickness is less constrained due to the absence of seismic reflection and borehole data, the thickness was interpolated over several hundred to thousand kilometers. Fortunately, most of these less constrained areas fall into the abyssal plains north of 70°S in the western Amundsen Sea sector, and north of 65°S in the eastern Amundsen Sea and Bellingshausen Sea sectors, where DSDP sites 322 and 323 hardly reported any sediment cover. Sediment thickness on the shelves of the Bellingshausen Sea and western Amundsen Sea could not be constrained by data but were based on observations from the central and eastern Amundsen Sea shelves. The largest uncertainties in the total sediment thickness grid are the limit of sedimentary cover and the sediment thickness on the inner Bellingshausen Sea.

7.3 AGE OF THE OCEANIC LITHOSPHERE AND BASEMENT DEPTH

In Figures 7.3 to 7.5 we present the derived set of digital grids that represent the South Pacific ocean floor ages, sediment-corrected basement depth, and oceanic residual basement depth. Collectively these provide an opportunity to study lithosphere dynamics of the West Antarctic margin. The residual basement depth (Figure 7.5) is the difference between the sediment-unloaded basement depth (Figure 7.4) and the predicted basement depth. The latter was derived from converting the crustal age

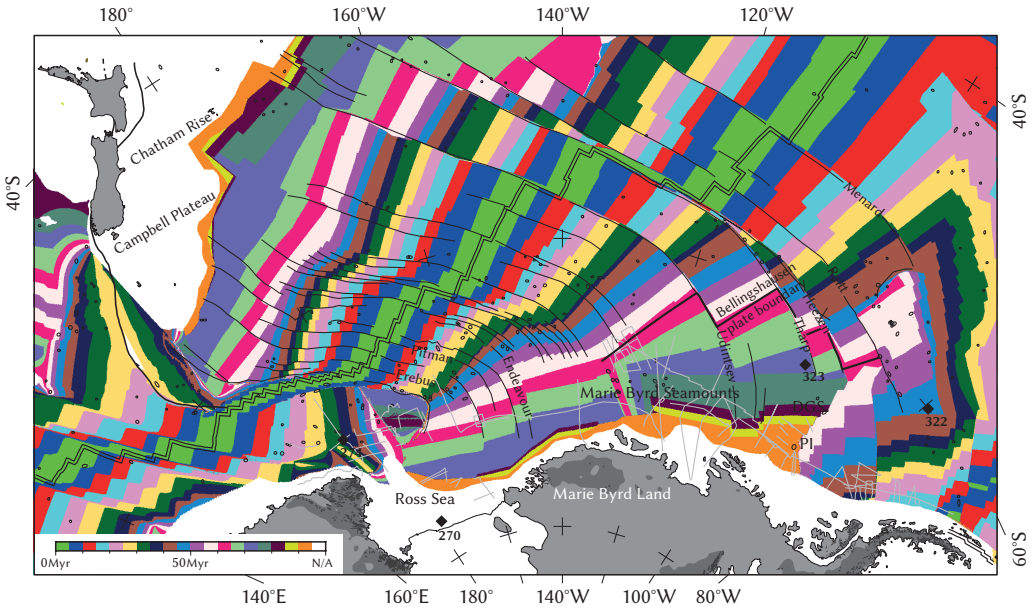

Figure 7.3. Age of the oceanic lithosphere (Wobbe et al. 2012) overlain with locations of seamounts (black circles, Global Seamount Database, Kim and Wessel 2011), fracture zones (black lines), and seismic and gravity profiles (light gray lines). Abbreviations same as Figure 7.2 and PI – Peter I Island. Lambert conformal conic projection with central meridian 160°W and standard parallels 75°S and 69°S referenced to WGS84.

(Figure 7.3, Wobbe et al. 2012) to basement depth by using Crosby et al.'s (2006) North Pacific depth–age relationship, $d = -2821 - 315\sqrt{t}$.

We decided to apply Crosby et al.'s (2006) model for converting age to depth because it is based on sediment-corrected basement depths from the Pacific, and because it is unbiased by igneous crustal thickening. Therefore, it is considered suitable for detecting anomalies in the basement depth caused by, e.g., hotspot swells, plateaus, and seamounts. It should be noted however, that the differences between this chosen model and models proposed by other authors such as Stein and Stein's (1992) GDH1 depth–age relationship are marginal (cf. profile 6 in Figure 7.7), and in the context of the scale of this study considered negligible for studying large-scale basement depth anomalies (see Müller et al. 2008). In brief, the differences between GDH1 and Crosby et al.'s (2006) depth–age relationship range from −32 to 360 m for ages less than or equal to 90 Myr. The mean difference is 87 m and the median difference equals 55 m during this time interval. Both models are remarkably similar for ages younger than 80 Myr, which encompasses more than 96 % of the area of interest (Figure 7.3). Subsequently, GDH1 follows a shallower trend than Crosby et al.'s (2006) depth–age relationship.

Sediment loading was estimated from our total sediment thickness grid (Figure 7.2), using the relationship between sediment thickness and isostatic correction from Sykes (1996). We calculated the sediment-unloaded basement depth by subtracting the isostatic effect using the water depths

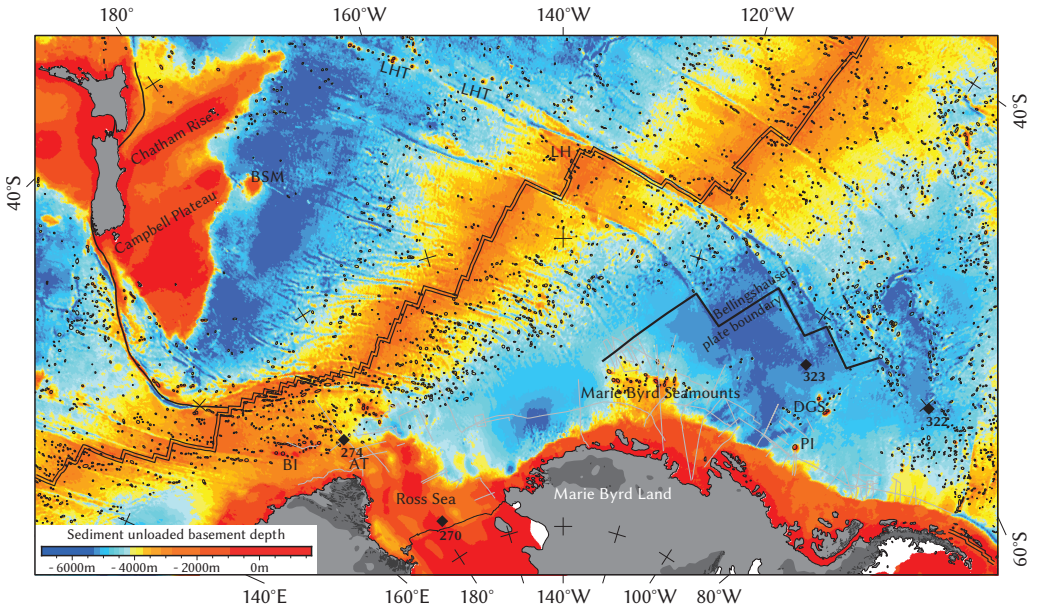

Figure 7.4. Sediment-unloaded basement depth determined by applying the correction from Sykes (1996) using the sediment thickness from Figure 7.2. Overlain with locations of seamounts (black circles, Global Seamount Database, Kim and Wessel 2011). Abbreviations same as in previous figures and BI – Balleny Islands hotspot/Charcot Ridge, BSM – Bollons Seamount, LH – Louisville hotspot, LHT – Louisville hotspot trail. Lambert conformal conic projection with central meridian 160°W and standard parallels 75°S and 69°S.

of the International Bathymetric Chart of the Southern Ocean (IBCSO, Arndt et al. 2013).

7.3.1 Residual basement depth anomalies

The residual basement depth of the South Pacific (Figure 7.5) is largely positive, with a few exceptions along the Udintsev, Hazen and Tharp fracture zones (labeled in Figure 7.3), southeast of the Campbell Plateau, and northwest of the Antarctic Peninsula. A positive residual basement depth anomaly indicates that the sediment-unloaded basement is shallower than expected based on Crosby et al.'s (2006) half-space cooling model. The magnitude of the residual basement depth anomaly and its irregular surface tend to correlate with hotspot trails, and with the size and abundance of seamounts. The sediment-unloaded basement is generally shallower in proximity to Antarctica. This is reflected in the values of the mean residual basement depth of the Antarctic and Pacific plate, being 485 and 204 m respectively. The depth variation is best expressed by the root mean square, 699 and 394 m respectively.

Figure 7.6 illustrates the sediment-unloaded basement depth and the predicted basement depth on selected profiles that are parallel to flow lines crossing the Pacific–Antarctic Ridge. The profiles, which were selected carefully to avoid undulations near fracture zones, confirm that the

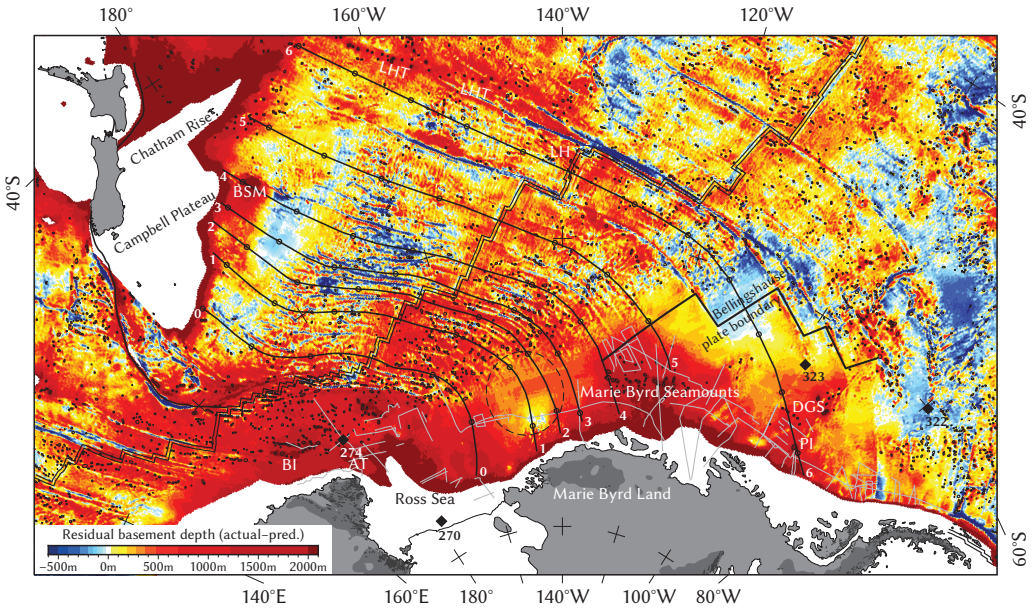

Figure 7.5. Residual basement depth of the oceanic crust determined by calculating the difference between sediment-unloaded basement depth (Figure 7.4) and predicted basement depth from applying Crosby et al.'s (2006) North Pacific depth–age relationship to the age distribution from Figure 7.3. Profiles 0–6 along flow lines shown in Figures 7.6, 7.7, and 7.10. Small circles along profiles placed 500 km apart. Dashed circle delineates Endeavour Anomaly. Abbreviations same as in previous figures. Lambert conformal conic projection with central meridian 160°W and standard parallels 75°S and 69°S.

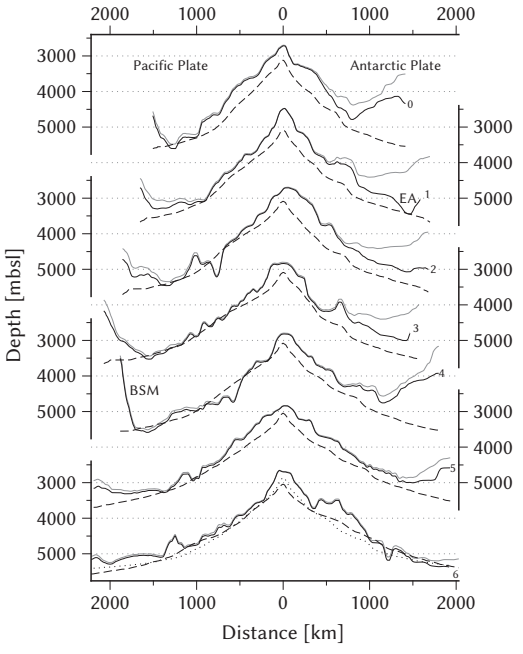

Figure 7.6. IBCSO/GEBCO_08 bathymetry (gray line), sediment-unloaded basement depth from Figure 7.4 (solid line), and predicted basement depth (dashed, Crosby et al. 2006) along profiles 0–6 across the Pacific–Antarctic Ridge (Figure 7.5). Predicted basement depth from Stein and Stein's (1992) depth–age relationship (dotted line, profile 6, cf. Section 7.3). Abbreviations same as in previous figures and EA – Endeavour Anomaly.

sediment-corrected basement depth of the Antarctic plate is considerably higher than that of the Pacific plate. Due to the excessive sediment cover offshore West Antarctica, seafloor topography is more than 1000 m shallower compared to the conjugate New Zealand margin (Figure 7.6). This is reflected by the isostatic correction for sediment thickness, which varies

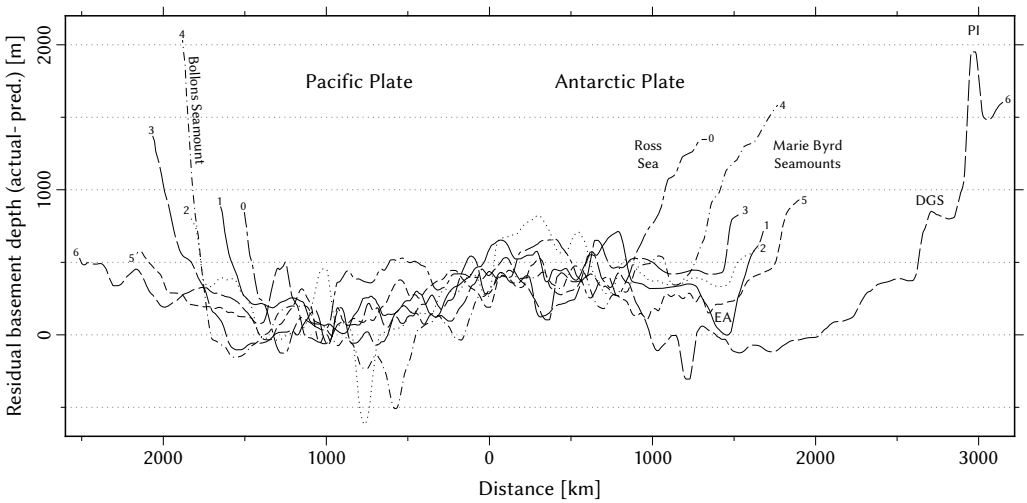

Figure 7.7. Residual basement depth vs. distance from Pacific–Antarctic Ridge along profiles from Figure 7.5. Abbreviations same as in previous figures.

from 100 to 500 m south of the Campbell Plateau and Chatham Rise but then reaches 800–1500 m and, occasionally, more than 2000 m in the Ross Sea and Amundsen Sea. Despite the large difference in seafloor topography between the two conjugate margins, the sediment-unloaded basement depth, and hence the residual basement depth off Marie Byrd Land, usually differs by less than 250 m (Figure 7.7 and Figure 7.14 in the supplement). Confined areas in the western Ross Sea, Marie Byrd Seamount area, and the Balleny Islands hotspot area south of the Pacific–Antarctic Ridge show residual basement depths exceeding 2000 m. Figure 7.7 demonstrates that the residual basement depth usually oscillates between 0 and 500 m, and that a local maximum is located 200–700 km southeast from the Pacific–Antarctic Ridge in an area with a significantly higher seamount density (Global Seamount Database, Kim and Wessel 2011, Figure 7.5). Another distinctive feature within a circular area north of Marie Byrd Land is defined by an anomalously deep sediment-unloaded basement depth with values 500 m below the surrounding region. We name this the Endeavour Anomaly. The acoustic basement topography and sediment thickness at the Endeavour Anomaly are only constrained along a single west–east directed seismic profile across the Endeavour Fracture Zone (cf. Figures 7.2 and 7.1). Further seismic data are not available in this region. The circular shape of the Endeavour anomaly is attributable to the interpolation algorithm used to grid the sediment thickness data, and its north–south expansion cannot be resolved.

7.3.2 Residual basement depth vs. seafloor roughness

Models explaining the morphology of mid-ocean ridge systems suggest that basement roughness depends on seafloor spreading rate and that an abrupt roughness intensification develops below a full spreading rate

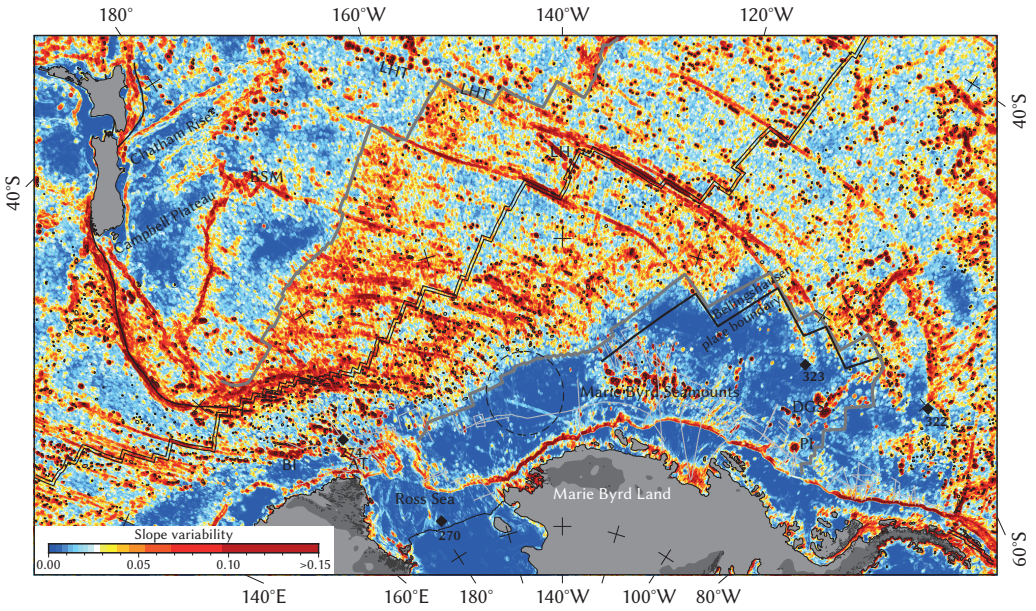

Figure 7.8. Seafloor roughness computed by calculating the slope variability, $S_v = S_{max} - S_{min}$, over a $10' \times 10'$ roving window from IBCSO/GEBCO_08 bathymetry. Thick gray lines are 55 Myr isochrons.

threshold of 60–70 mm Myr^{-1} (Small and Sandwell 1989; Malinverno 1991). This effect is readily visible in the roughness map in Figure 7.8, where morphologically flat basement close to New Zealand and its conjugate margin off West Antarctica, formed along an initially fast spreading Pacific–Antarctic Ridge (>60 mm Myr^{-1}, Wobbe et al. 2012). Other parts of the ocean floor with large slope variability were formed less than 55 Myr ago when full-spreading velocities dropped below 60 mm Myr^{-1} (e.g., Larter et al. 2002; Eagles et al. 2004a; Wobbe et al. 2012).

In the South Pacific, increased roughness is additionally caused by confined geological features including oceanic troughs, ridges, fracture zones, and seamounts. Cenozoic magmatism has been attributed to increased heat flow from the mantle (e.g., LeMasurier 1990; Rocchi et al. 2002; Finn et al. 2005; Kipf et al. 2013). While seamounts such as the Balleny Islands, Marie Byrd Seamounts, De Gerlache Seamounts, and Peter I Island are limited morphological surface expressions of these magmatic centers, oceanic crust may respond to the underlying heat source with thermal uplift. Consequently, residual basement depth and seafloor roughness of the Antarctic plate often correlate (Figures 7.5 and 7.8). However, the area with increased roughness between Campbell Plateau and Pacific–Antarctic Ridge, for example, shows an opposing trend. Hence, seafloor roughness alone cannot be used to explain the residual basement depth distribution.

7.3.3 Residual basement depth vs. shear wave velocity

Schaeffer and Lebedev (2013) recently published a global tomographic shear wave velocity model of the upper mantle, which extends to a depth

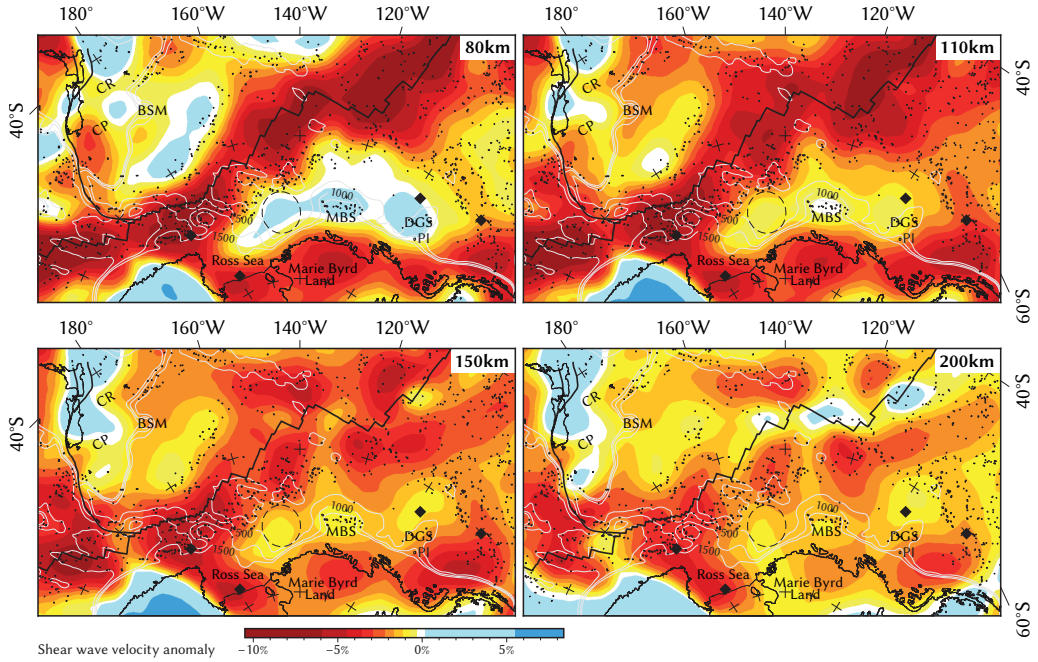

Figure 7.9. Shear wave velocity anomalies (SL2013sv model, Schaeffer and Lebedev 2013) of the upper mantle at 80, 110, 150, and 200 km depth with reference velocities of 4.38, 4.38, 4.39, and 4.45 km/s. Residual basement depth contours (500, 1000 and 1500 m) in gray.

of 660 km. Figure 7.9 displays the shear wave velocity anomaly of the uppermost mantle in four slices at different depths.

As expected, low shear wave velocities, which indicate increased heat flow in the mantle, coincide well with magmatic centers of Marie Byrd Land, Balleny Islands, and the Ross Sea area. In contrast, the Marie Byrd Seamounts, the De Gerlache Seamounts, and Peter I Island are underlain by mantle with anomalously high shear wave velocities that by implication may mean lower heat flow in the mantle. In these magmatic provinces off West Antarctica, the heat does not stem from the mantle directly below, as is the case in underplating, but may be provided by an upper mantle convective flow from warm mantle beneath the continental lithosphere of Marie Byrd Land (continental-insulation flow, Kipf et al. 2013, and references therein).

The distribution of seamounts that did not evolve from continental-insulation flow (e.g., Balleny Islands) matches the low shear wave velocity anomaly remarkably well. Similarly, the residual basement depth (Figures 7.5) matches the shear wave velocity anomaly too. Noticeably, the shear wave velocity anomaly minimum below the mid-ocean ridges shifts asymmetrically in all depth slices. Particularly south of 60°S, the shear wave velocity anomaly is located 500 km south of the Pacific–Antarctic Ridge, where it also coincides with a local maximum of the residual basement depth (Figures 7.7 and 7.10).

We chose Schaeffer and Lebedev's (2013) shear wave tomography as the most recently updated global mantle tomography model with ma-

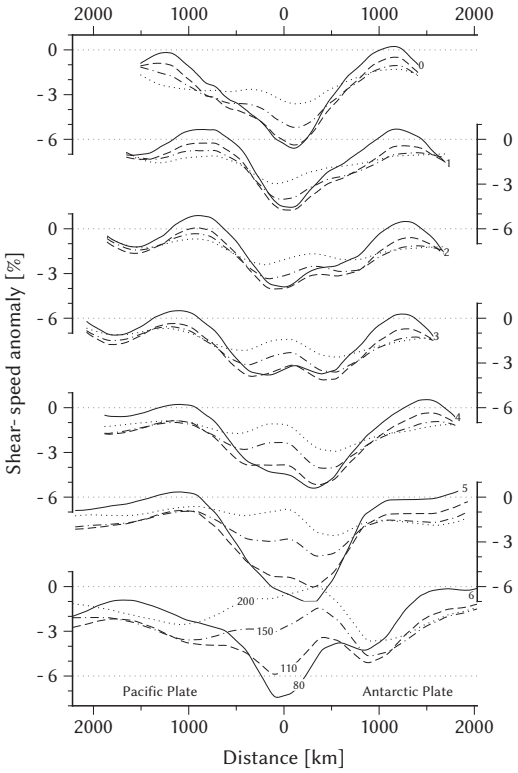

Figure 7.10. Shear wave velocity anomalies of the upper mantle at 80, 110, 150, and 200 km depth vs. distance from Pacific–Antarctic Ridge along profiles 0–6 from Figure 7.5.

jor improvements on the resolution in oceanic regions and the Southern Hemisphere. However, the amplitude of the shear wave velocity anomaly in the study area decreases with depth and deviates less than 1 % from zero at depths greater than 400 km. Distinct trends over the region or local extrema are absent. Well resolved shear wave velocity anomalies in this depth with an amplitude of less than 1 % would require seismic velocity uncertainties better than 50 m s^{-1}.

7.4 DISCUSSION

Improved paleoclimate and paleo-ice sheet models are subject to known limitations of current sediment volume approximations. With more robust sediment estimates, future reconstructions of paleotopography will improve our understanding of Antarctica's glaciation history. For instance, Wilson et al. (2013) estimated, based on the denudation history, that the total Antarctic ice volume since the Eocene–Oligocene transition was more than 1.4 times greater than previously assumed. This study and a recent work from Whittaker et al. (2013) both indicate that sediment thickness along the Antarctic margin has largely been underestimated. The landmass reduction of Antarctica due to erosion, therefore, has probably been larger than predicted (Wilson et al. 2012), and even larger ice sheet volumes may have covered Antarctica in the early times of glaciation. Of course, additional identifications of the volume and distribution of the pre-glacial to glacial components in the offshore sedimentary records are required

in order to reconstruct the past topography for periods associated with large changes in climate proxies, such as the Eocene–Oligocene transition. However, the construction of pre-glacial to glacial sediment thickness grids is beyond the scope of this publication.

The previous section shows that there is a connection between residual basement depth and shear wave velocity on the one hand and magmatic processes on the other. Residual basement depth should also resemble the present-day dynamic topography. As opposed to isostatic topography resulting from density and thickness contrasts in the lithosphere, dynamic topography refers to the earth surface elevation effect due to mantle density inhomogeneities (e.g. Flament et al. 2013, and references therein). It develops over tens of millions of years and can exhibit several hundreds of meters in surface elevation difference at long wavelengths. Dynamic topography models are derived from the present-day density structure of the mantle, subduction history, and plate-tectonic reconstructions. Uncertainties lie, for example, in the varying resolution of regional mantle convection models derived from global seismic tomography. As published dynamic topography models over the Southern Pacific suffer from large uncertainties, we compared our results with five different models (Ricard et al. 1993; Steinberger 2007; Conrad and Husson 2009; Spasojevic and Gurnis 2012; Flament et al. 2013, Figure 7.15 in the supplement). These global studies of dynamic topography are limited to a lateral resolution of about 3000–5000 km. There are regional mismatches at scales below 10 000 km and even inverse correlations, especially in the Pacific realm (Flament et al. 2013). None of the five above mentioned dynamic topography models resolve local residual basement anomalies in the South Pacific. Although absolute amplitudes vary as much as 1500 m, all models propose a topographic high beneath the Pacific Plate, north of 60°S/150°W, which is in contrast with the residual basement depth (Figure 7.5) and the shear wave anomaly (Figure 7.9). Depending on the chosen model, dynamic topography beneath the Antarctic Plate and West Antarctica varies between −500 and 1000 m, and the magnitude beneath New Zealand is usually consistent with that beneath Marie Byrd Land.

Mantle upwelling following the Gondwana subduction cessation around 100 Myr (e.g. Laird and Bradshaw 2004) has been suggested, but its extension beneath the West Antarctic margin remains unclear (e.g., Storey et al. 1999; Sieminski et al. 2003; Winberry and Anandakrishnan 2004; Finn et al. 2005). However, basement depth, mantle shear wave velocity anomaly (Schaeffer and Lebedev 2013), and Kipf et al.'s (2013) continental-insulation flow model show that upper mantle convective flow is solely confined to an area located beneath Marie Byrd Land and the Ross Sea. Spasojevic et al. (2010) and Sutherland et al. (2010) constructed models of Late Cretaceous to Cenozoic mantle flow, attributed to low density material above the Gondwana slab graveyard beneath Antarctica, to predict dynamic topography. Their models, which are based on present-day bathymetry, explain the high topography of the Ross Sea and Marie Byrd Land region

as well as anomalous postrift Campbell Plateau subsidence. Our findings complement Sutherland et al.'s (2010) dynamic topography model, and our total sediment thickness estimates confine areas of anomalous basement elevation more precisely. For example, Sutherland et al. (2010) attributed excess topography (0.5–2.0 km) offshore Marie Byrd Land and in the Ross Sea region to dynamic topography. Our results confirm this for the Ross Sea as well as the Balleny Islands hotspot area. However, the residual basement depth off Marie Byrd Land does not exceed that south of Campbell Plateau by more than 250 m (Figure 7.7 and Figure 7.14 in the supplement). East of the Ross Sea area, anomalously high basement topography is associated with magmatic processes driven by continental-insulation flow only (Marie Byrd Seamounts, De Gerlache Seamounts, Peter I Island, e.g., Kipf et al. 2013). Oceanic crust elsewhere in that region seems unaffected by mantle processes (e.g., Endeavour Anomaly). Sutherland et al.'s (2010) present day dynamic topography model coincides with our positive residual basement depth anomaly in the Ross Sea, but their proposed topography high beneath the Pacific Plate north of the Pacific–Antarctic Ridge lacks an equal counterpart anomaly in the residual basement depth.

A peculiar feature of the residual basement anomaly is its asymmetry over the Pacific–Antarctic Ridge, with a local maximum south of the spreading center, exactly where Campbell Plateau passed through—according to recent South Pacific plate motion models (e.g., Larter et al. 2002; Eagles et al. 2004a; Wobbe et al. 2012)—during 70–40 Myr (cf. Figure 7.16 in the supplement). This time interval also marks the peak subsidence of the Campbell Plateau as it moved away from Antarctica to its present-day position (Sutherland et al. 2010). Although residual basement depth represents only a snapshot of dynamic topography, which occurs over tens of millions of years (Flament et al. 2013), the anomalous basement elevation south of the Pacific–Antarctic Ridge seems to be caused by processes persisting since the Cretaceous separation of New Zealand from Antarctica. It should be kept in mind, though, that until more robust dynamic topography models become available, predictions of the South Pacific paleotopography remain highly speculative.

7.5 CONCLUSIONS

Seismic data, recently acquired along the West Antarctic margin, suggests that Divins' (2003) minimum sediment thickness estimates along the West Antarctic margin are much too low. We present a new total sediment thickness grid spanning the Ross Sea–Amundsen Sea–Bellingshausen Sea basins based on available seismic reflection, borehole, and gravity modeling data in West Antarctica (Figure 7.2). Our sediment thickness and volume estimates are consistent with previous analyses that indicate larger sediment amounts on Antarctica's margin than previously assumed

(e.g., Rebesco et al. 1997; Scheuer et al. 2006a; Whittaker et al. 2013). We therefore extended Divins' (2003) original NGDC grid further south by merging our new data with data from Scheuer et al. (2006a), Wilson and Luyendyk (2009), and Whittaker et al. (2013) into an updated 5 by 5 minute global grid of total ocean sediment thickness. The sediment thickness estimation involved interpolation over areas without data constraints, but fortunately most of the less constrained areas fall into the abyssal plains where sediment cover is usually sparse. Due to a wider, better constrained dataset, the presented sediment volume estimates off West Antarctica are considered to be fairly accurate. The sediment volume is the largest in the Bellingshausen Sea basin, with 3.61 million cubic kilometers, although its sediment source area is the smallest (15 % of all area draining into the South Pacific). Contrary, the Ross Sea basin, into which sediments are supplied from a much larger area (43 %), contains just 2.78 million cubic kilometers of sediment. The Amundsen Sea basin, into which 42 % of the present-day West Antarctic landmass on the Pacific side drain, is estimated to contain 3.58 million cubic kilometers of sediment.

We determined the sediment-corrected basement topography for the South Pacific from our total sediment thickness model (Figure 7.4). In addition, we obtained the residual basement depth of the oceanic crust (Figure 7.5) by subtracting the sediment-corrected basement depth from the theoretical basement depth, using a current South Pacific crustal age model (Wobbe et al. 2012) and Crosby et al.'s (2006) North Pacific depth–age relationship. The mean residual basement depths of the Antarctic and Pacific plate differ by about 300 m. The Antarctic Plate has a residual basement depth of nearly 500 m, but the excessive sediment cover offshore West Antarctica leads to seafloor depths in excess of 1000 m shallower than those of the conjugate New Zealand margin. No direct relationship between seafloor roughness (Figure 7.8) and residual basement depth or overlying sediment accumulation has been observed. Ocean floor with large slope variability rather formed from 55 Myr ago until present, when full-spreading velocities dropped below 60 mm Myr^{-1}.

Dynamic topography models (e.g., Ricard et al. 1993; Steinberger 2007; Conrad and Husson 2009; Spasojevic and Gurnis 2012; Flament et al. 2013) of the South Pacific are inconsistent with our local residual basement anomalies or even reversely correlate, and it remains unclear why. The pattern of residual basement depth, however, matches the distribution of seamounts and the shear wave velocity anomaly of the upper mantle (Figure 7.9). Collectively these observations suggest that mantle dynamics play a role and that the resolution of dynamic topography models still lack the precision to pinpoint present-day small-scale residual basement anomalies. Our findings support Sutherland et al.'s (2010) model of Late Cretaceous to Cenozoic persistent mantle flow beneath West Antarctica following the Gondwana subduction cessation, but show that basement elevation, estimated from seafloor topography only, has been overestimated off Marie Byrd Land. We demonstrate through our analysis that the Marie

Byrd Land margin is only affected by magmatic processes in the context of continental-insulation flow (Kipf et al. 2013, e.g., Marie Byrd Seamounts, De Gerlache Seamounts, Peter I Island). This seems to be supported by the observation that oceanic crust farther away from these magmatic centers is elevated less than 250 m higher than oceanic crust from the conjugate New Zealand margin. The Ross Sea as well as the Balleny Islands hotspot area, and a region south of the Pacific–Antarctic Ridge, however, have been subject to mantle processes that lead to anomalously high basement elevations more than 1500 m higher as expected. A persistent basement high south of the ridge would explain the rapid subsidence of the Campbell Plateau during 70–40 Myr en route to its present day position. Until more accurate dynamic topography models, that can explain the present-day anomalous basement depth both at the Pacific–Antarctic Ridge and along the continental margins, become available, predictions of the South Pacific paleotopography remain speculative.

ACKNOWLEDGMENTS

This project has been funded by the Earth System Sciences Research School (ESSReS), a graduate school of the Helmholtz Association of German Research Centres (HGF) at the Alfred Wegener Institute (AWI), and through the Priority Program 1158 'Antarctic Research' of the Deutsche Forschungsgemeinschaft under project number GO 724/10-1. We thank Doug Wilson and Carsten Scheuer, with whom we had helpful discussions, for sharing their results, and Nicolas Flament for the data exchange. Special thanks go to the New Zealand UNCLOS project for granting insight into seismic data off Chatham Rise. All of the figures in this publication were created using GMT (Generic Mapping Tools, Version 5, by Wessel et al. 2013). We thank Carmen Gaina and Joanne Whittaker for their constructive reviews.

7.6 SUPPLEMENT

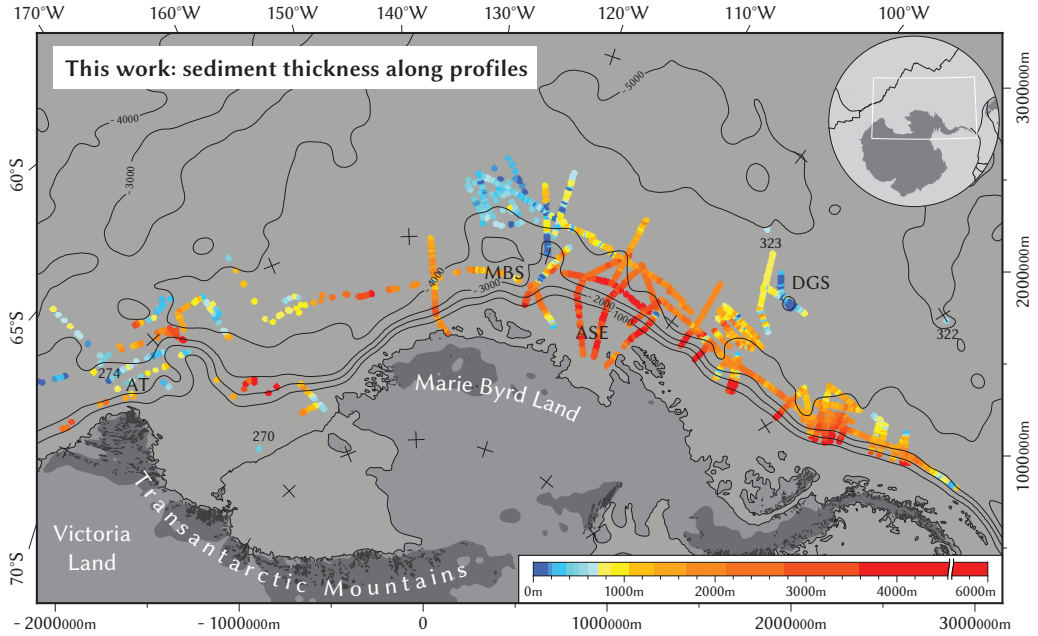

Figure 7.11. Sediment thickness along profiles (seismic and gravity, cf. Figure 7.1). Primary data were buffered by a distance of 20 km to make them visible on the map. Contour lines indicate water depth in meter. Same color coding and scale as in Figure 7.2.

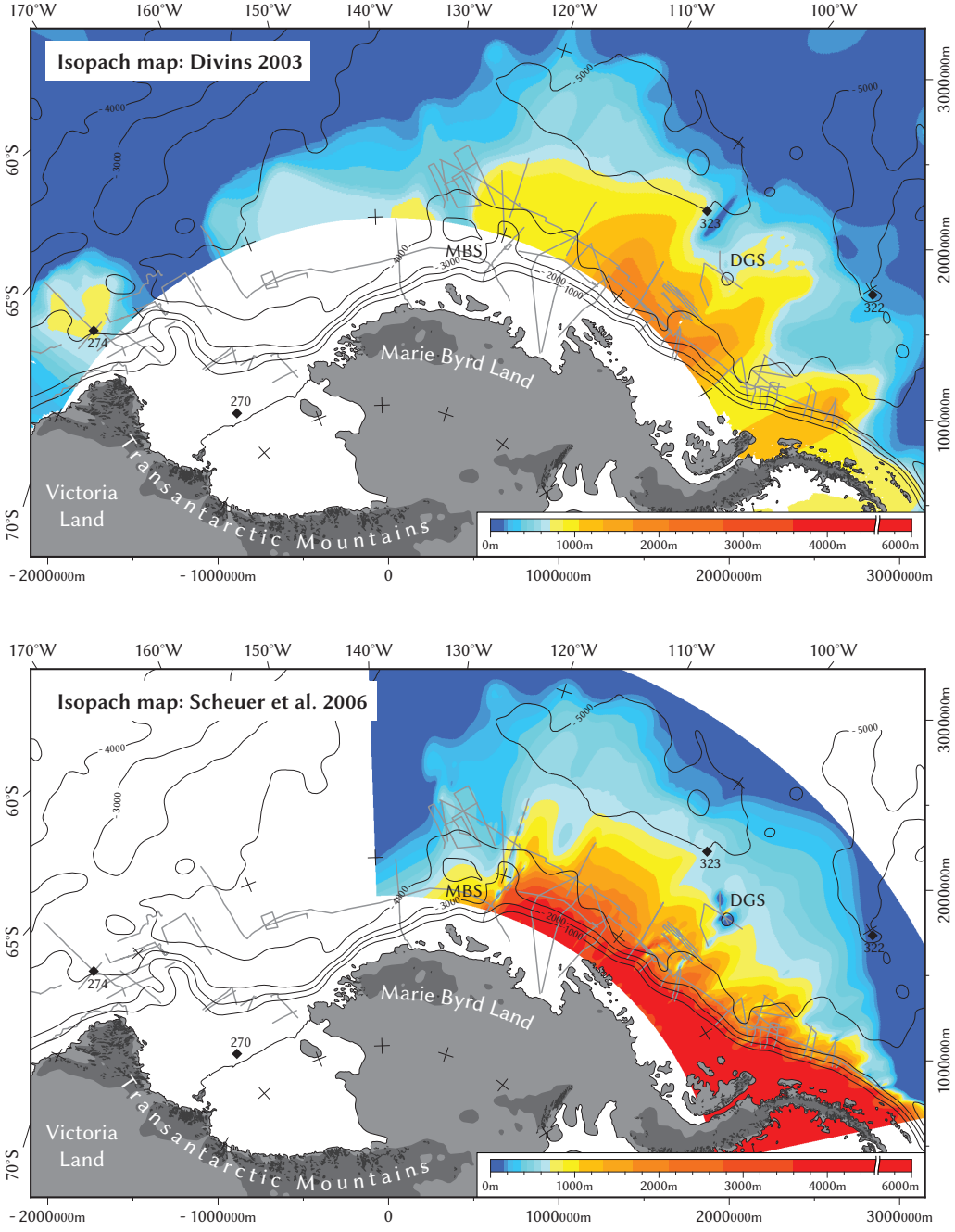

Figure 7.12. Sediment isopach maps of Divins (2003)/Whittaker et al. (2013) and Scheuer et al. (2006a). Same color coding and scale as in previous figure.

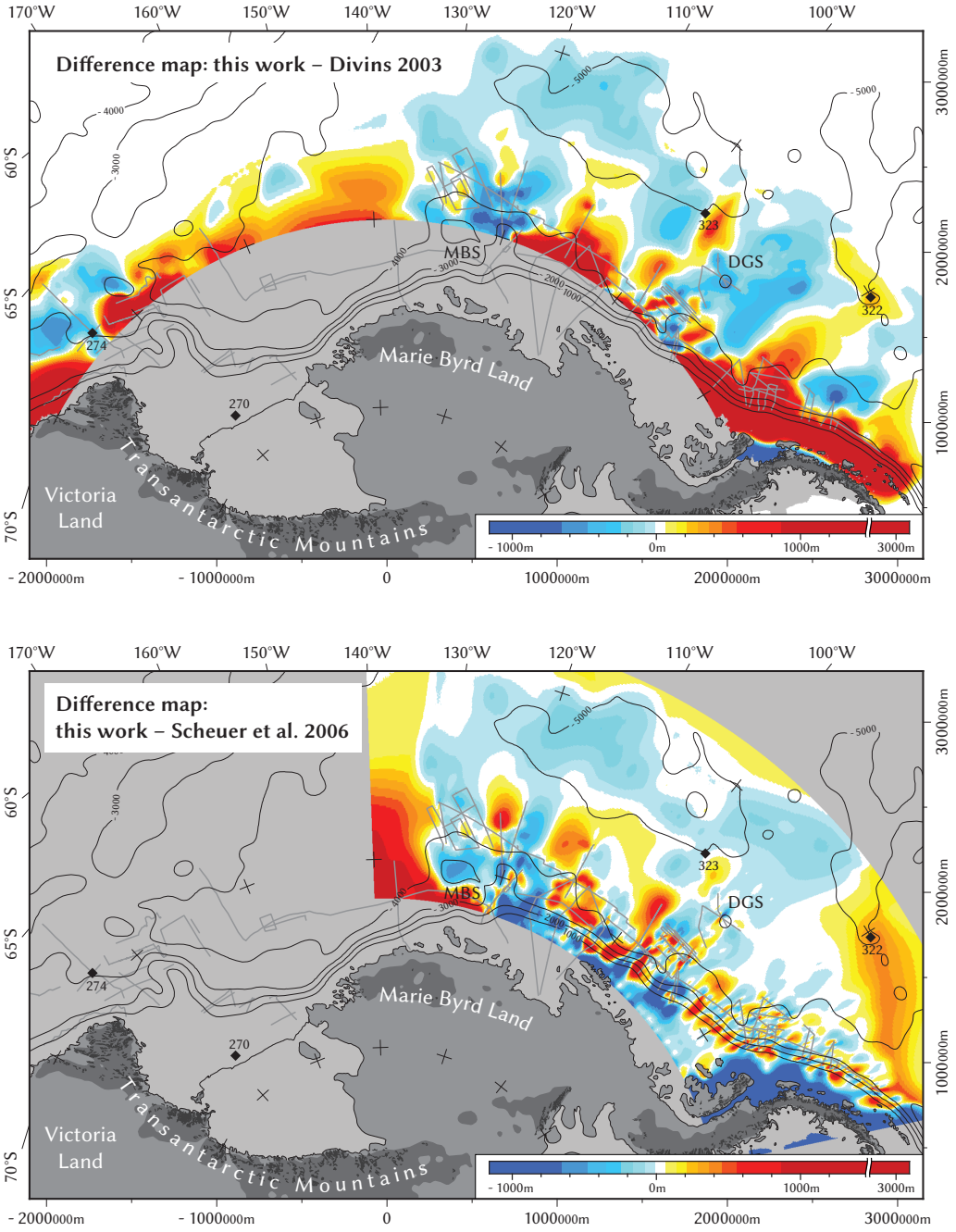

Figure 7.13. Sediment thickness difference maps: Divins (2003)/Whittaker et al. (2013) subtracted from this work (top) and Scheuer et al. (2006a) subtracted from this work (bottom). The sediment volume in the overlap areas are 1.14 $\times 10^6$ km^3 smaller in Divins (2003) and 0.35 $\times 10^6$ km^3 larger in Scheuer et al. (2006a) as compared to this work.

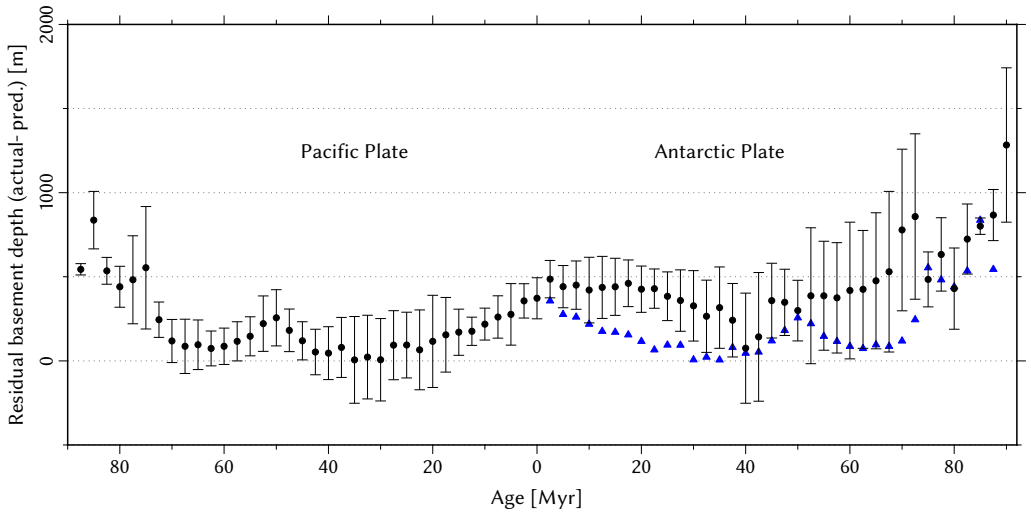

Figure 7.14. Residual basement depth vs. crustal age from Pacific–Antarctic Ridge. Bullets are mean values of 2.5 Myr bins along all profiles from Figure 7.5. Whiskers indicate standard deviation about the mean. Blue triangles represent values from the Pacific Plate mirrored to the right. The mean offset between residual basement values from the Pacific Plate vs. Antarctic Plate of the same age is about 240 m.

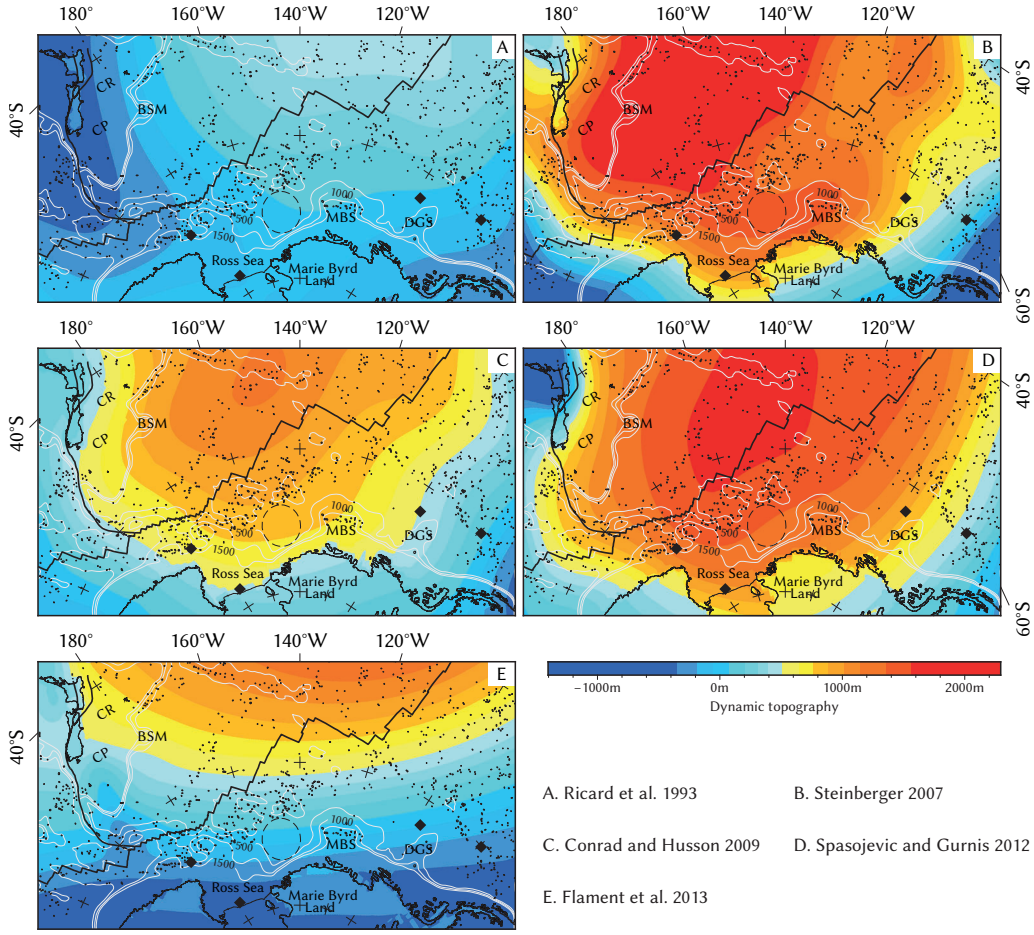

Figure 7.15. Present-day dynamic topography models of the South Pacific (Ricard et al. 1993; Steinberger 2007; Conrad and Husson 2009; Spasojevic and Gurnis 2012; Flament et al. 2013) vs. residual basement depth (500, 1000 and 1500 m contours).

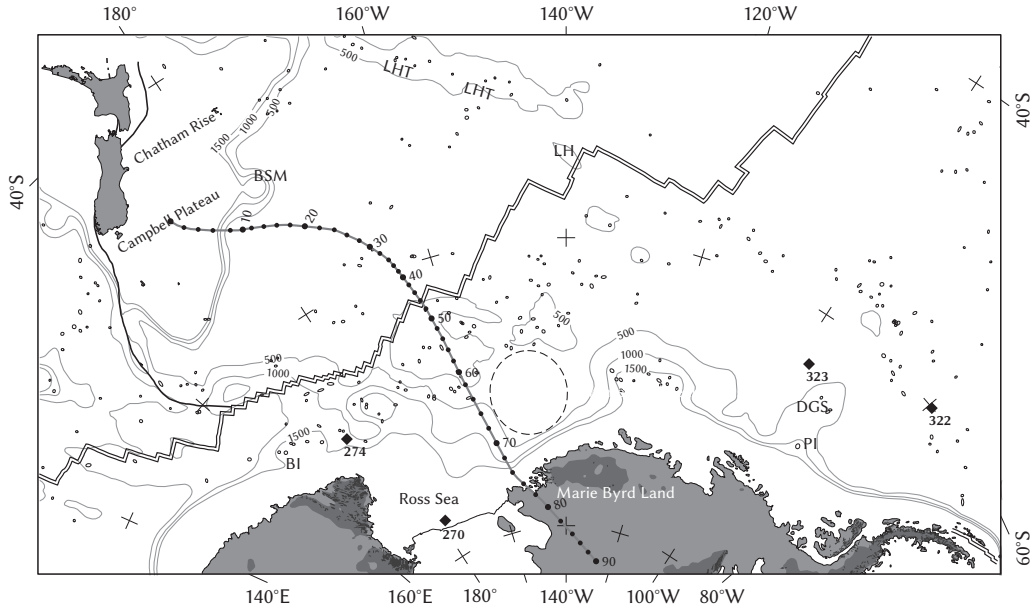

Figure 7.16. Motion path of Campbell Plateau from 90 Myr to present relative to Pacific hotspots (Wessel and Kroenke 2008) vs. residual basement depth (500, 1000 and 1500 m contours).

Table 7.1. Source-ID (values of source identification grid) vs. data origin of data used for compiling sediment thickness, including DSDP boreholes (1–4), data from the Antarctic Seismic Data Library System (SDLS, Wardell et al. 2007, 5–93, 161–207), recently acquired and processed seismic data (99–140), and data from previous work (e.g., Scheuer et al. 2006a, b; Wilson and Luyendyk 2009; Uenzelmann-Neben and Gohl 2012; Wobbe et al. 2012; Gohl et al. 2013b; Kalberg and Gohl 2014; Whittaker et al. 2013).

SID	Source	SID	Source	SID	Source
0	interpolated	32	AWI-94052	64	IT92A113
1	DSDP-28-270	33	AWI-94053	65	IT92A114
2	DSDP-28-274	34	AWI-94054-A	66	IT92A114A
3	DSDP-35-322	35	AWI-94054-B	67	IT92A115
4	DSDP-35-323	36	AWI-94054-C	68	IT92A124
5	AWI-010001	37	AWI-95200	69	IT97235
6	AWI-20060022	38	AWI-95201	70	IT97236
7	AWI-20060023	39	AWI-95210	71	PET-98401c
8	AWI-94002-A	40	BAS-92322	72	PET-98402a
9	AWI-94002-B	41	BAS-92323	73	PET-98403a
10	AWI-94002-C	42	BAS-92324	74	PET-98404
11	AWI-94002-D	43	BAS-92325	75	PET-98405b
12	AWI-94003-A	44	BAS-92327	76	PET-98405c
13	AWI-94003-B	45	BAS-92328	77	PET-98407
14	AWI-94003-C	46	BAS-92329	78	PET-98408
15	AWI-94030-A	47	BAS-92330	79	PET-98409
16	AWI-94030-B	48	I95130	80	TH86002A
17	AWI-94030-C	49	I95130A	81	TH86002B
18	AWI-94030-D	50	I95130B	82	TH86003A
19	AWI-94030-E	51	I95135	83	TH86003B
20	AWI-94040-A	52	I95135A	84	TH86003C
21	AWI-94040-B	53	I95136	85	TH86003D
22	AWI-94041-A	54	I95137	86	TH86003E
23	AWI-94041-B	55	I95138A	87	TH86003F
24	AWI-94041-C	56	IT89A45B	88	TH86004A
25	AWI-94042-A	57	IT89A48	89	TH86004B
26	AWI-94042-B	58	IT89A49	90	TH86004C
27	AWI-94042-C	59	IT92A106	91	TH86006
28	AWI-94043-A	60	IT92A107	92	TH86008
29	AWI-94043-B	61	IT92A108	93	TH86009
30	AWI-94050	62	IT92A109	95, 96	Scheuer et al. (2006a)
31	AWI-94051	63	IT92A110	97	assigned (this work)

Table 7.1. Source-ID vs. data origin (continued).

SID	Source	SID	Source	SID	Source
99	AWI-20060200	164	IT89AR36B	186	NBP9602-07H
107	AWI-20100107	165	NBP9601L010A	187	NBP9602-07I
108	AWI-20100108	166	NBP9601L010B	188	NBP9602-08A
109	AWI-20100109	167	NBP9601L010C	189	NBP9602-08B
110	AWI-20100110	168	NBP9601L082A	190	NBP9702-01A
111	AWI-20100111	169	NBP9601L082B	191	NBP9702-01C
112	AWI-20100112	170	NBP9601L08B	192	NBP9702-01D
113	AWI-20100113	171	NBP9602-01A	193	NBP9702-01E
117	AWI-20100117	172	NBP9602-01B	194	NBP9702-02C
118	AWI-20100118	173	NBP9602-04	195	NBP9702-05A
119	AWI-20100119	174	NBP9602-05A	196	NBP9702-05B
126	AWI-20100126	175	NBP9602-05B	197	NBP9702-05C
129	AWI-20100129	176	NBP9602-06A	198	NBP9702-06A
130	AWI-20100130	177	NBP9602-06C	199	NBP9702-06B
131	AWI-20100131	178	NBP9602-06D	200	SEV87-02B
132	AWI-20100132	179	NBP9602-07A	201	SEV87-07
139	AWI-20100139	180	NBP9602-07B	202	SEV87-11
140	AWI-20100140	181	NBP9602-07C	203	TH82-12
151	Wobbe et al. (2012)	182	NBP9602-07D	204	TH82-13
161	ATC82B-208	183	NBP9602-07E	205	TH82-14
162	BGR80-100	184	NBP9602-07F	206	TH82-16
163	IT89A37	185	NBP9602-07G	207	TH82-17
251	Ross Sea, Wilson and Luyendyk (2009)				
252	Ross Sea, Cooper et al. (1991)				
253	Divins (2003)/Whittaker et al. (2013)				

8 CONCLUSION AND OUTLOOK

New geophysical dataset acquired during R/V Polarstern cruises in the eastern Ross Sea and Bellingshausen Sea during 2006 and 2010 helped to better understand the tectonic and geodynamic processes that shaped this remote region after the breakup of Gondwana. An improved plate-tectonic reconstruction of the South Pacific is mostly consistent with previous works (e.g., Molnar et al. 1975; Larter et al. 2002; Stock and Cande 2002; Eagles et al. 2004a), but for the first time, considers continental extension during and after the rifting phase (Wobbe et al. 2012, Chapter 4). The initial seafloor formation propagated westward from the Bellingshausen sector between ~89 and 84 Myr. Seafloor magnetic anomalies adjacent to Marie Byrd Land indicate full-spreading rates of 60–74 mm yr^{-1} during 84–62 Myr, which then dropped to 22 mm yr^{-1} at 50 Myr. A brief rifting phase formed a typical magma-poor margin with little continental deformation (<90 km) prior to the breakup. This margin type is only preserved in the Ross Sea area. Further east, subsequent motion of the Bellingshausen plate over a period of 22 Myr modified the initial rift morphology. In this region the margin was extended by 106–304 km and intraplate magmatism further altered the lithosphere in the Early Cenozoic (Kipf et al. 2013). Distinct zones of patterns in the magnetic anomaly map of the Amundsen Sea Embayment further indicate that parts of the West Antarctic Rift system have been active in this region during the Eocene (Gohl et al. 2013a, Chapter 6).

Continental margin restorations elsewhere in Antarctica show a very heterogenous pattern of continental extension with each domain displaying a different amount of continental stretching (Wobbe and Gohl 2013, Chapter 5). The breakup of Gondwana lasted for about 100 million years and in some places, such as the Australian–Antarctic conjugated margin, the rifting velocity was sufficiently low to allow a margin extension of up to 300–400 km. The concept of passive margin restoration is known since the late 1980s (e.g., Dunbar and Sawyer 1987, 1989), yet reliable quantitative plate-tectonic reconstructions considering stretched continental crust appeared only lately (e.g., Whittaker et al. 2010; Williams et al. 2011; Heine et al. 2013). Due to the lack of data constraining the crustal structure of Antarctica's passive margins, the calculation of the pre-rift plate boundary geometries along these margins is difficult and may contain large errors. However, it is the only way to obtain full-fit reconstructions that complete the global plate circuit.

A first cross-regional total sediment thickness grid for the Pacific margin of Antarctica reveals a sediment thickness about 3–4 km larger than previously assumed (Wobbe et al. 2014a, Chapter 7). New magnetic data helped to define the extent of the sediment-covered area on the middle

to outer Amundsen Sea Embayment shelf (Gohl et al. 2013a, Chapter 6). The computed sediment volume in the Ross Sea basin is consistent with previous investigations (Wilson and Luyendyk 2009). Sediment volumes in the Bellingshausen and Amundsen Sea, however, have been underestimated. Sediment corrected basement depth and residual basement depth of the South Pacific could be derived from the sediment thickness. The results show that the residual basement depth is distributed unevenly and the mean value of the Antarctic plate is about 300 m higher than that of the Pacific plate. However, dynamic topography models (e.g., Ricard et al. 1993; Steinberger 2007; Conrad and Husson 2009; Spasojevic and Gurnis 2012; Flament et al. 2013) of the South Pacific show an opposing trend. The cause is still unclear. The residual basement depth anomalies support suggestions of persistent mantle flow beneath West Antarctica (Sutherland et al. 2010), but restrict the area affected by the plume to the Ross Sea and the Balleny Islands hotspot area. These findings have implications for further research:

- Paleobathymetric reconstructions of the South Pacific require the consideration of the dynamic topography. However, current dynamic topography models have a limited lateral resolution and disagree with the basement topography of the South Pacific. Hence, predictions of the South Pacific paleotopography remain speculative until better dynamic topographies are available.

- So far, the timing of the sedimentation (age of sediments, sedimentation rate) along the Pacific margin of West Antarctica is investigated rudimentarily. These parameters are only known for sparsely distributed drill sites in the South Pacific and must be estimated for large areas in-between. A cross-regional seismic horizon stratigraphic correlation is another prerequisite for modeling the paleobathymetry.

- A recently published study by Wilson et al. (2013) indicates that West Antarctica's topography lay above sea level in the Early Oligocene and that, consequently, the total Antarctic ice volume since the Eocene–Oligocene transition was greater than previously assumed. This thesis concludes that the sediment thickness along the Antarctic margin has been underestimated for the most part. Possibly, Antarctica supported even larger ice sheet volumes in the early times of glaciation. In this theses it is therefore suggested that erosion rates should be re-evaluated with the new sediment thickness data. This would improve the Eocene paleotopography and the derived climate-ice sheet models.

BIBLIOGRAPHY

Amante, C. and B. W. Eakins, 2009. ETOPO1 1 Arc-Minute Global Relief Model: Procedures, Data Sources and Analysis. Technical Report, NOAA Technical Memorandum NESDIS NGDC-24. Available from: http://www.ngdc.noaa.gov/mgg/global/global.html.

Andersen, O. B. and P. Knudsen, 2009. DNSC08 mean sea surface and mean dynamic topography models. *J. Geophys. Res.*, **114**(C11), C11001. doi:10.1029/2008JC005179.

Arndt, J. E., H. W. Schenke, M. Jakobsson, F. O. Nitsche, G. Buys, B. Goleby, M. Rebesco, F. Bohoyo, J. Hong, J. Black, R. Greku, G. Udintsev, F. Barrios, W. Reynoso-Peralta, M. Taisei, and R. Wigley, 2013. The International Bathymetric Chart of the Southern Ocean (IBCSO) Version 1.0 – A new bathymetric compilation covering circum-Antarctic waters. *Geophys. Res. Lett.* doi:10.1002/grl.50413.

Barker, P. F., B. Diekmann, and C. Escutia, 2007a. Onset of Cenozoic Antarctic glaciation. *Deep-Sea Res. II*, **54**(21–22), 2293–2307. doi:10.1016/j.dsr2.2007.07.027.

Barker, P. F., G. M. Filippelli, F. Florindo, E. E. Martin, and H. D. Scher, 2007b. Onset and role of the Antarctic Circumpolar Current. *Deep-Sea Res. II*, **54**(21–22), 2388–2398. doi:10.1016/j.dsr2.2007.07.028.

Bayer, B., W. H. Geissler, A. Eckstaller, and W. Jokat, 2009. Seismic imaging of the crust beneath Dronning Maud Land, East Antarctica. *Geophys. J. Int.*, **178**(2), 860–876. doi:10.1111/j.1365-246X.2009.04196.x.

Blaich, O. A., J. I. Faleide, and F. Tsikalas, 2011. Crustal breakup and continent-ocean transition at South Atlantic conjugate margins. *J. Geophys. Res.*, **116**(B1), B01402. doi:10.1029/2010JB007686.

Block, A. E., R. E. Bell, and M. Studinger, 2009. Antarctic crustal thickness from satellite gravity: Implications for the Transantarctic and Gamburtsev Subglacial Mountains. *Earth Planet. Sci. Lett.*, **288**(1–2), 194–203. doi:10.1016/j.epsl.2009.09.022.

Boyden, J. A., R. D. Müller, M. Gurnis, T. H. Torsvik, J. A. Clark, M. Turner, H. Ivey-Law, R. J. Watson, and J. S. Cannon, 2011. Next-generation plate-tectonic reconstructions using GPlates. In G. R. Keller and C. Baru, editors, *Geoinformatics: Cyberinfrastructure for the Solid Earth Sciences*. Cambridge University Press.

Cande, S. C. and J. M. Stock, 2004. Cenozoic reconstructions of the Australia-New Zealand-South Pacific sector of Antarctica. In N. F. Exon,

J. P. Kennett, and M. J. Malone, editors, *The Cenozoic Southern Ocean: Tectonics, Sedimentation and Climate Change Between Australia and Antarctica*, volume 151, pp. 5–18. AGU Monograph Series.

Cande, S. C., C. A. Raymond, J. Stock, and W. F. Haxby, 1995. Geophysics of the Pitman Fracture Zone and Pacific-Antarctic Plate Motions During the Cenozoic. *Science*, **270**(5238), 947–953. doi:10.1126/science.270.5238.947.

Cande, S. C., J. M. Stock, R. D. Müller, and T. Ishihara, 2000. Cenozoic motion between East and West Antarctica. *Nature*, **404**(6774), 145–150. doi:10.1038/35004501.

Carlson, R. L., A. F. Gangi, and K. R. Snow, 1986. Empirical Reflection Travel Time Versus Depth and Velocity Versus Depth Functions for The Deep-Sea Sediment Column. *J. Geophys. Res.*, **91**(B8), 8249–8266. doi:10.1029/JB091iB08p08249.

Chian, D., K. E. Louden, and I. Reid, 1995. Crustal structure of the Labrador Sea conjugate margin and implications for the formation of nonvolcanic continental margins. *J. Geophys. Res.-Sol. Ea.*, **100**(B12), 24239–24253. doi:10.1029/95JB02162.

Conrad, C. P. and L. Husson, 2009. Influence of dynamic topography on sea level and its rate of change. *Lithosphere*, **1**(2), 110–120. doi:10.1130/L32.1.

Cook, R. A., R. Sutherland, and H. Zhu, 1999. Cretaceous - Cenozoic geology and petroleum systems of the Great South Basin, New Zealand. In *Institute of Geological & Nuclear Sciences monograph 20*, p. 188. Lower Hutt, New Zealand: Institute of Geological & Nuclear Sciences Limited.

Cooper, A. K., F. J. Davey, and K. Hinz, 1991. Crustal extension and origin of sedimentary basins beneath the Ross Sea and Ross Ice Shelf. In M. R. A. Thomson, J. A. Crame, and J. W. Thomson, editors, *Geological Evolution of Antarctica*, Cambridge World and Regional Geology, pp. 285–291. Cambridge University Press, Cambridge. ISBN 978-0521372664.

Cox, A., 1973. *Plate Tectonics and Geomagnetic Reversals*. W. H. Freeman. ISBN 978-0-7167-0258-0.

Cox, A. and R. B. Hart, 1986. *Plate Tectonics: How It Works*. Blackwell Scientific Publications. ISBN 978-0-86542-313-8.

Croon, M. B., S. C. Cande, and J. M. Stock, 2008. Revised Pacific-Antarctic plate motions and geophysics of the Menard Fracture Zone. *Geochem. Geophys. Geosyst.*, **9**(7), Q07001. doi:10.1029/2008GC002019.

Crosby, A. G., D. McKenzie, and J. G. Sclater, 2006. The relationship between depth, age and gravity in the oceans. *Geophys. J. Int.*, **166**(2), 553–573. doi:10.1111/j.1365-246X.2006.03015.x.

Cunningham, A. P., R. D. Larter, P. F. Barker, K. Gohl, and F. O. Nitsche, 2002. Tectonic evolution of the Pacific margin of Antarctica 2. Structure of Late Cretaceous–early Tertiary plate boundaries in the Bellingshausen Sea from seismic reflection and gravity data. *J. Geophys. Res.*, **107**(B12), 2346. doi:10.1029/2002JB001897.

Czaja, A. and J. Marshall, 2006. The Partitioning of Poleward Heat Transport between the Atmosphere and Ocean. *J. Atmos. Sci.*, **63**(5), 1498–1511. doi:10.1175/JAS3695.1.

Dalziel, I. W. D., 2006. On the extent of the active West Antarctic rift system. In C. S. Siddoway and C. A. Ricci, editors, *Proceedings of the Workshop Frontiers and Opportunities in Antarctic Geosciences 2004*, volume 12 of *Terra Antartica Reports*, pp. 193–202. Siena, Italy.

Dalziel, I. W. D. and D. H. Elliot, 1982. West Antarctica: Problem child of Gondwanaland. *Tectonics*, **1**(1), 3–19. doi:10.1029/TC001i001p00003.

Davy, B., 2006. Bollons Seamount and early New Zealand–Antarctic seafloor spreading. *Geochem. Geophys. Geosyst.*, **7**(6), Q06021. doi:10.1029/2005GC001191.

Davy, B., K. Hoernle, and R. Werner, 2008. Hikurangi Plateau: Crustal structure, rifted formation, and Gondwana subduction history. *Geochem. Geophys. Geosyst.*, **9**(7), Q07004. doi:10.1029/2007GC001855.

DeConto, R. M., D. Pollard, P. A. Wilson, H. Palike, C. H. Lear, and M. Pagani, 2008. Thresholds for Cenozoic bipolar glaciation. *Nature*, **455**(7213), 652–656. doi:10.1038/nature07337.

Divins, D. L., 2003. Total Sediment Thickness of the World's Oceans & Marginal Seas. NOAA National Geophysical Data Center, Boulder, CO. Available from: http://www.ngdc.noaa.gov/mgg/sedthick/.

Dunbar, J. A. and D. S. Sawyer, 1987. Implications of continental crust extension for plate reconstruction: An example from the Gulf of Mexico. *Tectonics*, **6**(6), 739–755. doi:10.1029/TC006i006p00739.

Dunbar, J. A. and D. S. Sawyer, 1989. Patterns of continental extension along the conjugate margins of the central and North ATLANTIC Oceans and Labrador Sea. *Tectonics*, **8**(5), 1059–1077. doi:10.1029/TC008i005p01059.

Eagles, G. and M. König, 2008. A model of plate kinematics in Gondwana breakup. *Geophys. J. Int.*, **173**(2), 703–717. doi:10.1111/j.1365-246X.2008.03753.x.

Eagles, G., K. Gohl, and R. Larter, 2004a. High-resolution animated tectonic reconstruction of the South Pacific and West Antarctic margin. *Geochem. Geophys. Geosyst.*, **5**, Q07002. doi:10.1029/2003GC000657.

Eagles, G., K. Gohl, and R. D. Larter, 2004b. Life of the Bellingshausen plate. *Geophys. Res. Lett.*, **31**, L07603. doi:10.1029/2003GL019127.

Eagles, G., R. D. Larter, K. Gohl, and A. P. M. Vaughan, 2009. West Antarctic Rift System in the Antarctic Peninsula. *Geophys. Res. Lett.*, **36**(21), L21305. doi:10.1029/2009GL040721.

Fasullo, J. T. and K. E. Trenberth, 2008. The Annual Cycle of the Energy Budget. Part II: Meridional Structures and Poleward Transports. *J. Climate*, **21**(10), 2313–2325. doi:10.1175/2007JCLI1936.1.

Ferraccioli, F., M. Gambetta, and E. Bozzo, 1998. Microlevelling procedures applied to regional aeromagnetic data: an example from the Transantarctic Mountains (Antarctica). *Geophys. Prospect.*, **46**(2), 177–196. doi:10.1046/j.1365-2478.1998.00080.x.

Ferraccioli, F., T. A. Jordan, D. G. Vaughan, J. Holt, M. James, H. Corr, D. D. Blankenship, J. D. Fairhead, and T. M. Diehl, 2007. New aerogeophysical survey targets the extent of the West Antarctic Rift System over Ellsworth Land. In A. K. Cooper, C. R. Raymond, and the 10th ISAES Editorial Team, editors, *Antarctica: A Keystone in a Changing World – Online Proceedings of the 10th International Symposium on Antarctic Earth Sciences*, USGS Open-File Report 2007-1047, Extended Abstract 113. USGS. doi:10.3133/of2007-1047.

Finlay, C. C., S. Maus, C. D. Beggan, T. N. Bondar, A. Chambodut, T. A. Chernova, A. Chulliat, V. P. Golovkov, B. Hamilton, M. Hamoudi, R. Holme, G. Hulot, W. Kuang, B. Langlais, V. Lesur, F. J. Lowes, H. Lühr, S. Macmillan, M. Mandea, S. McLean, C. Manoj, M. Menvielle, I. Michaelis, N. Olsen, J. Rauberg, M. Rother, T. J. Sabaka, A. Tangborn, L. Tøffner-Clausen, E. Thébault, A. W. P. Thomson, I. Wardinski, Z. Wei, and T. I. Zvereva, 2010. International Geomagnetic Reference Field: the eleventh generation. *Geophys. J. Int.*, **183**(3), 1216–1230. doi:10.1111/j.1365-246X.2010.04804.x.

Finn, C. A., R. D. Müller, and K. S. Panter, 2005. A Cenozoic diffuse alkaline magmatic province (DAMP) in the southwest Pacific without rift or plume origin. *Geochem. Geophys. Geosyst.*, **6**(2). doi:10.1029/2004GC000723.

Flament, N., M. Gurnis, and R. D. Müller, 2013. A review of observations and models of dynamic topography. *Lithosphere*, **5**(2), 189–210. doi:10.1130/L245.1.

Gaina, C., R. D. Müller, B. Brown, T. Ishihara, and S. Ivanov, 2007. Breakup and early seafloor spreading between India and Antarctica. *Geophys. J. Int.*, **170**(1), 151–169. doi:10.1111/j.1365-246X.2007.03450.x.

Gardner, G. H. F., L. W. Gardner, and A. R. Gregory, 1974. Formation velocity and density—The diagnostic basics for stratigraphic traps. *Geophysics*, **39**(6), 770–780. doi:10.1190/1.1440465.

Gohl, K., editor, 2007. *The Expedition ANTARKTIS-XXIII/4 of the Research Vessel Polarstern in 2006*, volume 557 of *Berichte zur Polar- und Meeresforschung = Reports on polar and marine research*. Alfred Wegener Institute for Polar and Marine Research. doi:10013/epic.27102.d001.

Gohl, K., 2008. Antarctica's Continent–Ocean Transitions: Consequences for Tectonic Reconstructions. In A. K. Cooper, P. Barrett, H. Stagg, B. Storey, E. Stump, W. Wise, and the 10th ISAES editorial team, editors, *Antarctica: A Keystone in a Changing World*, Proceedings of the 10th International Symposium on Antarctic Earth Sciences, Santa Barbara, California, August 26 to September 1, 2007, pp. 29–38. The National Academies Press, Washington, D.C. ISBN 978-0-309-11854-5.

Gohl, K., editor, 2010. *The expedition of the Research Vessel Polarstern to the Amundsen Sea, Antarctica, in 2010 (ANT-XXVI/3)*, volume 617 of *Berichte zur Polar- und Meeresforschung = Reports on polar and marine research*. Alfred Wegener Institute for Polar and Marine Research. doi:10013/epic.35668.d001.

Gohl, K., 2012. Basement control on past ice sheet dynamics in the Amundsen Sea Embayment, West Antarctica. *Palaeogeogr. Palaeoclimatol. Palaeoecol.*, **335–336**, 35–41. Cenozoic Evolution of Antarctic Climates, Oceans and Ice Sheets. doi:10.1016/j.palaeo.2011.02.022.

Gohl, K., F. Nitsche, and H. Miller, 1997. Seismic and gravity data reveal Tertiary interplate subduction in the Bellingshausen Sea, southeast Pacific. *Geology*, **25**(4), 371–374. doi:10.1130/0091-7613(1997)025<0371:SAGDRT>2.3.CO;2.

Gohl, K., G. L. Leitchenkov, N. Parsiegla, B. M. Ehlers, C. Kopsch, D. Damaske, Y. B. Guseva, and V. V. Gandyukhin, 2007a. Crustal types and continent-ocean boundaries between the Kerguelen Plateau and Prydz Bay, East Antarctica. In A. K. Cooper, C. R. Raymond, and the 10th ISAES Editorial Team, editors, *Antarctica: A Keystone in a Changing World – Online Proceedings of the 10th International Symposium on Antarctic Earth Sciences*, USGS Open-File Report 2007-1047, Extended Abstract 038. USGS. doi:10.3133/of2007-1047.

Gohl, K., D. Teterin, G. G. Eagles, G. Netzeband, J. W. G. Grobys, N. Parsiegla, P. Schlüter, V. Leinweber, R. D. Larter, G. Uenzelmann-Neben, and G. B. Udintsev, 2007b. Geophysical Survey Reveals Tectonic Structures in the Amundsen Sea Embayment, West Antarctica. In A. K. Cooper, C. R. Raymond, and the 10th ISAES Editorial Team, editors, *Antarctica: A Keystone in a Changing World – Online Proceedings of the 10th International Symposium on Antarctic Earth Sciences*, USGS Open-File Report 2007-1047, Short Research Paper 047. USGS. doi:10.3133/of2007-1047.srp047.

Gohl, K., G. Uenzelmann-Neben, E. Weigelt, A. Lindeque, T. Kalberg, G. Kuhn, C. D. Hillenbrand, and R. D. Larter, 2011. Sedimentary and glacial processes of the Amundsen Sea Embayment, West Antarctica.

Poster presentation at General Assembly of European Geoscience Union (EGU), Vienna, 3–8 April 2011. doi:10013/epic.37078.

Gohl, K., A. Denk, G. Eagles, and F. Wobbe, 2013a. Deciphering tectonic phases of the Amundsen Sea Embayment shelf, West Antarctica, from a magnetic anomaly grid. *Tectonophysics*, **585**(0), 113–123. doi:10.1016/j.tecto.2012.06.036.

Gohl, K., G. Uenzelmann-Neben, R. D. Larter, C.-D. Hillenbrand, K. Hochmuth, T. Kalberg, E. Weigelt, B. Davy, G. Kuhn, and F. O. Nitsche, 2013b. Seismic stratigraphic record of the Amundsen Sea Embayment shelf from pre-glacial to recent times: Evidence for a dynamic West Antarctic ice sheet. *Mar. Geol.*, **344**(0), 115–131. doi:10.1016/j.margeo.2013.06.011.

Gradstein, F. M., J. G. Ogg, A. G. Smith, W. Bleeker, and L. J. Lourens, 2004. A new Geologic Time Scale with special reference to Precambrian and Neogene. *Episodes*, **27**(2), 83–100.

Graham, A. G. C., R. D. Larter, K. Gohl, C.-D. Hillenbrand, J. A. Smith, and G. Kuhn, 2009. Bedform signature of a West Antarctic palaeo-ice stream reveals a multi-temporal record of flow and substrate control. *Quaternary Sci. Rev.*, **28**(25–26), 2774–2793. doi:10.1016/j.quascirev.2009.07.003.

Green, A., 1983. A comparison of adjustment procedures for leveling aeromagnetic survey data. *Geophysics*, **48**(6), 745–753. doi:10.1190/1.1441504.

Grobys, J. W. G., K. Gohl, and G. Eagles, 2008. Quantitative tectonic reconstructions of Zealandia based on crustal thickness estimates. *Geochem. Geophys. Geosyst.*, **9**(1), Q01005. doi:10.1029/2007GC001691.

Grobys, J. W. G., K. Gohl, G. Uenzelmann-Neben, B. Davy, and D. Barker, 2009. Extensional and magmatic nature of the Campbell Plateau and Great South Basin from deep crustal studies. *Tectonophysics*, **472**(1–4), 213–225. doi:10.1016/j.tecto.2008.05.003.

Grunow, A. M., D. V. Kent, and I. W. D. Dalziel, 1991. New paleomagnetic data from Thurston Island: Implications for the tectonics of west Antarctica and Weddell Sea opening. *J. Geophys. Res.*, **96**(B11), 17935–17954. doi:10.1029/91JB01507.

Halliday, A. N., D.-C. Lee, S. Tommasini, G. R. Davies, C. R. Paslick, J. G. Fitton, and D. E. James, 1995. Incompatible trace elements in OIB and MORB and source enrichment in the sub-oceanic mantle. *Earth Planet. Sci. Lett.*, **133**(3–4), 379–395. doi:10.1016/0012-821X(95)00097-V.

Hayes, D. E., L. A. Frakes, P. J. Barrett, D. A. Burns, P.-H. Chen, A. B. Ford, A. G. Kaneps, E. M. Kemp, D. W. McCollum, D. J. W. Piper, R. E. Wall, and P. N. Webb, editors, 1975. *Initial Reports of the Deep Sea Drilling*

Project, volume 28. U.S. Government Printing Office, Washington, D.C. doi:10.2973/dsdp.proc.28.1975.

Heine, C., J. Zoethout, and R. D. Müller, 2013. Kinematics of the South Atlantic rift. *Solid Earth*, **4**(2), 215–253. doi:10.5194/se-4-215-2013.

Hellinger, S. J., 1981. The Uncertainties of Finite Rotations in Plate Tectonics. *J. Geophys. Res.*, **86**(B10), 9312–9318. doi:10.1029/JB086iB10p09312.

Hillier, J. K. and A. B. Watts, 2005. Relationship between depth and age in the North Pacific Ocean. *J. Geophys. Res.-Sol. Ea.*, **110**, B02405. doi:10.1029/2004JB003406.

Hollister, C. D., C. Craddock, Y. A. Bogdanov, N. T. Edgar, J. M. Gieskes, B. U. Haq, J. R. Lawrence, F. Roegl, H.-J. Schrader, B. E. Tucholke, W. R. Vennum, F. M. Weaver, V. N. Zhivago, and P. Worstell, editors, 1976. *Initial Reports of the Deep Sea Drilling Project*, volume 35. U.S. Government Printing Office, Washington, D.C. doi:10.2973/dsdp.proc.35.1976.

Huismans, R. and C. Beaumont, 2011. Depth-dependent extension, two-stage breakup and cratonic underplating at rifted margins. *Nature*, **473**(7345), 74–78. doi:10.1038/nature09988.

Jokat, W., T. Boebel, M. König, and U. Meyer, 2003. Timing and geometry of early Gondwana breakup. *J. Geophys. Res.-Sol. Ea.*, **108**(B9). doi:10.1029/2002JB001802.

Jokat, W., O. Ritzmann, C. Reichert, and K. Hinz, 2004. Deep Crustal Structure of the Continental Margin off the Explora Escarpment and in the Lazarev Sea, East Antarctica. *Mar. Geophys. Res.*, **25**, 283–304. doi:10.1007/s11001-005-1337-9.

Jokat, W., Y. Nogi, and V. Leinweber, 2010. New aeromagnetic data from the western Enderby Basin and consequences for Antarctic-India break-up. *Geophys. Res. Lett.*, **37**(21), L21311. doi:10.1029/2010GL045117.

Jordan, T. A., F. Ferraccioli, D. G. Vaughan, J. W. Holt, H. Corr, D. D. Blankenship, and T. M. Diehl, 2010. Aerogravity evidence for major crustal thinning under the Pine Island Glacier region (West Antarctica). *Geol. Soc. Am. Bull.*, **122**(5–6), 714–726. doi:10.1130/B26417.1.

Kalberg, T. and K. Gohl, 2014. The crustal structure and tectonic development of the continental margin of the Amundsen Sea Embayment margin, West Antarctica: implications from geophysical data. *Geophys. J. Int.*, **198**(1), 327–341. doi:10.1093/gji/ggu118.

Kim, S.-S. and P. Wessel, 2011. New global seamount census from altimetry-derived gravity data. *Geophys. J. Int.*, **186**(2), 615–631. doi:10.1111/j.1365-246X.2011.05076.x.

Kipf, A., R. Werner, K. Gohl, F. Hauff, P. van den Bogaard, and K. Hoernle, 2008. Age and origin of magmatism at the Marie Byrd Seamounts (Amundsen Sea). Poster presentation at General Assembly of the European Geoscience Union, Vienna, 13–18 April 2008.

Kipf, A., N. Mortimer, R. Werner, K. Gohl, P. van den Bogaard, F. Hauff, and K. Hoernle, 2012. Granitoids and dykes of the Pine Island Bay region, West Antarctica. *Antarctic Science*, **24**, 473–484. doi:10.1017/S0954102012000259.

Kipf, A., F. Hauff, R. Werner, K. Gohl, P. van den Bogaard, K. Hoernle, and A. Maicher, D .and Klügel, 2013. Seamounts off the West Antarctic margin of the Pacific: A case of non-hotspot intraplate volcanism. *Gondwana Res.* doi:10.1016/j.gr.2013.06.013.

König, M., 2006. *Processing of shipborne magnetometer data and revision of the timing and geometry of the Mesozoic break-up of Gondwana*. Ph.D. thesis, University of Bremen. doi:10013/epic.24879.d001.

König, M. and W. Jokat, 2006. The Mesozoic breakup of the Weddell Sea. *J. Geophys. Res.*, **111**, B12102. doi:10.1029/2005JB004035.

Laird, M. G. and J. D. Bradshaw, 2004. The Break-up of a Long-term Relationship: the Cretaceous Separation of New Zealand from Gondwana. *Gondwana Res.*, **7**(1), 273–286. doi:10.1016/S1342-937X(05)70325-7.

Larter, R. D., A. P. Cunningham, P. F. Barker, K. Gohl, and F. O. Nitsche, 2002. Tectonic evolution of the Pacific margin of Antarctica 1. Late Cretaceous tectonic reconstructions. *J. Geophys. Res.*, **107**(B12), 2345. doi:10.1029/2000JB000052.

Larter, R. D., A. G. C. Graham, K. Gohl, G. Kuhn, C.-D. Hillenbrand, J. A. Smith, T. J. Deen, R. A. Livermore, and H.-W. Schenke, 2009. Subglacial bedforms reveal complex basal regime in a zone of paleo–ice stream convergence, Amundsen Sea embayment, West Antarctica. *Geology*, **37**(5), 411–414. doi:10.1130/G25505A.1.

Leinweber, V. T. and W. Jokat, 2012. The Jurassic history of the Africa–Antarctica corridor – new constraints from magnetic data on the conjugate continental margins. *Tectonophysics*, **530–531**(0), 87–101. doi:10.1016/j.tecto.2011.11.008.

LeMasurier, W. E., 1990. Late Cenozoic volcanism on the Antarctic Plate: An overview. In W. E. LeMasurier, J. W. Thomson, P. Baker, P. Kyle, P. Rowley, J. Smellie, and W. Verwoerd, editors, *Volcanoes of the Antarctic Plate and Southern Oceans*, volume 48 of *Antarct. Res. Ser.*, pp. 1–17. AGU, Washington, D.C. ISBN 978-0-87590-172-5. doi:10.1029/AR048p0001.

Lindeque, A. and K. Gohl, 2010. Western Antarctic palaeostratigraphy: implications for palaeobathymetry and palaeoclimate modelling. Poster

presentation at IPY Oslo Science Conference, Oslo, 8–12 June 2010. Available from: http://elsevier.conference-services.net/resources/247/1976/pdf/Oslo2010_0377.pdf.

Livermore, R., C.-D. Hillenbrand, M. Meredith, and G. Eagles, 2007. Drake Passage and Cenozoic climate: An open and shut case? *Geochem. Geophys. Geosyst.*, **8**, Q01005. doi:10.1029/2005GC001224.

Llubes, M., N. Florsch, B. Legresy, J.-M. Lemoine, S. Loyer, D. Crossley, and F. Remy, 2003. Crustal thickness in Antarctica from CHAMP gravimetry. *Earth Planet. Sci. Lett.*, **212**(1–2), 103–117. doi:10.1016/S0012-821X(03)00245-0.

Lowe, A. L. and J. B. Anderson, 2002. Reconstruction of the West Antarctic ice sheet in Pine Island Bay during the Last Glacial Maximum and its subsequent retreat history. *Quaternary Sci. Rev.*, **21**(16–17), 1879–1897. doi:10.1016/S0277-3791(02)00006-9.

Luyendyk, B. P., 1995. Hypothesis for Cretaceous rifting of east Gondwana caused by subducted slab capture. *Geology*, **23**(4), 373–376. doi:10.1130/0091-7613(1995)023<0373:HFCROE>2.3.CO;2.

Luyendyk, B. P., D. S. Wilson, and C. S. Siddoway, 2003. Eastern margin of the Ross Sea Rift in western Marie Byrd Land, Antarctica: Crustal structure and tectonic development. *Geochem. Geophys. Geosyst.*, **4**(10), 1090. doi:10.1029/2002GC000462.

Malinverno, A., 1991. Inverse square-root dependence of mid-ocean-ridge flank roughness on spreading rate. *Nature*, **352**(6330), 58–60. doi:10.1038/352058a0.

McFadden, R. R., C. Teyssier, C. S. Siddoway, D. L. Whitney, and C. M. Fanning, 2010. Oblique dilation, melt transfer, and gneiss dome emplacement. *Geology*, **38**(4), 375–378. doi:10.1130/G30493.1.

Mendel, V., M. Munschy, and D. Sauter, 2005. MODMAG, a MATLAB program to model marine magnetic anomalies. *Comput. Geosci.*, **31**(5), 589–597. doi:10.1016/j.cageo.2004.11.007.

Molnar, P., T. Atwater, J. Mammerickx, and S. M. Smith, 1975. Magnetic Anomalies, Bathymetry and the Tectonic Evolution of the South Pacific since the Late Cretaceous. *J. R. Astron. Soc.*, **40**(3), 383–420. doi:10.1111/j.1365-246X.1975.tb04139.x.

Müller, R. D., K. Gohl, S. C. Cande, A. Goncharov, and A. V. Golynsky, 2007. Eocene to Miocene geometry of the West Antarctic Rift System. *Aust. J. Earth. Sci.*, **54**(8), 1033–1045. doi:10.1080/08120090701615691.

Müller, R. D., M. Sdrolias, C. Gaina, and W. R. Roest, 2008. Age, spreading rates, and spreading asymmetry of the world's ocean crust. *Geochem. Geophys. Geosyst.*, **9**, Q04006. doi:10.1029/2007GC001743.

NGDC, 2007. Marine Trackline Geophysics Data (GEODAS), Data Announcement 2003-MGG-02. National Geophysical Data Center, National Oceanic and Atmospheric Administration, Boulder, Colorado. Available from: http://www.ngdc.noaa.gov/mgg/gdas/gd_sys.html.

Nitsche, F. O., S. S. Jacobs, R. D. Larter, and K. Gohl, 2007. Bathymetry of the Amundsen Sea continental shelf: Implications for geology, oceanography, and glaciology. *Geochem. Geophys. Geosyst.*, **8**(10), Q10009. doi:10.1029/2007GC001694.

Nogi, Y. and K. Kaminuma, 1999. Measurements of vector magnetic anomalies on board the icebreaker Shirase and the magnetization of the ship. *Ann. Geofis.*, **42**(2), 161–170. doi:10.4401/ag-3711.

Oppenheim, A. V. and R. W. Schafer, 2009. *Discrete-Time Signal Processing*. Prentice Hall Signal Processing. Prentice Hall, 3 edition. ISBN 978-0-13-198842-2.

Pankhurst, R. J., I. L. Millar, A. M. Grunow, and B. C. Storey, 1993. The Pre-Cenozoic magmatic history of the Thurston Island Crustal Block, West Antarctica. *J. Geophys. Res.-Sol. Ea.*, **98**(B7), 11835–11849. doi:10.1029/93JB01157.

Parsons, B. and J. G. Sclater, 1977. An analysis of the variation of ocean floor bathymetry and heat flow with age. *J. Geophys. Res.*, **82**(5), 803–827. doi:10.1029/JB082i005p00803.

Paulsen, T. S. and T. J. Wilson, 2010. Evolution of Neogene volcanism and stress patterns in the glaciated West Antarctic Rift, Marie Byrd Land, Antarctica. *J. Geol. Soc. London*, **167**(2), 401–416. doi:10.1144/0016-76492009-044.

Phipps Morgan, J. and W. H. F. Smith, 1992. Flattening of the sea-floor depth-age curve as a response to asthenospheric flow. *Nature*, **359**(6395), 524–527. doi:10.1038/359524a0.

Pilet, S., M. B. Baker, and E. M. Stolper, 2008. Metasomatized Lithosphere and the Origin of Alkaline Lavas. *Science*, **320**(5878), 916–919. doi:10.1126/science.1156563.

Planke, S. and O. Eldholm, 1994. Seismic response and construction of seaward dipping wedges of flood basalts: Vøring volcanic margin. *J. Geophys. Res.-Sol. Ea.*, **99**(B5), 9263–9278. doi:10.1029/94JB00468.

Pollard, D. and R. M. DeConto, 2009. Modelling West Antarctic ice sheet growth and collapse through the past five million years. *Nature*, **458**(7236), 329–332. doi:10.1038/nature07809.

Powell, C. M., S. R. Roots, and J. J. Veevers, 1988. Pre-breakup continental extension in East Gondwanaland and the early opening of the eastern Indian Ocean. *Tectonophysics*, **155**(1–4), 261–283. doi:10.1016/0040-1951(88)90269-7.

Pritchard, H. D., R. J. Arthern, D. G. Vaughan, and L. A. Edwards, 2009. Extensive dynamic thinning on the margins of the Greenland and Antarctic ice sheets. *Nature*, **461**(7266), 971–975. doi:10.1038/nature08471.

Reading, A. M., 2006. The seismic structure of Precambrian and early Palaeozoic terranes in the Lambert Glacier region, East Antarctica. *Earth Planet. Sci. Lett.*, **244**(1–2), 44–57. doi:10.1016/j.epsl.2006.01.031.

Rebesco, M., R. D. Larter, P. F. Barker, A. Camerlenghi, and L. E. Vanneste, 1997. The History of Sedimentation on the Continental Rise West of the Antarctic Peninsula. In P. F. Barker and A. K. Cooper, editors, *Geology and Seismic Stratigraphy of the Antarctic Margin, 2*, volume 71 of *Antarct. Res. Ser.*, pp. 29–49. AGU, Washington, D.C. doi:10.1029/AR071p0029.

Reid, A., J. Allsop, H. Granser, A. Millett, and I. Somerton, 1990. Magnetic interpretation in three dimensions using Euler deconvolution. *Geophysics*, **55**(1), 80–91. doi:10.1190/1.1442774.

Ricard, Y., M. Richards, C. Lithgow-Bertelloni, and Y. Le Stunff, 1993. A geodynamic model of mantle density heterogeneity. *J. Geophys. Res.-Sol. Ea.*, **98**(B12), 21895–21909. doi:10.1029/93JB02216.

Rignot, E., J. L. Bamber, M. R. van den Broeke, C. Davis, Y. Li, W. J. van de Berg, and E. van Meijgaard, 2008. Recent Antarctic ice mass loss from radar interferometry and regional climate modelling. *Nat. Geosci.*, **1**(2), 106–110. doi:10.1038/ngeo102.

Rocchi, S., P. Armienti, M. D'Orazio, S. Tonarini, J. R. Wijbrans, and G. Di Vincenzo, 2002. Cenozoic magmatism in the western Ross Embayment: Role of mantle plume versus plate dynamics in the development of the West Antarctic Rift System. *J. Geophys. Res.-Sol. Ea.*, **107**(B9). doi:10.1029/2001JB000515.

Royer, J. and N. Rollet, 1997. Plate-tectonic setting of the Tasmanian region. *Aust. J. Earth Sci.*, **44**(5), 543–560. doi:10.1080/08120099708728336.

Royer, J.-Y. and D. T. Sandwell, 1989. Evolution of the eastern Indian Ocean since the Late Cretaceous: Constraints from Geosat altimetry. *J. Geophys. Res.-Sol. Ea.*, **94**(B10), 13755–13782. doi:10.1029/JB094iB10p13755.

Sanger, E. A. and J. M. G. Glen, 2003. Density and magnetic susceptibility values for rocks in the Talkeetna mountains and adjacent region, south-central Alaska. Open-File Report 03-268, U.S. Geological Survey. Available from: http://geopubs.wr.usgs.gov/open-file/of03-268/.

Schaeffer, A. J. and S. Lebedev, 2013. Global shear-speed structure of the upper mantle and transition zone. *Geophys. J. Int.* doi:10.1093/gji/ggt095.

Scheuer, C., K. Gohl, and G. Eagles, 2006a. Gridded isopach maps from the South Pacific and their use in interpreting the sedimentation history of the West Antarctic continental margin. *Geochem. Geophys. Geosyst.*, **7**(11), Q11015. doi:10.1029/2006GC001315.

Scheuer, C., K. Gohl, R. D. Larter, M. Rebesco, and G. Udintsev, 2006b. Variability in Cenozoic sedimentation along the continental rise of the Bellingshausen Sea, West Antarctica. *Mar. Geol.*, **227**(3–4), 279–298. doi:10.1016/j.margeo.2005.12.007.

Siddoway, C. S., 2008. Tectonics of the West Antarctic Rift System: new light on the history and dynamics of distributed intracontinental extension. In A. K. Cooper, P. Barrett, H. Stagg, B. Storey, E. Stump, W. Wise, and the 10th ISAES editorial team, editors, *Antarctica: A Keystone in a Changing World*, Proceedings of the 10th International Symposium on Antarctic Earth Sciences, Santa Barbara, California, August 26 to September 1, 2007, pp. 91–114. The National Academies Press, Washington, D.C. ISBN 978-0-309-11854-5.

Siddoway, C. S., S. L. Baldwin, P. G. Fitzgerald, C. M. Fanning, and B. P. Luyendyk, 2004. Ross Sea mylonites and the timing of intracontinental extension within the West Antarctic rift system. *Geology*, **32**(1), 57–60. doi:10.1130/G20005.1.

Sieminski, A., E. Debayle, and J.-J. Lévêque, 2003. Seismic evidence for deep low-velocity anomalies in the transition zone beneath West Antarctica. *Earth Planet. Sci. Lett.*, **216**(4), 645–661. doi:10.1016/S0012-821X(03)00518-1.

Small, C. and D. T. Sandwell, 1989. An abrupt change in ridge axis gravity with spreading rate. *J. Geophys. Res.-Sol. Ea.*, **94**(B12), 17383–17392. doi:10.1029/JB094iB12p17383.

Smith, W. H. F. and D. T. Sandwell, 1997. Global Sea Floor Topography from Satellite Altimetry and Ship Depth Soundings. *Science*, **277**(5334), 1956–1962. doi:10.1126/science.277.5334.1956.

Smith, W. H. F. and P. Wessel, 1990. Gridding with continuous curvature splines in tension. *Geophysics*, **55**, 293–305.

Spasojevic, S. and M. Gurnis, 2012. Sea level and vertical motion of continents from dynamic earth models since the Late Cretaceous. *AAPG Bulletin*, **96**(11), 2037–2064. doi:10.1306/03261211121.

Spasojevic, S., M. Gurnis, and R. Sutherland, 2010. Inferring mantle properties with an evolving dynamic model of the Antarctica–New Zealand region from the Late Cretaceous. *J. Geophys. Res.-Sol. Ea.*, **115**(B5). doi:10.1029/2009JB006612.

Stagg, H. M. J., J. B. Colwell, N. G. Direen, P. E. O'Brien, B. J. Brown, G. Bernardel, I. Borissova, L. Carson, and D. B. Close, 2005. Geological framework of the continental margin in the region of the Australian Antarctic Territory. In *Geoscience Australia Record 2004/25*. Petroleum & Marine Division, Geoscience Australia, Canberra. ISBN 978-1-920871-20-8.

Stein, C. A. and S. Stein, 1992. A model for the global variation in oceanic depth and heat flow with lithospheric age. *Nature*, **359**(6391), 123–129. doi:10.1038/359123a0.

Steinberger, B., 2007. Effects of latent heat release at phase boundaries on flow in the Earth's mantle, phase boundary topography and dynamic topography at the Earth's surface. *Phys. Earth Planet. Inter.*, **164**(1–2), 2–20. doi:10.1016/j.pepi.2007.04.021.

Stickley, C. E., H. Brinkhuis, S. A. Schellenberg, A. Sluijs, U. Röhl, M. Fuller, M. Grauert, M. Huber, J. Warnaar, and G. L. Williams, 2004. Timing and nature of the deepening of the Tasmanian Gateway. *Paleoceanography*, **19**(4), PA4027. doi:10.1029/2004PA001022.

Stock, J. and P. Molnar, 1987. Revised history of early Tertiary plate motion in the south-west Pacific. *Nature*, **325**(6104), 495–499. doi:10.1038/325495a0.

Stock, J. M. and S. C. Cande, 2002. Tectonic history of Antarctic seafloor in the Australia–New Zealand–South Pacific sector: Implications for Antarctic continental tectonics. In J. A. Gamble, D. N. B. Skinner, and S. Henrys, editors, *Antarctica at the close of a millennium*, volume 35 of *Royal Society of New Zealand Bulletin*, pp. 251–259.

Storey, B. C., 1991. The crustal blocks of West Antarctica within Gondwana: reconstruction and break-up model. In M. R. A. Thomson, J. A. Crame, and J. W. Thomson, editors, *Geological Evolution of Antarctica*, pp. 587–592. Cambridge University Press, Cambridge. ISBN 978-0-521-37266-4.

Storey, B. C., P. T. Leat, S. D. Weaver, R. J. Pankhurst, J. D. Bradshaw, and S. Kelley, 1999. Mantle plumes and Antarctica–New Zealand rifting: evidence from mid-Cretaceous mafic dykes. *J. Geol. Soc. London*, **156**(4), 659–671. doi:10.1144/gsjgs.156.4.0659.

Suckro, S. K., K. Gohl, T. Funck, I. Heyde, A. Ehrhardt, B. Schreckenberger, J. Gerlings, V. Damm, and W. Jokat, 2012. The crustal structure of southern Baffin Bay: implications from a seismic refraction experiment. *Geophys. J. Int.*, **190**(1), 37–58. doi:10.1111/j.1365-246X.2012.05477.x.

Sutherland, R., 1999. Basement geology and tectonic development of the greater New Zealand region: an interpretation from regional magnetic data. *Tectonophysics*, **308**(3), 341–362. doi:10.1016/S0040-1951(99)00108-0.

Sutherland, R., S. Spasojevic, and M. Gurnis, 2010. Mantle upwelling after Gondwana subduction death explains anomalous topography and subsidence histories of eastern New Zealand and West Antarctica. *Geology*, **38**(2), 155–158. doi:10.1130/G30613.1.

Sykes, T. J. S., 1996. A correction for sediment load upon the ocean floor: Uniform versus varying sediment density estimations—implications for isostatic correction. *Mar. Geol.*, **133**(1–2), 35–49. doi:10.1016/0025-3227(96)00016-3.

Thompson, D., 1982. EULDPH: A new technique for making computer-assisted depth estimates from magnetic data. *Geophysics*, **47**(1), 31–37. doi:10.1190/1.1441278.

Tikku, A. and S. Cande, 1999. The oldest magnetic anomalies in the Australian-Antarctic Basin: Are they isochrons? *J. Geophys. Res.*, **104**(B1), 661–677. doi:10.1029/1998JB900034.

Totterdell, J. M., J. E. Blevin, H. I. M. Struckmeyer, B. E. Bradshaw, J. B. Colwell, and J. M. Kennard, 2000. A new sequence framework for the great Australian Bight: starting with a clean slate. *APPEA J.*, **40**, 95–118.

Trenberth, K. E. and J. M. Caron, 2001. Estimates of Meridional Atmosphere and Ocean Heat Transports. *J. Climate*, **14**(16), 3433–3443. doi:10.1175/1520-0442(2001)014<3433:EOMAAO>2.0.CO;2.

Uenzelmann-Neben, G. and K. Gohl, 2012. Amundsen Sea sediment drifts: Archives of modifications in oceanographic and climatic conditions. *Mar. Geol.*, **299–302**(0), 51–62. doi:10.1016/j.margeo.2011.12.007.

Uenzelmann-Neben, G., K. Gohl, R. D. Larter, and P. Schlüter, 2007. Differences in ice retreat across Pine Island Bay, West Antarctica, since the Last Glacial Maximum: indications from multichannel seismic reflection data. In A. K. Cooper, C. R. Raymond, and the 10th ISAES Editorial Team, editors, *Antarctica: A Keystone in a Changing World – Online Proceedings of the 10th International Symposium on Antarctic Earth Sciences*, USGS Open-File Report 2007-1047, Short Research Paper 084. USGS. doi:10.3133/of2007-1047.

van Wijk, J. W. and S. A. P. L. Cloetingh, 2002. Basin migration caused by slow lithospheric extension. *Earth Planet. Sci. Lett.*, **198**(3–4), 275–288. doi:10.1016/S0012-821X(02)00560-5.

Vaughan, D. G., H. F. J. Corr, F. Ferraccioli, N. Frearson, A. O'Hare, D. Mach, J. W. Holt, D. D. Blankenship, D. L. Morse, and D. A. Young, 2006. New boundary conditions for the West Antarctic ice sheet: Subglacial topography beneath Pine Island Glacier. *Geophys. Res. Lett.*, **33**(9), L09501. doi:10.1029/2005GL025588.

Vine, F. J. and D. H. Matthews, 1963. Magnetic Anomalies Over Oceanic Ridges. *Nature*, **199**(4897), 947–949. doi:10.1038/199947a0.

Voss, M. and W. Jokat, 2007. Continent-ocean transition and voluminous magmatic underplating derived from P-wave velocity modelling of the East Greenland continental margin. *Geophys. J. Int.*, **170**(2), 580–604. doi:10.1111/j.1365-246X.2007.03438.x.

Wardell, N., J. R. Childs, and A. K. Cooper, 2007. Advances through Collaboration: Sharing Seismic Reflection Data via the Antarctic Seismic Data Library System for Cooperative Research (SDLS). In A. K. Cooper, C. R. Raymond, and the 10th ISAES Editorial Team, editors, *Antarctica: A Keystone in a Changing World – Online Proceedings of the 10th International Symposium on Antarctic Earth Sciences*, USGS Open-File Report 2007-1047, Short Research Paper 001. USGS. doi:10.3133/of2007-1047.srp001.

Watts, A. B., 1988. Gravity anomalies, crustal structure and flexure of the lithosphere at the Baltimore Canyon Trough. *Earth Planet. Sci. Lett.*, **89**(2), 221–238. doi:10.1016/0012-821X(88)90174-4.

Watts, A. B. and J. D. Fairhead, 1999. A process-oriented approach to modeling the gravity signature of continental margins. *Leading Edge*, **18**(2), 258–263. doi:10.1190/1.1438270.

Weigelt, E., K. Gohl, G. Uenzelmann-Neben, and R. D. Larter, 2009. Late Cenozoic ice sheet cyclicity in the western Amundsen Sea Embayment – Evidence from seismic records. *Glob. Planet. Change*, **69**(3), 162–169. Cenozoic Antarctic glacial history. doi:10.1016/j.gloplacha.2009.07.004.

Wessel, P. and L. W. Kroenke, 2008. Pacific absolute plate motion since 145 Ma: An assessment of the fixed hot spot hypothesis. *J. Geophys. Res.*, **113**(B6), B06101. doi:10.1029/2007JB005499.

Wessel, P. and W. H. F. Smith, 1991. Free software helps map and display data. *EOS Trans. AGU*, **72**(41), 441. doi:10.1029/90EO00319.

Wessel, P., W. H. F. Smith, R. Scharroo, J. Luis, and F. Wobbe, 2013. Generic Mapping Tools: Improved Version Released. *EOS Trans. AGU*, **94**(45), 409–410. doi:10.1002/2013EO450001.

White, R. S., D. McKenzie, and R. K. O'Nions, 1992. Oceanic Crustal Thickness From Seismic Measurements and Rare Earth Element Inversions. *J. Geophys. Res.*, **97**(B13), 19683–19715. doi:10.1029/92JB01749.

Whittaker, J., S. Williams, N. Kusznir, and R. D. Müller, 2010. Restoring the continent-ocean boundary: constraints from lithospheric stretching grids and tectonic reconstructions. *ASEG Ext. Abstr.*, **2010**(1), 1–4. doi:10.1071/ASEG2010ab251.

Whittaker, J., A. Goncharov, S. Williams, R. D. Müller, and G. Leitchenkov, 2013. Global sediment thickness dataset updated for the Australian–Antarctic Southern Ocean. *Geochem. Geophys. Geosyst.* doi:10.1002/ggge.20181.

Whittaker, J. M., R. D. Müller, G. Leitchenkov, H. Stagg, M. Sdrolias, C. Gaina, and A. Goncharov, 2007. Major Australian-Antarctic Plate Reorganization at Hawaiian-Emperor Bend Time. *Science*, **318**(5847), 83–86. doi:10.1126/science.1143769.

Williams, S. E., J. M. Whittaker, and R. D. Müller, 2011. Full-fit, palinspastic reconstruction of the conjugate Australian–Antarctic margins. *Tectonics*, **30**(6), TC6012. doi:10.1029/2011TC002912.

Wilson, D. S. and B. P. Luyendyk, 2009. West Antarctic paleotopography estimated at the Eocene–Oligocene climate transition. *Geophys. Res. Lett.*, **36**(16), L16302. doi:10.1029/2009GL039297.

Wilson, D. S., S. S. R. Jamieson, P. J. Barrett, G. Leitchenkov, K. Gohl, and R. D. Larter, 2012. Antarctic topography at the Eocene–Oligocene boundary. *Palaeogeogr. Palaeoclimatol. Palaeoecol.*, **335–336**(0), 24–34. Cenozoic Evolution of Antarctic Climates, Oceans and Ice Sheets. doi:10.1016/j.palaeo.2011.05.028.

Wilson, D. S., D. Pollard, R. M. DeConto, S. S. Jamieson, and B. P. Luyendyk, 2013. Initiation of the West Antarctic Ice Sheet and estimates of total Antarctic ice volume in the earliest Oligocene. *Geophys. Res. Lett.*, **40**(16), 4305–4309. doi:10.1002/grl.50797.

Winberry, J. P. and S. Anandakrishnan, 2004. Crustal structure of the West Antarctic rift system and Marie Byrd Land hotspot. *Geology*, **32**(11), 977–980. doi:10.1130/G20768.1.

Wobbe, F. and K. Gohl, 2013. Continental deformation of Antarctica during Gondwana's breakup. In G. Lohmann, K. Grosfeld, D. Wolf-Gladrow, V. Unnithan, J. Notholt, and A. Wegner, editors, *Earth System Science: Bridging the Gaps between Disciplines — Perspectives from a Multi-Disciplinary Helmholtz Graduate Research School*, SpringerBriefs in Earth System Sciences, pp. 83–89. Springer, Berlin Heidelberg. ISBN 978-3-642-32234-1. doi:10.1007/978-3-642-32235-8_4.

Wobbe, F., K. Gohl, A. Chambord, and R. Sutherland, 2012. Structure and breakup history of the rifted margin of West Antarctica in relation to Cretaceous separation from Zealandia and Bellingshausen plate motion. *Geochem. Geophys. Geosyst.*, **13**(4), Q04W12. doi:10.1029/2011GC003742.

Wobbe, F., A. Lindeque, and K. Gohl, 2014a. Anomalous South Pacific lithosphere dynamics derived from new total sediment thickness estimates off the West Antarctic margin. *Glob. Planet. Change*, **123**, 139–149. doi:10.1016/j.gloplacha.2014.09.006.

Wobbe, F., A. Lindeque, and K. Gohl, 2014b. Total sediment thickness grid of the Southern Pacific Ocean off West Antarctica, data repository. PANGAEA. doi:10.1594/PANGAEA.835589.

Wolfenden, E., C. Ebinger, G. Yirgu, P. R. Renne, and S. P. Kelley, 2005. Evolution of a volcanic rifted margin: Southern Red Sea, Ethiopia. *Geol. Soc. Am. Bull.*, **117**(7–8), 846–864. doi:10.1130/B25516.1.

Zwally, H. J., M. B. Giovinetto, M. A. Beckley, and J. L. Saba, 2012. Antarctic and Greenland Drainage Systems, GSFC Cryospheric Sciences

Laboratory [online]. Available from: http://icesat4.gsfc.nasa.gov/cryo_data/ant_grn_drainage_systems.php.